Modeling of the Vertical Heat Exchange in Shallow Lakes

DISSERTATION

zur Erlangung des akademischen Grades
Doctor rerum naturalium
(*Dr. rer. nat.*)
im Fach Geographie

eingereicht an der
Mathematisch-Naturwissenschaftliche Fakultät II
der Humboldt-Universität zu Berlin

von

Dipl.-Ing. Georgiy Kirillin
geb. am 26 August 1969 in Karaganda, UdSSR

Präsident der Humboldt-Universität zu Berlin
Prof. Dr J. Mlynek
Dekan der Mathematisch-Naturwissenschaftlichen Fakultät II
Prof. Dr E. Kulke

Gutachter:
1. Prof. Dr G. Nützmann
2. Prof. Dr W. Endlicher
3. Prof. Dr G. Jirka

Tag der mündlichen Prüfung: 19.11.2002

Berlin 2002

Abstract

This study aims at (i) providing improved understanding of the vertical heat exchange in shallow lakes with intermittent thermal stratification and (ii) developing of a computationally inexpensive model, which should take into account general mechanisms of vertical heat exchange in a lake. A special attention is paid to parameterization of the turbulent exchange in the thermocline: the strongly stratified layer developing below the upper mixed layer. In addition, the mechanisms of stratification formation are considered with account of the vertically distributed absorption of the solar radiation within the upper water column, and possible influence of biological production on the thermal budget in a lake is analyzed.

The concept of self-similarity of the thermocline is used for parameterization of the vertical heat exchange in stratified media. A new self-similarity function is proposed based on solution of the heat transfer equation in one-dimensional form in propagating wave form. The temperature gradient at the thermocline bottom is included into the governing parameters extending applicability of the self-similarity description on wider class of natural processes including boundary layer development in stably stratified atmosphere and mixed layer deepening in shallow lakes.

A one-dimensional model of temperature evolution in lakes is developed. The self-similar description of the thermocline allows achieving a fully parameterized, computationally inexpensive algorithm that make it possible to use the model in various environmental applications including ecological modeling and numerical weather predictions.

The model is tested against observations in the Lake Müggelsee, Berlin. Thermal regime of the lake during summer periods of 1980-1996 is modeled, general mechanisms of the temperature structure formation in a shallow polymictic lake are discussed, the role of water transparency variability is analyzed.

Convection driven by solar radiation absorption is considered in frames of the bulk mixed layer approach. The radiatively-driven convection proper only for fresh-water lakes in late winter represents a rare natural example of purely convective mixing providing a good test case for mixed layer scaling. A mixed layer model including the effect of salt concentration on stability is developed and applied to a number of temperate and polar lakes. The similarity of the turbulent kinetic energy and dissipation rate profiles within the convective mixed layer is demonstrated, the influence of very small salt concentrations on vertical mixing at temperatures close to the maximum density value is discussed.

Modellierung des vertikalen Wärmeaustausches in Flachseen

Zusammenfassung zur Dissertation

Zielstellung und Methoden. Diese Arbeit hat zum Ziel (*i*) ein erweitertes Verständnis des vertikalen Wärmeaustausches in Flachseen mit intermittierender thermischer Schichtung zur Verfügung zu stellen sowie (*ii*) ein wenig Rechenkapazität beanspruchendes Modell zu entwickeln, welches die generellen Mechanismen des vertikalen Wärmeaustausches in Seen berücksichtigt. Besondere Aufmerksamkeit wird der Parametrisierung des turbulenten Austauschs innerhalb der Sprungschicht – der stabilen Schicht, die sich unterhalb der oberen, durchmischten Zone entwickelt – gewidmet. Außerdem werden die Mechanismen der Schichtungsbildung mit Blick auf die vertikale Absorptionsverteilung der Sonnenstrahlung im oberen Wasserkörper sowie der möglichen Einfluss der biologischen Primärproduktion auf den Wärmehaushalt des Sees analysiert. Eine weitere Fragestellung dieser Arbeit betrifft die Vorhersagbarkeit kurzer Schichtungsereignisse, die sich mit Perioden vertikaler Homogenität abwechseln. Diese sogenannte "*Polymixis*" ist typisch für Flachseen in Sommern gemäßigter Zonen.

Eine eindimensionale, über die Horizontale gemittelte Darstellung eines Sees wurde als Grundlage für die Modellentwicklung gewählt. Das Konzept der Selbstähnlichkeit der Sprungschicht wird für die Parametrisierung des vertikalen Wärmeaustausches im geschichteten Teil des Wasserkörpers benutzt. Eine neue Selbstänlichkeitsfunktion wird in der vorliegenden Arbeit vorgeschlagen. Sie basiert auf der Lösung der Wärmetransportgleichung einer sich nach unten ausbreitenden Welle. Der Temperaturgradient am Boden der Sprungschicht wird dabei als ein wesentlich bestimmender Parameter mit einbezogen. Dieser Schritt öffnet die Anwendbarkeit des Konzepts der Selbstähnlichkeit für die Beschreibung anderer natürliche Prozesse, wie zum Beispiel die Entwicklung von Grenzschichten in stabil geschichteter Atmosphäre oder die Vertiefung der durchmischten Zone in Flachseen.

Selbstähnlichkeitsanalyse des Temperaturprofils in der Sprungschicht. Das Konzept der Selbstähnlichkeit der Sprungschicht wird diskutiert und der physikalische Hintergrund der Selbstähnlichkeitshypothese analysiert. Dabei wird gezeigt, dass die Selbstähnlichkeit des Temperaturprofils sich äquivalent zu der Lösung einer sich fortbewegenden Welle in der eindimensionalen Wärmetransportgleichung verhält (Kirillin, 2001a).

Die Lösung wird unter Berücksichtigung der Schichtungsverhältnisse unterhalb der Sprungschicht erreicht. Sie erweitert die Anwendbarkeit des Selbstähnlichkeitsprinzips der Sprungschicht auf eine Reihe von geophysikalischen Strömungen, einschließlich Flachseen, konvektiven Grenzschichten in der Atmosphäre und jahreszeitlich bedingten Sprungschichten in Ozeanen. In nicht-turbulenten Fluiden werden die unterhalb der Sprungschicht liegenden Schichtungsverhältnisse durch die Berücksichtigung eines dimensionslosen Temperaturgradienten am Boden der Sprungschicht mit in die Lösung einbezogen. Dies erlaubt eine Variation der Form des Temperaturprofils innerhalb der Sprungschicht, insbesondere die Annäherung an einen asymptotischen Temperatursprung am Boden der oberen durchmischten Schicht.

Die vorgestellte Lösung verallgemeinert bisher vorgeschlagene empirische Beschreibungen des Temperaturprofils in der Sprungschicht. Das von ihr resultierende Profil des turbulenten Wärmetransports zeigt das direkte Verhältnis zwischen Mischungsintensität und potentieller Energie. Dies liegt in Übereinstimmung mit der Theorie über die durch das Brechen interner Wellen angetriebene Mischung in geschichteten Fluiden (Kantha, 1977).

Der Lösungsansatz wird anhand von Beobachtungen in Ozeanen, der Erd- und Marsatmosphäre, Laboruntersuchungen und Messungen in Seen überprüft (Kirillin, 2001b). Die vertikale

Ausdehnung der natürlichen Prozesse variiert von einigen Metern zu mehreren 10 Kilometern. Werden diese jedoch mit der in dieser Arbeit vorgeschlagenen dimensionslosen Variablen skaliert, so gruppieren sich alle Temperaturprofile um die Kurve, die sich aus dem vorgeschlagenen Lösungsansatz ergibt.

Die Beschreibung des Temperaturprofils mit dem Konzept der Selbstähnlichkeit ermöglicht es, Ansätze der "*bulk*"-Modellierung analog zur Modellierung gemischter Zonen auf geschichteten Teil des Wasserkörpers anzuwenden. Die Tatsache, dass der Wärmetransport am Boden der Sprungschicht mit in das Modell einbezogen wird, erlaubt die Berücksichtigung dieser Beziehung in der Modellierung von Flachseen, in denen der Wärmefluss an der Wasser-Sediment Grenzschicht beträchtlich sein kann, sowie in der Modellierung von Konvektionen, die von starken Inversionen in der konvektiven Grenzschicht der Atmosphäre überdeckt sind.

Das Modell über die Temperaturentwicklung in Seen. Das Modell der jahreszeitlichen Temperaturentwicklung in Seen wurde unter Verwendung des Quellenkodes sowie des generellen Konzepts des TeMix-Modells abgeleitet (Mironov *et al.* , 1991). Das Modell verwendet eine Zwei-Schichten-Darstellung des Temperaturprofils, welche auf dem Lösungsansatz der Selbstähnlichkeit beruht.

Im Gegensatz zum bisherigen TeMix-Algorithmus wird eine durch Sonneneinstrahlung verursachte differntielle Erwärmung der Wasserschicht berücksichtigt. Dies verbessert die Modellvorhersagen entscheidend, insbesondere unter den in Flachseen vorherrschenden Bedingungen.

Die Leistungsfähigkeit des Modells wird anhand von Daten des Müggelsees (Driescher *et al.* , 1993) untersucht. Ein Vergleich zwischen den Modellergebnissen und den gemachten Beobachtungen zeigt, dass das Modell den vertikalen Temperaturverlauf in Flachseen ausreichend gut voraussagt. Die Modellberechnungen für die Sommer der Jahre 1980-1996 erlaubten die Detektion von zu hohen Messwerten der Sonneneinstrahlung auf der Seeoberfläche in den Jahren 1980-1989. Dies demonstriert die Sensitivität des Modells in Abhängigkeit von der Qualität der Eingangsdaten und bestätigt die Zuverlässigkeit der Modellvorhersagen.

Ein Vergleich der Modellergebnisse mit denen von Zweigleichungssystem basierten Turbulenzmodellen wurde durchgeführt. Vorhersagen über die Tiefe der durchmischten Zone des in dieser Arbeit vorgeschlagenen Modells liegen in guter Übereinstimmung mit der vertikalen Turbulenzstruktur, wie sie das k-ϵ-Modell vorhersagt. Gleichzeitig liefert der dem TeMix-Modell zu Grunde liegende "*bulk*"-Algorithmus bessere Ergebnisse der Oberflächentemperatur in Flachseen als die des k-ϵ- und des Mellor-Yamada-Modells. Letztere zeigen große numerische Instabilität, wenn sie für flache Wasserkörper mit an der Oberfläche stark variierenden Wärmeflüssen angewendet werden. Diese Tatsache sowie die hohen rechentechnischen Anforderungen machen die praktische Anwendung der Zweigleichungs-Turbulenzmodelle in ökologischen und meteorologischen Fragestellungen, wo die Vorhersage der thermalen Struktur in Flachseen notwendig ist, schwierig. Das TeMix-Modell weist im Gegensatz dazu keine Limitierungen auf, da hier adäquate Vorhersagen mit geringen Rechenanforferungen miteinander verbunden sind.

Das Modell sagt recht gut die jahreszeitlichen sowie die zwischenjährlichen thermischen Schwankungen – inklusive Schichtungsbildung und -zerstörung – in einem polymiktischen See voraus. Die Outputcharakteristiken des Modells – die Durchschnittstemperatur, die Tiefe und die Temperatur der oberen durchmischten Zone – liefern ausreichende Informationen für vielfältige Anwendungen im Bereich der Seenphysik.

Die Rolle der Variabilität der Lichtdurchlässigkeit des Wassers im Wärmehaushalt eines Flachsees wird anhand von Modellergebnissen und Beobachtungsdaten des Müggelsees untersucht. Es wurde herausgefunden, dass in Sommermonaten mit geringer mittlerer Windgeschwindigkeit, die Variationen der Oberflächentemperatur mit der Lichtextinktion des Seewassers korreliert. Eine kann folglich ein Einfluss des Algenwachstums auf die Seetemperatur vermutet werden.

Die Konvektion in Eis bedeckten Seen. Die typischen Mischungsverhältnisse unterhalb der Eisschicht als Resultat von Konvektion werden analysiert (Mironov *et al.* , 2002). Es wird gezeigt, dass die für die Beschreibung der Wärmefluss induzierten Konvektion in der Atmosphäre und in Ozeanen geeignete *Gleichung des Turbulenten Entrainments*, auch für Konvektionen unterhalb der Eisschicht von Seen angewendet werden kann. Dies gilt allerdings nur unter der Voraussetzung, dass die auf dem oberflächennahen Wärmefluss basierende Deardorff-Skala für die Konvektionsgeschwindigkeit durch eine geeignete Skala ersetzt wird, die den Charakter der vertikal verteilten Strahlungswärme berücksichtigt.

Ein “*bulk*”-Modell wird für die durchmischte Zone angewendet, um eine sich in die Tiefe ausbreitende konvektiv durchmischte Zone zu simulieren. Das Modell verwendet das Konzept der Selbstähnlichkeit für die Darstellung des sich entwickelnden Temperaturprofils. Eine stationäre Lösung der Wärmetransportgleichung wird verwendet, um die Struktur der stabil geschichteten Zone unterhalb der Eisoberfläche zu beschreiben. Die Skalierung der durchmischten Zone und die über die durchmischte Zone integrierte Bilanzgleichung für die turbulente kinetische Energie werden für die Ableitung der *Gleichung des Entrainments* benutzt. Die auf dieser Basis erlangten Modellvorhersagen stimmen gut mit Beobachtungsdaten von sowohl in gemäßigten als auch in polaren Klimazonen gelegenen Seen überein.

Eine Erweiterung des für die durchmischte Zone entwickelten Modells auf Salzwasser wird vorgeschlagen und anhand von Beobachtungsdaten geprüft (Kirillin *et al.* , 2001). Obwohl der Salzgehalt in den meisten Seen der gemäßigten und polaren Klimazonen sehr gering ist, kann er bei Temperaturen um das Dichtemaximum signifikanten Einfluss auf die Dynamik ausüben. Unter Bedingungen von mit zunehmender Tiefe steigenden Temperaturen und mit dem Übersteigen der Temperatur des Dichtemaximums in der Bodenschicht wäre die Wassersäule einer konvektiven Umkehrströmung ausgesetzt. Das ist jedoch nicht der Fall, wenn der Salzgehalt mit der Tiefe ansteigt und damit für statische Bedingungen sorgt.

Strahlungsinduzierte Konvektion in Eis bedeckten Seen bietet ein nahezu ideales Testgebiet für die Anwendung von Turbulenzmodellen. Wie bereits von Farmer (1975) beschrieben, handelt es sich hierbei um ein seltenes Beispiel geophysikalischer Konvektionsströmung, bei der keine bedeutende Scherung auftritt. Dies bedeutet eine Vereinfachung von besonderem Wert bei Untersuchungen von Gravitationsinstabilitäten und ihren Konsequenzen. Datensätze, die durch Turbulenz- und Temperaturmessungen in der konvektiven Grenzschicht unterhalb des Eises und durch Simulation von großen Strudeln gewonnen werden, können benutzt werden, um turbulente Konvektionsströmungsmodelle zu testen und weiter zu entwickeln.

Praktische Anwendungen. Eine Integration des hier vorgestellten Modells in ein Ökosystemmodell von Flachseen (Schellenberger *et al.* , 1983) ist eine folgerichtige Erweiterung der vorliegenden Arbeit. Eine wesentliche Verbesserung der Vorhersagen der ökologischen Komponenten kann bei Einbeziehung der vertikalen Temperaturschichtung erwartet werden (Denman & Gargett, 1983). Die Tiefe der durchmischten Zone ist die Skala, welche die vertikale Verteilung des Seeplanktons und die Biomasseproduktion bestimmt. Das Schichtungsregime bestimmt auch die externe und interne Nährstofffracht, und somit den trophischen Zustand des Sees (Golosov & Kirillin, 2000).

Die hier vorgestellte parametrisierte Beschreibung der vertikalen Temperaturverteilung kann ebenso in zwei- und dreidimensionalen Zirkulationsmodellen verwendet werden, insbesondere wenn eine vereinfachte jedoch physikalisch solide Parametrisierung des vertikalen Transports erwünscht ist. Dieses wurde zum Beispiel von Kirillin *et al.* (1998) anhand der Modellierung von ufernahen Strömungen in großen Seen untersucht.

Seen verändern die Struktur und Transporteigenschaften der oberen Atmosphärenschicht. Diese Problemstellung wurde zwar bisher noch nicht ausreichend beschrieben, jedoch in den meisten numerischen Ansätzen Umwelt bezogener Modellanwendungen, insbesondere in numerischen Wettervorhersage- und Klimamodellen, wird der von Seen ausgehende Effekt entweder vollständig ignoriert oder nur äußerst primitiv in die Parametrisierung mit einbezogen. Folglich wird ein Seenmodell für Umwelt bezogene Anwendungen benötigt, das einerseits physikalisch solide ist, jedoch anderseits Computerresourcen effizient nutzt. Mit dem in dieser Arbeit vorgeschlagenen Modellansatz, der sich das Prinzip der Selbstähnlichkeit des Temperaturprofils in der Sprungschicht zur Beschreibung der Schichtungsstruktur zwischen der oberen durchmischten Zone und dem Beckenboden zu Nutze macht, kann ein vernünftiger Kompromiss zwischen physikalischer Realität und Rechenökonomie erreicht werden.

Contents

Chapter 1

Introduction

1.1 Objectives and scope of the study

The subject of the study are the physical processes of heat and mass exchange in shallow lakes. There is a number of reasons stimulating our interest to the shallow lakes dynamics. Some of them are listed below.

- Physical background for ecological modeling.

  Modeling aquatic ecosystems is a rapidly growing branch of ecological science. A large number of small freshwater lakes is located in highly urbanized areas and undergoes strong anthropogenic impact. Their small spatial scales provide relatively fast response to this impact followed by ecological equilibrium disturbance. Scenarios of ecological changes need adequate description of main physical processes in a lake, which processes determine in many ways the behavior of lake ecosystems.

- Climate modeling and numerical weather prediction.

  In most numerical modeling systems for environmental applications, most notably numerical weather prediction (NWP) and climate modeling (CM) systems, the effect of small-to-medium size lakes is either entirely ignored or is parameterized very crudely. The problem urgently calls for further investigation, in particular, due to the increase of the horizontal resolution of models. Such increase is envisaged for most NWP systems in the near future. Then, a physically realistic and at the same time computationally cheap model is required to predict the evolution of the heat exchange at the air-lake interface.

- Lake as a model of the ocean.

  When Forel (1892) introduced the term *limnology*, he classified this science as *l'océanographie des lacs*: the oceanography of lakes. Lakes as dynamical systems are less complicated than oceans or the atmosphere and monitoring of physical processes can be carried out here at relatively low cost. In this sense, a lake can be considered as taking an intermediate place between laboratory models and the global atmosphere-ocean system, allowing us to distinguish general physical principles of the geophysical fluid dynamics. Significant progress in limnology is clearly marked as one of the first priorities in future development of physical oceanography:

  > *Lakes can be useful analogs of the ocean, with wind and thermally driven circulations, developing coastal fronts, and topographically steered currents. Lakes*

> *are important as model ecosystems which are simpler and more accessible than ocean ecosystems. Significant progress can be foreseen in the coming decades in limnology, helped by the tools and ideas developed for the ocean. (Royer & Young, 1997)*

When considering a lake as a physical model of the ocean, one can expect lake data to present additional information about vertical turbulent transport in stratified media, whose characteristics and origin in the ocean are still not clearly defined (Webb & Suginohara, 2001).

Among the physical factors determining biological processes in lake ecosystems, the vertical mixing conditions are of the first importance (Denman & Gargett, 1983). On the other hand, ecosystem modeling involves parameterization of a number of biological and chemical interactions that usually leaves no room for detailed description of lake physics. At once simple and physically sound algorithms are required, linking the biological processes with overall physical characteristics.

Integration of sophisticated models of lake dynamics into NWP systems is also rarely possible on account of high computational requirements of latter. Nonetheless, an adequate prediction of vertical stratification in a lake can lead to essential improvement of heat and mass exchange estimation at the air-lake interface.

Based on these considerations, the main goal of this work is formulated as development of a computationally inexpensive model, which should take into account general mechanisms of vertical heat exchange in a lake. A special attention is paid to parameterization of the turbulent exchange in the thermocline: the strongly stratified layer developing below the upper mixed layer. In addition, the mechanisms of stratification formation are considered with account of the vertically distributed absorption of the solar radiation within the upper water column, and possible influence of biological production on the thermal budget in a lake is analyzed. Another question to consider is predictability of short stratification events alternating with periods of vertical homogeneity (so-called *polymixis* phenomenon), which is typical for temperate shallow lakes in summer. Destroying of the vertical temperature stratification leads to enrichment of the upper photosynthetically active layer by nutrients from the sediments and determines in this way the primary production in a lake. Thus, an estimation of ecological changes in shallow lakes is impossible without adequate description of the polymixis, which can be achieved in its turn from one-dimensional modeling of the vertical temperature structure in a lake.

1.2 General approaches and methods

The one-dimensional, horizontally averaged representation of a lake is used here as the background for the model development. The scales of horizontal movements in a lake exceed in several orders the vertical ones, providing relatively homogeneous distribution of main characteristics across a lake. At the same time, the vertical exchange is arrested by the stratification occurring due to gravitational forces. That makes possible considering a lake as a horizontally mixed water column, where the energy exchange appears only in vertical direction or, to be meticulous, parallel to the Earth gravitation vector.

The applicability of the one-dimensional approximation to an individual lake can be limited due to additional horizontal inhomogeneity introduced by interaction of external forces and lake morphometry. Horizontal variability in atmospheric forcing, river in- and outflow and wind-driven upwelling of deep water in coastal areas are usually declared as the main sources of such inhomogeneity. None of these effects, however, will introduce horizontal inhomogeneity in a temperature field until the density distribution is uniform in the lake and inflows. The aforementioned mechanisms should be considered in interaction with the vertical density stratification, formed in freshwater lakes by radiative heating and by the heat input at the lake-atmosphere interface. Wind mixing and convective mixing driven by surface cooling, destroy, in their turn, the stratification in the upper part of a lake leading to formation of the upper mixed layer. Hence, a simple criterion, indicating whether this vertical structure develops in a lake or it is fully mixed vertically, can be achieved from comparison of the lake's depth with a characteristic scale for mixed layer thickness. The *upper* estimation for the mixing depth is the *Eckman depth*: $h_e = 0.3u_*/f$, where u_* is the momentum flux at the lake surface and f is the Coriolis parameter. The estimation is rough since the constant 0.3 is derived for open waters and does not take into account the fetch influence, and the Eckman formula does not include stabilization by vertical stratification and by surface heating and dissipation of the wind energy at coastal slopes. In reality, wind mixing will occupy much shallower layer at the surface. The depth of wind-driven mixed layer in case of stabilizing surface buoyancy flux can be estimated from a typical value of the Monin-Obukhov length scale, modified for taking into account the volumetric absorption of the incoming short-wave solar radiation I_0 within the water column.

$$l = \frac{\rho C_p u_*^3}{\alpha g[Q_s + I_0(1 - (1 - e^{-\gamma D})/\gamma D)]}, \tag{1.1}$$

where γ is the light extinction coefficient and α and C_p are the thermal expansion coefficient and the specific heat of water, correspondingly. The mixed layer depth can be then estimated as $h_l = 0.2l$ and, given the characteristic lake depth D, the stratification criterion can be written:

$$h_{mix}/D < 1, \quad h_{mix} = \min(h_l, h_e). \tag{1.2}$$

When the condition holds true, a two-layered vertical structure develops in a lake, where the well-mixed upper layer is separated from the stratified lower part by a density front - the pycnocline. Under wind drag forcing, the declination of the pycnocline takes place counterbalancing the slope of the lake surface that introduces horizontal inhomogeneity in the density distribution. At strong winds the pycnocline can climb to the lake's surface at the upwind shore resulting in upwelling of deep water and in formation of horizontal density front at the surface. A criterion characterizing the balance between the wind drag and the slope of the thermocline resulting from it can be written in form of the *Wedderburn Number* W as it introduced by Thompson & Imberger (1980):

$$W = g' h_{mix}^2/(u_*^2 L), \tag{1.3}$$

with $g' = g\Delta\rho/\rho_0$ is the reduced gravity, $\Delta\rho$ is the density jump across the pycnocline, ρ_0 is the reference density, and L is the characteristic horizontal length scale of the lake. If $W < 1$ than the pycnocline will surface at the upwind end, and resulting longitudinal inhomogeneity should be generally taken into account. It is clear that the lake's morphometry will strongly influence the inclination of the pycnocline. A criterion, similar to the Wedderburn Number but incorporating the stability of the water column at z's horizon $St = \rho_0^{-1}\int_0^D (h_V - z) g\rho A(z)\mathrm{d}z$ (Schmidt, 1915), was introduced by Imberger & Patterson (1990) as the *Lake Number* L_N:

$$L_N = \frac{h_{mix} St}{u_*^2 (D - h_V) A_S^{3/2}}, \tag{1.4}$$

where, $A(z)$ is the lake's area at the depth z, A_S is that at the lake's surface, h_V is the height of the center of the volume. As for the Wedderburn Number, the critical value of $L_N = 1$ indicates the transition to horizontally inhomogeneous state.

Another important mechanism potentially producing essential horizontal temperature gradients is the throughflow. Again, as in case of wind circulation, the degree of inhomogeneity introduced by a river inflow will be determined by the density stratification, which can be expressed here as the density difference between the lake water and the inflow. Its influence can be expressed in terms of the internal *Froude number*:

$$Fr = \frac{V}{(g'D)^{1/2}}, \tag{1.5}$$

where V is the inflow velocity, and the reduced gravity g' is based now on the difference between inflow and surface densities. The number represents the relationship between inertial forces of the inflow and pressure gradient forces on account of density difference. Thus, if $Fr < 1$, the pressure forces dominate and lead normally to fast adjustment of gradients in vicinity of inflow area. If, however, the river density is higher than that of the lake surface, the inflow can plunge to a depth of zero density difference, where it leaves the lake bottom and propagates further along isopycnal surfaces, forming so-called intrusive flow and leading to local inhomogeneities. A discussion on intrusions in lakes can be found in (Imberger & Hamblin, 1982). In case $Fr > 1$, the inertial forces can potentially destroy the one-dimensional structure in the lake. Imberger & Hamblin (1982) have proposed the *modified Wedderburn Number* for estimation of introduced inhomogeneity in form:

$$\tilde{W} = \frac{g'D^2}{V^2 L}, \tag{1.6}$$

where term definitions are the same as in (1.5). Small $\tilde{W}$ lead to an active mixing by inflow with longitudinal density gradients. At large $\tilde{W}$ the situation stays close to one-dimensional. A similar criterion was derived by Jirka & Watanabe (1980) named the *Pond Number*, which can be written in our terms as:

$$Pn = C\frac{u_*^2 L}{g'D^2} = C\frac{D}{L}Fr_*^2 = C\,\tilde{W}_*^{-1}. \tag{1.7}$$

Here, u_* is the friction velocity at the bottom of the mixed layer and the coefficient C describes damping of the inflow velocity on account of the entrainment at the density interface.

In some cases, wind mixing can be complicated by configuration of a lake: presence of sidearms, shadowed areas etc. The heating and cooling processes, in their turn, can be influenced by variations in lake depth. Thus, the shallow coastal zone cools at night to a lower temperature than that in the deeper interior that results in convective mixing at sloping bottom and introduces additional vertical mixing mechanism. A faster heating of sidearms and coastal areas during the daytime can also lead to the horizontal density gradient formation in a lake. The following criterion was proposed by Imberger (2001) for estimation of littoral flushing driven by night cooling of lake waters, balancing the gravitational flow along a bottom slope and the convective mixing:

$$C_V = (b\,L)^{-1/3}\frac{D}{L\tan\phi\,T_c}, \tag{1.8}$$

where, $b = (C_p\,\rho)^{-1}g\alpha Q_s$ is the convective buoyancy flux at the surface, ϕ is the bottom slope and T_c is the time scale of the night convective period. If $C_V < 1$ then the littoral zone will be flushed during the night cooling period. If $C_V > 1$ no essential water exchange appears.

Thus, in order to justify the application of the 1-dimensional approximation to a stratified lake, one should perform an analysis of the balance between stratification and disturbing forces with help of the criteria (1.1-1.8). When a lake is fully mixed vertically, horizontal variations in the wind field and in the surface heat exchange remain the only inhomogeneity sources. These are usually small in lakes with horizontal scales less than the synoptical scales in the atmosphere. Hence, one can neglect these variations for lakes with horizontal size $\lesssim 50$km., which are the majority of lakes on the Earth. This estimation can be also applied approximately to all polymictic lakes, which have being fully mixed vertically at least once during the summer and where no seasonal thermocline exists in the strict sense. Moreover, if we exclude from consideration diurnal oscillations, all variations associated with diurnal cycle in a lake can be parameterized as subscale processes in frames of the one-dimensional approach when modeling the seasonal evolution of lake temperature. A simple estimation of one-dimensional approximation applicability based on time scales of processes under investigation can be achieved from following considerations. The temporal scales of physical processes in natural waters are known to be in a certain relationship to the spatial scales (Kamenkovich *et al.* , 1987): phenomena with larger spatial dimensions appear to have also longer duration (Fig. 1.1). The particular case represent

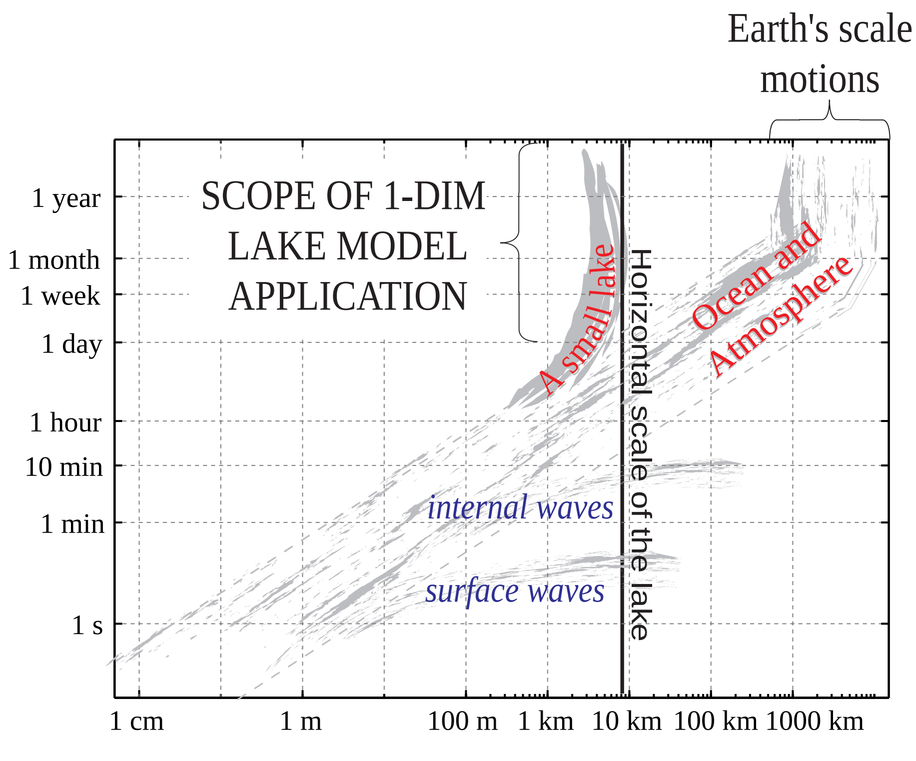

Figure 1.1: Time and space scales typical for physical processes in natural water bodies and applicability domain of one-dimensional horizontally averaged lake models.

wave motions, which are essentially non-local and can transport the energy far away from its source. In their turn, the spatial extension of the motions in a lake is limited by lake's horizontal dimensions. Thus, all oscillations with essentially large temporal scales can be related as occupying the whole lake, making the one-dimensional representation of the lake well-grounded. With a good accuracy, we can assume all oscillations with temporal scales larger than diurnal ones to have the one-dimensional nature in lakes with horizontal dimensions 1-10 km. Thereby, we exclude diurnal variations from consideration and operate with daily averaged characteristics when applying a one-dimensional model to lake dynamics.

Two approaches to one-dimensional lake modeling are commonly used nowadays. The principal difference between them consists in the way of vertical turbulent exchange representation. The *turbulence closure models* (Mellor & Yamada, 1974; Rodi, 1987) are based on local closure of the Reynolds-averaged motion equations using fickian analogy for turbulent mixing parameterization and empirical hypotheses about vertical profiles of higher turbulent moments to determine profiles of turbulent exchange coefficients. The models are relative cumbersome and the underlying parameterizations have ambiguous physical meaning.

The *bulk-models* are based on vertically integrated budget of heat and momentum within a certain layer arrived in assumption of temperature and velocity profiles in the layer be known. The most widely used kind of these models are mixed-layer models applied to upper layers of lakes and oceans (Gill & Turner, 1976; Niiler & Kraus, 1977) assuming homogeneous vertical temperature distribution there and approximating the underlying thermocline by temperature jump at the mixed layer base. Additional hypotheses about similarity of turbulence characteristics within the Upper Mixed Layer (UML) allow arriving at the *entrainment equation* for the UML depth evolution, which equation is a vertically integrated form of turbulent kinetic energy (TKE) budget within the UML. The similarity of the TKE and of the TKE dissipation rate profiles within the UML is reported in numerous laboratory and field studies (see Zilitinkevich 1987 for review) and will be also tested in the current work on observational and large-eddy simulation (LES) data for radiatively-driven convection in ice-covered lakes. The hypothesis about self-similarity of vertical profiles of main characteristics can be also extended on the stably stratified thermocline underlying the UML (Barenblatt, 1996). The essence of the concept consist of representation of vertical temperature profile under the mixed layer by an universal function of depth. In couple with upper mixed layer approach, it allows achieving two-layered entirely parameterized temperature representation that excludes the vertical heat conductivity coefficient from a model and reduces computational costs to a minimum conserving the physical soundness of a model.

Existing approaches to self-similar description of the thermocline are summarized here and underlying physical mechanisms are analyzed. The analysis has allowed arriving at the solution of the vertical heat transport equation within the thermocline in terms of dimensionless similarity variables: the non-dimensional thermocline depth and the temperature jump across it. The solution generalize a number of previously proposed empirical approximations and gives a theoretical explanation of the observed self-similarity. It allows also taking into account stratification in non-turbulent quiescent water underlying the thermocline by means of dimensionless temperature gradient at the thermocline base, that extends the scope of application on wider range of geophysical phenomena including the convective boundary layer (CBL) development in the atmosphere and the thermocline on lakes where the near-bottom temperature gradients are not negligible. The solution is tested against observational data from lakes. Furthermore, data from the Ocean, the Earth and the Mars atmospheres are compared with the proposed model, revealing the good adequacy of the model in the wide range of spatial and temporal scales and justifying the validity of proposed scaling. Finally, we incorporate the achieved solution into a bulk-model of seasonal temperature evolution in a lake.

The model of seasonal temperature evolution in a lake `TeMix` (TEmperature and MIXing) (Mironov *et al.* , 1991) is used here as the basis for development of the current model. The model is also based on two-layered self-similar representation of the temperature profile but make use of empirical temperature profile approximation within the thermocline and does not take into account the vertically distributed absorption of the solar radiation in the water column. We rederive the model equations with account of the new solution paying the particular attention to the entrainment equation derivation with account of volumetric radiation absorption.

The model is tested on lake temperature data for 16 years collected in the Lake Müggelsee. The Lake Müggelsee is located near Berlin, Germany. The comprehensive monitoring have been performed in the lake by the Institute of Water Ecology and Inland Fisheries (IGB) during last 20 years and includes a set of hydrological and meteorological parameters allowing to trace medium-scale variations and long-term trends in thermal regime of the lake.

The model displays a good agreement with observational data allowing us to estimate the validity of underlying approximations for shallow conditions. The comparison of the model performance with turbulence closure models is also performed. Despite the high level of formalization in `TeMix` description of the turbulent mixing processes, the model predicts the vertical temperature profile in a lake quite well and its results are comparable with those given by more sophisticated but computationally more expensive turbulent closure models.

The role of vertically distributed heating in the heat budget of shallow lakes is analyzed based on modeling results and on measurements data from the the Lake Müggelsee. Finally, a special case of radiatively-driven convection in ice-covered lakes is considered in more detail. The phenomenon exists only in fresh-water lakes and provides an excellent example for testing the hypothesis about similarity of turbulence characteristics profiles within the convectively-driven mixed layer.

The study includes following main steps.

- Analysis of thermocline self-similarity concept including overview of previous studies, theoretical analysis of the thermocline's self-similarity and development of improved parameterizations of vertical heat exchange mechanisms.

- Development of a new model scheme based on new parameterizations.

- Analysis of main mechanisms governing the heat exchange in a shallow lake and trends in air-lake interaction based on the Lake Müggelsee data collected in the IGB during 1980-1996. Verification of the current version of the `TeMix` model on these data.

- Application of the bulk mixed layer model to the convection under ice.

1.3 Structure of the thesis

The thesis is divided into the following parts:

- The present chapter, where the problem is formulated and general solution methods are proposed.

- Chapter 2 includes formulation of the self-similarity concept; review of previous studies dedicated to the concept application; solution of the vertical heat transfer equation in dimensionless variables providing the self-similar thermocline representation and comparison of the solution with observational data.

- Chapter 3 contains description of the `TeMix` model. Results achieved in the previous chapter are used here in derivation of the model equations. The entrainment equation is derived accounting for the vertically distributed radiation absorption within the water column.

- Chapter 4 is dedicated to application of the model to the Lake Müggelsee. The model performance is analyzed here by comparison with observations and with results of two-equational k-ϵ model. General characteristics of vertical heat exchange in a shallow lake are discussed here based on modeling results and observational data. The role of the water transparency in heat budget is analyzed and the possible feedback between biological production and water temperature is discussed.

- Chapter 5: The convection in ice-covered lakes is considered here in terms of mixed-layer modeling; general description of the phenomenon is given; previous studies are reviewed; the mixed layer model is developed and tested against data from different lakes; the role of small salt concentration in vertical mixing at temperatures close to the maximum density value is discussed.

- Chapter 6 presents an overview of achieved results. Conclusions are made about adequacy of bulk modeling for shallow lake conditions. Possible practical applications and possible improvements of the model are discussed.

Chapter 2

Self-similarity of the thermocline

2.1 The concept formulation and overview of previous studies

As it was mentioned in the previous chapter, the vertical density distribution in lakes has generally two-layered structure. From the physical point of view, these two layers appear to be outcomes of two main harmonics in external forcing: the seasonal and the diurnal one. Features, specific for all natural water bodies, – positive dependence of water density on temperature and the free upper boundary, – determine the reaction of lakes to these oscillations. On seasonal scales, the downward flux of the solar radiation warms up the upper layers resulting in stable vertical density stratification. The anomalous property of freshwater density should be mentioned here, namely the non-linear dependence of freshwater density on temperature; at temperatures below the maximum density point (about $4°C$) the density decreases with temperature increasing, and heating from above will result in destabilizing the water column. This effect will be considered in more detail in Chapter 5. The most intensive heat exchange takes place in summer at temperatures exceeding the maximum density point and stable seasonal stratification develops in lakes. At the same time, the secondary effect of the heat exchange at the upper boundary with the atmosphere disturbs the stratification. Main components of this exchange include turbulent exchange at the interface, emission and absorption of the long-wave infrared radiation and heat losses due to evaporation. The boundary heat exchange becomes especially important during nighttime periods, when the short-wave radiative flux disappears. The high heat capacity of water determines in this case higher heat content of lakes in comparison to lower layers of the atmosphere and, as a result, intensive heat losses at the surface. It follows in convective boundary layer formation near the lake surface. Additional contribution in mixing near the surface make the velocity stresses and waves breaking driven by winds. Wind and convective mixing has time scales from diurnal to synoptic ones, so the depth of the well-mixed boundary layer varies during the stratification period. It can be schematically represented by time evolution of the depth of the interface between the homogeneous boundary layer and the stratified layer, the thermocline, below it (see Fig. 2.1). The overall vertical structure can be assumed to remain approximately the same, or in other words, to have a *self-similar* structure. This phenomenological, *bulk* representation of physical processes has been widely used in modeling of boundary layers and can be a very effective tool for prediction of macro-characteristics of a physical system without detailed description of microscale interactions inside it. The key condition of successful modeling in this case is the proper choice of physical scales for a process. Bulk modeling of the upper mixed layer (UML) in the Ocean and in lakes has been gained intensive development starting from works of Kitaigorodski (1960) and Kraus & Turner (1967). Here were extend the method on the stratified thermocline layer below the UML in order to achieve a fully parameterized bulk-description of the whole water column from the lake surface to the water-sediments boundary.

The essence of the thermocline's self-similarity idea can be illustrated by following citation from the paper of Munk & Anderson (1948):

> *... the upper layers are stirred until an almost homogeneous layer is formed, bounded beneath by a region of marked temperature gradient, the thermocline. ... If the wind increases in intensity the thermocline moves downward, but the characteristic* ***shape*** *of the temperature-depth curve remains essentially unchanged* (original authors' emphasis).

Self-similar solutions are closely related to the dimensional analysis in physics. In fact, they are different formulations of the same method. Indeed, postulating of self-similarity of a physical process is adequate to a choice of appropriate scaling or, in other words, to introducing of dimensionless co-ordinates. The Monin-Obukhov similarity hypothesis is a famous example of the power of the approach. Another example, which is often not associated in literature with similarity approach directly, is mixed-layer (or bulk) modeling of the upper ocean. The first oceanic mixed layer model (Kitaigorodski, 1960) was namely the application of the Monin-Obukhov theory to the upper ocean. The generalized theory of homogeneous upper ocean layer was developed later by Kraus & Turner (1967). In terms of similarity analysis, the basic assumption of homogeneous boundary layer near the surface corresponds to the choice of this layer's depth h as a scaling variable. Following Barenblatt (1996):

> *A time-dependent phenomenon is called self-similar if the spatial distributions of its properties at different times can be obtained from one another by a similarity transformation.*

In case of the well-mixed UML (see Fig. 2.1), the temperature self-similarity function is:

$$T(z,t) = T_s f(z/h), \tag{2.1}$$

where:

$$T_s = T(0,t); \qquad f(z/h) = 1.$$

The *thermocline* is a layer with strong temperature stratification (the part of the temperature curve between vertical co-ordinates h and D in Fig. 2.1) and typically develops between the highly turbulized UML and the rest non-turbulent fluid. This layer exists in lakes either permanently during the summer until the surface temperature falls to the maximum density value and mixing achieves lake's bottom (so-called *dimictic* lakes) or forms intermittently in shallow lakes alternating with periods of vertical uniformity (*polymictic* lakes). The seasonal thermocline develops also in ocean and has an analog in the atmosphere: the interfacial layer developing during convective entrainment driven by surface heating. In many cases the thermocline tends to have a universal shape, especially at sufficiently large time scales, when the balance of external forces becomes close to the steady state. Evidence of this generality in thermocline's shape argues to the advantage of modeling the thermocline by using the self-similarity idea, analogous to the UML concept. Taking into account the thermocline's structure, it is consistent to adopt the thermocline depth $\Delta h \equiv D - h$ and the temperature jump across it $\Delta T \equiv T_s - T_D$ as universal length and temperature scales (Fig. 2.1). The similarity function can be written then as follows:

$$T(z,t) = \Delta T f(z/\Delta h). \tag{2.2}$$

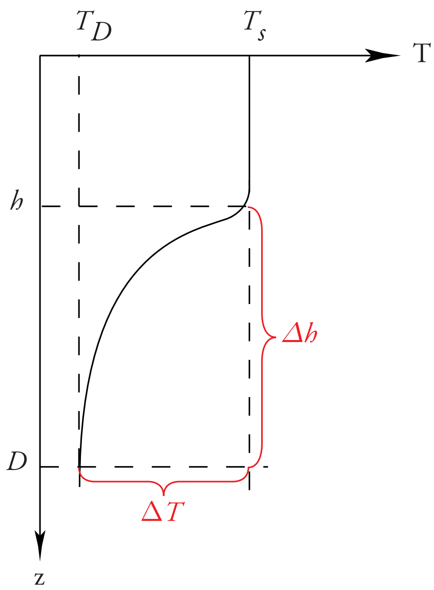

Figure 2.1: The model representation of the vertical temperature profile in a lake.

In this connection, two originating works dedicated to the analysis of the thermocline should be mentioned here. In the paper of Munk & Anderson (1948) a model of the open sea thermocline was developed and tested against oceanic and lake data. Ertel (1954) has proposed an analytical solution of the heat transfer equation describing vertical temperature jump formation and deepening during summer heating in a lake. The similarity transformation (2.2) was not used in both of the papers directly, but some results of their preliminary analysis have found a logical continuation in self-similar theories of the thermocline. Ertel (1954) investigated time evolution of a lake thermocline, which he defined following Birge as a layer with temperature gradient $\geq 1°C$. His analysis has shown (Ertel, 1954, Eq. 58), that the ratio of depth from the upper thermocline's boundary to the bend point $\partial^2 T/\partial z^2$ and that from the bend point to the bottom of the thermocline is constant or, in other words, *the shape of thermocline is independent on time*. The same idea lied in background of the Munk & Anderson (1948) analysis.

The first direct application of the thermocline self-similarity idea to the oceanic active layer was performed by Kitaigorodski & Miropolski (1970). Using the above mentioned scales, the authors introduce dimensionless coordinates,

$$\vartheta = \frac{T_s - T(z)}{\Delta h}; \ \zeta = \frac{z - h}{\Delta h}. \tag{2.3}$$

The variables $\vartheta \in [0; 1]$ and $\zeta \in [0; 1]$ denote here dimensionless temperature and vertical coordinate, respectively.

The explicit expression for the function $\vartheta(\zeta)$ was derived by Kitaigorodski & Miropolski (1970) using Polhausen approach. The approach is widely applied in boundary-layer physics and consist of approximation of a function in question by an $(n-1)$-st order polynomial from n boundary conditions the function must fulfill. The following five boundary conditions were used by the authors:

$$\vartheta\ (0) = 0, \tag{2.4a}$$
$$\vartheta\ (1) = 1, \tag{2.4b}$$
$$\vartheta'\ (1) = 0, \tag{2.4c}$$
$$\vartheta''\ (1) = 0, \tag{2.4d}$$
$$\vartheta'''(0) = 0. \tag{2.4e}$$

Prime denotes here differentiation on ζ.

The conditions (2.4a, 2.4b) follow directly from the self-similarity co-ordinates definition (2.3). The condition (2.4c) relies on the assumption of the vertically uniform temperature distribution below the thermocline, that is close to the reality for deep-water conditions of the open ocean. In this case, the point $\zeta = 1$ is also the bend point (Eq. 2.4d). The last condition (2.4e) means the curvature maximum existence at the upper thermocline's boundary and arises from the thermocline definition given in (Munk & Anderson, 1948). The following 4^{th}-order polynomial fulfills Eqs. (2.4a-2.4e):

$$\vartheta(\zeta) = \frac{8}{3}\zeta - 2\zeta^2 + \frac{1}{3}\zeta^4. \tag{2.5}$$

The representation (2.5) was tested against monthly averaged observational data in (Miropolsky *et al.* , 1970) and the satisfactory agreement was demonstrated for summer heating periods.

The approach had encountered further development in (Arsenyev & Felsenbaum, 1977). Using the same co-ordinates (2.3) and the Polhausen procedure, the authors discarded a validity of the condition (2.4e) and confined the approximating polynomial with 3^{rd} degree, that gives:

$$\vartheta(\zeta) = 1 - (1-\zeta)^3. \tag{2.6}$$

The shape of the function (2.6) differs only slightly from that given by (2.5). The temperature profile representation (2.6) was subsequently widely used in thermocline modeling and have found a theoretical justification as it will be shown below.

The self-similar behavior of the function $\vartheta(\zeta)$ was confirmed by laboratory experiments on turbulent mixing in stratified fluids (Linden, 1975; Wyatt, 1978). Linden (1975) has modified the expression (2.5) for the case of linear stratification in quiescent water under the thermocline in order to describe the situation existing in his experiments [1]:

$$\vartheta(\zeta) = \zeta + [1 - \vartheta'(1)] \left[\frac{5}{3}\zeta - 2\zeta^2 + \frac{1}{3}\zeta^4\right]. \tag{2.7}$$

Analysis of field data shows much more scatter over an universal self-similarity curve than that of laboratory experiments (Miropolsky *et al.* , 1970; Reshetova & Chalikov, 1977). An attempt of extending the self-similarity description by including additional mechanisms of temperature profile formation was performed in (Mälkki & Tamsalu, 1985). The authors classified the temperature profiles observed in the Baltic Sea, based on the regime of the UML formation or destroying. For the mixed layer deepening, the equation (2.6) was adopted. In case of mixed layer decay, a polynomial was built from the assumption of vertical density gradient disappearance at the UML bottom: $\vartheta'(0) = 0$. In couple with conditions (2.4a–2.4d) that gives

$$\vartheta(\zeta) = 1 - 4\,(1-\zeta)^3 + 3\,(1-\zeta)^4\,. \tag{2.8}$$

A plausible theoretical explanation of the observed temperature profile self-similarity in the thermocline was proposed simultaneously and independently by Barenblatt (1978) and Turner (1978). Taking into account that ζ co-ordinate origin is moving along the vertical with the velocity $\dot{h} \equiv \mathrm{d}h/\mathrm{d}t$, the heat transfer equation can be rewritten as

$$\Delta h\dot{\vartheta} - (\dot{h} + \dot{\Delta h})\vartheta' = -\frac{\Delta h}{\Delta T}\frac{\mathrm{d}Q}{\mathrm{d}z}, \tag{2.9}$$

[1] The final formula in the original paper is inconsistent with the reported underlying gradient, apparently on account of a typing error.

where Q is the vertical heat flux, dots over variables $\dot{()}$ denote time differentiation and primes $()'$ are, as before, derivatives regarding to ζ co-ordinate. The first term in (2.9) is of minor magnitude and can be neglected in most of cases (Barenblatt, 1978), leaving us with ordinary differential equation with regard to ζ. Some additional assumptions about the heat flux profile $Q(t,\zeta)$ allow achieving an analytical solution of (2.9). The additional condition of a solution existence is $\dot{h} + \dot{\Delta h} > 0$, i.e. the thermocline should propagate in positive direction, otherwise the equation (2.9) has no stable solution. Solutions of this kind, usually called propagating or traveling wave type solutions, are widely used in different branches of mathematical physics (the introduction of a moving co-ordinate system is nothing but another formulation of physical self-similarity, see e.g. Barenblatt 1996). Both Barenblatt (1978) and Turner (1978) examined the case of infinitely deep ocean, neglecting the term $\dot{\Delta h}$ in (2.9) and using the Fickian type expression for the turbulent heat flux, i.e.

$$-\Delta h \dot{h} \vartheta' = (K\,\vartheta')'. \tag{2.10}$$

The simplest model assumption of constant heat conductivity K was examined in (Barenblatt, 1978) and as a first guess in (Turner, 1978). In case of $K = const$, the solution of (2.10) in co-ordinates (2.3) is

$$\vartheta(\zeta) = \left(1 - \exp\left[-\frac{\dot{h}\Delta h}{K}\,\zeta\right]\right) \Big/ \left(1 - \exp\left[-\frac{\dot{h}\Delta h}{K}\right]\right). \tag{2.11}$$

As one can see, the exact form of the solution (2.11) depends on the dimensionless parameter $\dot{h}\Delta h/K$. An attempt of the parameter estimation based on observational data from ocean weather stations was performed in (Efimov & Tsarenko, 1980)[2]. They found, that the value $\dot{h}/K$ is nearly constant during the summer periods as well as during convective mixed layer deepening in autumn. Values of K in the thermocline, estimated on the data, are sufficiently higher than the molecular value and reach 10^{-4} m^2/s.

An interesting analysis of the traveling thermal wave equation (2.10) in application to the thermocline was performed by Shapiro (1980). In order to take into account oscillations taking place on the lower thermocline border during the UML deepening, the author has applied Reynolds-averaging procedure to the entrainment rate $\dot{h} = \dot{H} + \dot{\widetilde{h}}(t)$, where $\dot{\widetilde{h}}$ denotes small-amplitude fluctuations of the mean entrainment rate $\dot{H}$. After averaging a new source term appears in the equation for the mean temperature (2.10), describing heat redistribution on account of the boundary fluctuations:

$$-\dot{h}\vartheta' = K\vartheta''/\Delta h + \left\langle \dot{\widetilde{h}}\widetilde{\vartheta}\,' \right\rangle. \tag{2.12}$$

An additional equation for temperature fluctuations $\widetilde{\vartheta}$ follows from the Reynolds averaging applied to the heat transfer equation (2.9), and a solution of this equation was achieved in (Shapiro, 1980) in Fourier quadratures, that allowed estimating the role of the last term on the r.h.s. in (2.12) if spectral characteristics of the boundary oscillations are given. Particularly, it was shown that, in an idealized case of single-frequency oscillations of the interface, these oscillations result in overall cooling through the thermocline and in sharpening of the temperature gradient at the UML base, as there were an additional energy sink here.

[2] Barenblatt (1978) made use of co-ordinates $\tilde{z} = z - h$ and $\tilde{T} = (T - T_s)/T_s$ with conditions $\tilde{T}(0) = 1$ and $\tilde{T}(\infty) = 0$ that gave the solution of (2.10) as $\tilde{T} = 1 - \exp(-\dot{h}\tilde{z}/K)$ and resulted in the infinite thermocline depth. In (Efimov & Tsarenko, 1980) this solution was incorrectly transformed into co-ordinates (2.3).

In addition to the case of depth-constant K, Turner (1978) examined one other, more complicated case, $K \propto \mathrm{d}T/\mathrm{d}z$. Using the co-ordinates (2.3), the Turner's expression for K becomes:

$$K = \frac{1}{4}\dot{h}\Delta h \vartheta'. \tag{2.13}$$

Then, the equation (2.10) has the solution:

$$\vartheta(\zeta) = 2\zeta - \zeta^2. \tag{2.14}$$

It worth to be mentioned here, that the same expression was achieved in (Golosov & Kreiman, 1992) from phenomenological considerations in application to vertical thermal wave propagation in lake sediments.

Physical relevance of the vertical heat conductivity representation (2.13) was discussed in (Zilitinkevich *et al.* , 1988; Zilitinkevich & Mironov, 1992). If we assume internal gravity waves breaking to be the main mechanism of turbulence generation in the thermocline, then the mixing intensity should be in direct ratio on stratification and, consequently, on vertical temperature gradient $\mathrm{d}T/\mathrm{d}z$ (in contrast to inverse dependence on density gradient for weakly stable conditions). In any case, an expression for K should include a dependence on the thermal expansion coefficient $\alpha_T = (\partial\varrho/\partial T)_{s,p}$ as well, in order to reflect an influence of temperature stratification on mixing. Based on these considerations, Zilitinkevich *et al.* (1988) have proposed the following formula, derived from dimensional arguments:

$$K = l^2 N. \tag{2.15}$$

Here, $N = \sqrt{g\varrho^{-1}\partial\varrho/\partial z}$ is the Brunt-Väisälä frequency, and l is a length scale. Assuming the water density to be a function of the temperature only, one can write:

$$N^2 = \beta \partial T/\partial z,$$

where $\beta = g\alpha_T$ is the buoyancy parameter, and the solution of (2.10) with conditions (2.4a), (2.4b) and (2.4c) is

$$\vartheta(\zeta) = 1 - (1-\zeta)^3; \qquad \Delta h = 3\sqrt[3]{\beta \Delta T l^4/\dot{h}^2}. \tag{2.16}$$

The expression for ϑ in (2.16) is exactly the same as that achieved before from phenomenological considerations (see Eq.2.6) and verified numerously on field data (Arsenyev & Felsenbaum, 1977; Mälkki & Tamsalu, 1985; Rumiantsev *et al.* , 1986; Tamsalu & Myrberg, 1998). Thus, a theoretical explanation of the observed self-similarity of thermocline profile was found, at least for certain mixing conditions.

An analytical model of the thermocline was built in (Zilitinkevich & Mironov, 1992) invoking the turbulent kinetic energy (TKE) equation in couple with the expression for TKE:

$$b = (lN)^2$$

which follows directly from (2.15) and from the classical formula of the k-l theory of turbulence: $K = l\sqrt{b}$. An additional scaling variable arises in this case describing the TKE scale in the thermocline. The value $b_s \equiv b|_{z=h}$ was chosen as this scale in (Zilitinkevich & Mironov, 1992). The dependence $\vartheta(\zeta, b_s)$ achieved with the model was compared with those from laboratory experiments (Deardorff *et al.* , 1980; Deardorff & Willis, 1982), where direct measurements of turbulent characteristics were available.

An attempt of extending of the self-similarity hypothesis on the vertical heat flux distribution across the thermocline was undertaken in (Tamsalu *et al.* , 1997). Following the same reasoning as that in derivation of Eq. (2.8), two different regimes of heat exchange in the thermocline were distinguished: one existing during the UML deepening ($\dot{h} > 0$) and one other associated with the mixed layer recession ($\dot{h} \leq 0$). As a result, two scales were proposed for the heat flux description: $Q|_{z=h}$ if $\dot{h} > 0$ and $\bar{Q} \equiv 1/\Delta h \int_h^{h+\Delta h} Q(z)\mathrm{d}z$ if $\dot{h} \leq 0$ leading to two polynomial representations of dimensionless vertical flux profiles. These representations were tested against field measurements data in (Tamsalu & Myrberg, 1998) and have shown a reasonable agreement with observations.

Most of the self-similarity functions discussed above assume directly or indirectly a homogeneous vertical temperature distribution in the water column below the thermocline. Nevertheless, stratification in the underlying layers plays an important role in entrainment interface formation during UML deepening. When the assumption of no density gradient in deep layers is traditionally applied in the ocean modeling with more or less success, the problem of stratification account becomes of key value in modeling of the convective boundary layer in the atmosphere. Development of a convective boundary layer (CBL) capped with temperature inversion above during daytime is an atmospheric analog of the UML deepening in the ocean. This process is quite similar also to that appearing in lakes, when nocturnal convection is developed on the background of stable stratification. The self-similarity idea was applied by Fedorovich & Mironov (1995) to modeling of CBL with account of temperature gradient in inversion layer. The authors implement the co-ordinates (2.3) but define, the upper boundary of interfacial layer (IL) h following Deardorff (1979) as the point where the temperature (buoyancy) flux changes it's sign ($\mathrm{d}Q/\mathrm{d}z = 0$). This condition means also density homogeneity in the lower part of the IL (at the top of the thermocline in the ocean case): $\vartheta'(0) = 0$, and differs from the common UML definition. The last condition was combined with (2.4a), (2.4b) and with the empirical expression derived by Deardorff (1979):

$$C_b = \int_0^1 \vartheta(\zeta)\mathrm{d}\zeta = \mathrm{A}\exp\left(\alpha\Gamma\right), \tag{2.17}$$

where $\Gamma \equiv \vartheta'(1)$, A= 0.55 and $\alpha = -0.27$. The Polhausen method was then applied in order to achieve the function $\vartheta(\zeta,\Gamma)$ in form of a 4$^{\mathrm{th}}$ order polynomial:

$$\vartheta(\zeta,\Gamma) = \left(\frac{3}{2}\Gamma - 12 + 30C_b\right)\zeta^2 + (28 - 4\Gamma - 60C_b)\zeta^3 + \left(\frac{5}{2}\Gamma - 15 + 30C_b\right)\zeta^4. \tag{2.18}$$

The one-dimensional lake model `TeMix` is an example of implementation of the self-similarity approach in applied modeling (Zilitinkevich & Rumyantsev, 1990; Mironov *et al.* , 1991; Zilitinkevich *et al.* , 1992). In the model the two asymptotic polynomials were adopted (see Eqs. 2.6 and 2.8):

$$\vartheta(\zeta) = \begin{cases} 1 - (1-\zeta)^3 & \text{if} \quad \dot{h} > 0 \\ 1 - 4(1-\zeta)^3 + 3(1-\zeta)^4 & \text{if} \quad \dot{h} \leq 0 \end{cases}, \tag{2.19}$$

The exact shape of the temperature profile is assumed in the model to slip between the two asymptotical bounds, that is parameterized by introducing a characteristic time scale

$$t_* = \Delta h^2[(C_l h)^2 N]^{-1},$$

where C_l is an dimensionless constant (cf. Eq.2.15), and a simple time relaxation formula:

$$(C_T - C_T^0)/(C_T^* - C_T^0) = (t - t^0)/t_*. \tag{2.20}$$

Here, $C_T \equiv \int_0^1 \vartheta(\zeta)\mathrm{d}\zeta$ is the so-called integral shape factor (cf. Eq.2.17). A superscript 0 means values at the moment of the last $\dot{h}$ sign change. C_T^* is the asymptotical value, which depends on the current sign of $\dot{h}$ as it defined by (2.19). Together with the conditions (2.4a)-(2.4d) that leads to the 4$^{\mathrm{th}}$ order polynomial:

$$\vartheta(\zeta) = (15 - 20C_T)\zeta^4 - (44 - 60C_T)\zeta^3 + (42 - 60C_T)\zeta^2 - (12 - 20C_T)\zeta. \tag{2.21}$$

The model was numerously applied to the simulation of the seasonal cycle of temperature and mixing in large (Rumiantsev *et al.* , 1986; Zilitinkevich, 1991) and medium-depth lakes (Zilitinkevich & Rumyantsev, 1990; Mironov *et al.* , 1991; Zilitinkevich *et al.* , 1992).

Thus, a description of the thermocline in terms of self-similarity variables could be a versatile and inexpensive tool in geophysical modeling. In the background of self-similarity assumption lies the physically sound representation of the thermocline as a downward propagating thermal wave. It provides the generality of the description in application to various natural examples of entrainment in stratified media: seasonal thermocline formation in lakes and the ocean, convective boundary layer development in the atmosphere.

At the same time, a dependence of the density profile in the thermocline on the background stratification in adjoining layers has no adequate description yet. This dependence is crucial for the thermocline formation in many cases, as that of convection in the atmosphere, where stably stratified inversion layer bounds the interfacial layer from above. In addition, strong gradients in the bottom layer caused by the heat flux from the sediments can influence the diurnal thermocline formation in shallow lakes.

2.2 Heat transfer equation for downward propagating heat wave

As it was mentioned in section 2.1, a theoretical explanation of thermocline's self-similarity can be given in terms of so-called traveling (or propagating) wave type solution of the heat transfer equation . Here some possible solutions of such equation are considered, corresponding to idealized conditions which can be however applied to many real situations.

The heat transfer equation (HTE) in one-dimensional form can be written as

$$\frac{\partial T}{\partial t} = -\frac{\partial Q}{\partial z} \tag{2.22}$$

where T is the temperature, Q is the kinematic heat flux, t and z are time and space co-ordinates correspondingly.

The idea of the propagating wave representation of HTE consist in a co-ordinates transformation allowing reducing the partial differential equation (2.22) to an ordinary differential equation with regard to a new co-ordinate $\zeta(t, z)$.

Rewriting the equation (2.22) in co-ordinates (2.3) one gets:

$$\frac{\mathrm{d}T_s}{\mathrm{d}t}(1-\vartheta) + \frac{\mathrm{d}T_D}{\mathrm{d}t}\vartheta - \frac{\mathrm{d}\vartheta}{\mathrm{d}\zeta}\frac{\Delta T}{\Delta h}\left[\frac{\mathrm{d}h}{\mathrm{d}t}(1-\zeta) + \frac{\mathrm{d}D}{\mathrm{d}t}\zeta\right] = -\frac{1}{\Delta h}\frac{\mathrm{d}Q}{\mathrm{d}\zeta}$$

or, using notation introduced in the previous section:

$$\frac{\mathrm{d}T_s}{\mathrm{d}t} - \frac{\mathrm{d}\Delta T}{\mathrm{d}t}\vartheta - \vartheta' \frac{\Delta T}{\Delta h}\left[\dot{h} - \frac{\mathrm{d}\Delta h}{\mathrm{d}t}\zeta\right] = -\frac{1}{\Delta h}Q' \tag{2.23}$$

The derivatives regarding to t and ζ are split in equation (2.23). Thereafter, the equation can be solved as an ordinary differential equation with regard to ζ, if the functions $\mathrm{d}T_s/\mathrm{d}t$, $\mathrm{d}T_D/\mathrm{d}t$, $\mathrm{d}h/\mathrm{d}t$ and $\mathrm{d}D/\mathrm{d}t$ are known. The first two of those derivatives are usually assumed to be negligible when investigating turbulent entrainment in geophysical boundary layers. Deepening of the upper mixed layer base $\mathrm{d}h/\mathrm{d}t$ and that of the interfacial layer bottom $\mathrm{d}D/\mathrm{d}t$ can be parameterized in two different ways depending on real situation to be modeled. For the ocean, the assumption of infinitely deep basin is often applied. Then, it is consistent to treat the thickness of the thermocline Δh to be constant in time, or $\mathrm{d}h/\mathrm{d}t = \mathrm{d}D/\mathrm{d}t$.

In this case, equation (2.23) takes the simple form:

$$\Delta T \dot{h} \vartheta' = Q' \tag{2.24}$$

It follows directly from (2.24) that the vertical heat flux profile in the thermocline has the same shape as the temperature curve. The assumption of similarity of the temperature and heat flux profiles was used by Zilitinkevich *et al.* (1988); Zilitinkevich & Mironov (1992) for modeling thermocline formation in lakes.

The other possible simplification, agreeing well with many natural situations, is that the position of the thermocline's lower boundary is fixed, i.e. $\mathrm{d}D/\mathrm{d}t = 0$. It gives when combined with (2.23):

$$\Delta T(1-\zeta)\dot{h}\vartheta' = Q' \tag{2.25}$$

Indeed, if stratification below the thermocline is strong, the deepening of the lower thermocline border is arrested by density gradient and becomes much slower than the entrainment velocity d*h*/d*t*. In this case, $\mathrm{d}\Delta h/\mathrm{d}t \approx \mathrm{d}h/\mathrm{d}t$ and the expression (2.25) is valid. In particular, this approximation was used in the model of the thermocline proposed by Tamsalu *et al.* (1997). The situation becomes exactly true in shallow lakes and reservoirs, where the non-turbulent quiescent layer does not exist so that seasonal thermocline extends from the lower edge of the mixed layer down to the basin's bottom.

If we suppose thermocline's bottom deepening to be arrested by underlying stratification, it is necessary to take this stratification into account when parameterizing the temperature distribution inside the thermocline. As it was already mentioned in the previous chapter, it can be made by including the dimensionless temperature gradient Γ below the IL into governing parameters of the problem (see Eq. 2.17). The gradient Γ is defined as:

$$\Gamma = \frac{\Delta h}{\Delta T}\left(\frac{\partial T}{\partial z}\right)_{z=D} \tag{2.26}$$

The temperature curve inside the thermocline changes its shape depending on Γ. We do not stipulate *a priori* an exact form of this dependence. A proposition can be made that in case $\Gamma = 0$ the shape of the curve $\vartheta(\zeta)$ should be close to that, given by previous parameterizations (2.5, 2.6, 2.16). Increasing of Γ should result in collapsing of the IL (see Fig. 2.2), i.e. in decreasing of the integral shape factor $\int_0^1 \vartheta(\zeta)\mathrm{d}\zeta$ (see e.g., Deardorff, 1979). For the asymptotic case $\Gamma \to \infty$

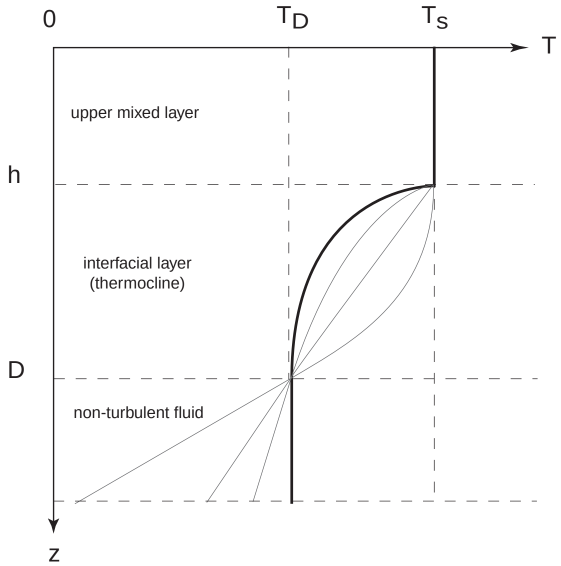

Figure 2.2: Sketch illustrating dependence of the temperature distribution in the thermocline on stratification in non-turbulent fluid.

we can postulate then, $\int_0^1 \vartheta(\zeta)\mathrm{d}\zeta \to 0$ that means collapsing of the IL to a temperature jump at $\Gamma \to \infty$ (see Fig. 2.2). This is the only additional condition we introduce for description of $\vartheta(\Gamma)$ dependence.

Considering the physical mechanism of turbulent entrainment into a stratified fluid, the average gradient through the non-turbulent quiescent layer $\left(\frac{\overline{\partial T}}{\partial z}\right)_{z>D}$ should be used rather than the temperature gradient just below the thermocline. The influence of the stratification displays itself in this case through generation of internal waves, which intensity is proportional, in its turn, to the average squared Brunt-Väisälä frequency $\overline{N^2}$ and consequently, to the average temperature gradient (see e.g., Thorpe 1973). Avoiding redundant complication, we can assume the temperature below the thermocline to develop linearly regarding to depth, in which case both gradients are coincident.

None of the parameterizations $\vartheta(\zeta)$ cited in section 2.1 describes adequately the thermocline behavior in the whole range of Γ variability. Moreover, when using polynomial approximation of temperature profile as it is done in Polhausen approach, it is impossible to reproduce collapse of the thermocline at infinitely growing Γ. Below, a parameterization based on self-similar exponential temperature profile is proposed and possible theoretical explanation of the self-similarity is discussed.

The following conditions have to be satisfied in order to represent the real situation with account of underlying stratification:

$$\vartheta = 0 \,\mathrm{at}\, \zeta = 0; \quad \vartheta = 1 \,\mathrm{at}\, \zeta = 1; \quad \frac{d\vartheta}{d\zeta} = \Gamma \,\mathrm{at}\, \zeta = 1; \quad \int_0^1 \vartheta \to 0 \,\mathrm{at}\, \Gamma \to \infty. \tag{2.27}$$

The first two conditions follow directly from the dimensionless co-ordinates definition (2.3). The second pair expresses the dependence on underlying stability, where the last condition reproduces the behavior of the integral shape function in the asymptotic case of two-layered fluid. We search the function $\vartheta(\zeta, \Gamma)$ in form $\vartheta = \zeta \cdot f(\zeta, \Gamma)$, satisfying the first two conditions automatically. Analyzing the second two conditions, the function in question can be written as:

$$\boxed{\vartheta = \zeta \mathrm{e}^{(\zeta-1)(\Gamma-1)}}. \tag{2.28}$$

According to (2.28), the infinitely increasing underlying stability Γ will lead to degeneracy of the interfacial layer down to the density jump at its lower border. In the second asymptotical case $\Gamma = 0$, the expression (2.28) reduces to

$$\boxed{\vartheta = \zeta \mathrm{e}^{1-\zeta}}. \tag{2.29}$$

The shape of dimensionless temperature profile is very close in this case to those found previously using Polhausen method (Eqs. 2.5, 2.6) as it can be seen in Fig. 2.3. The case of $\Gamma = 1/5$ is also shown in the figure in comparison with the function (2.7) achieved by Linden (1975) from laboratory modeling.

Thus, we can state that the solution adequately describes the entrainment interface between two non-stratified layers, the situation, most often modeled and approximating many real physical situations.

In case $\Gamma = 1$ the solution diminishes to the linear temperature profile within IL $\vartheta = \zeta$ with the gradient equal to that in non-turbulent underlayer. It is the simplest temperature profile corresponding the condition $\int_0^1 \vartheta(\zeta)\mathrm{d}\zeta = 1/2$ and coincides to the temperature profile in the idealized case of non-penetrative convection, so-called "encroachment" regime (Zubov, 1943). It should be mentioned, however, that the co-ordinates ζ and ϑ are not relevant in case of encroachment (which regime is also physically impossible), since there is no IL in this case at all, and scales Δh and ΔT are undefined. The impossibility of a thermocline existence with $\Gamma = 1$ is expressed in the solution by indefiniteness of the heat flux within the IL, which expression is derived below (2.32) and leads to division by zero in case $\Gamma = 1$. Further increasing of Γ results in concave shape of the temperature profile within the IL, which also observed in real situation of entrainment in strongly stratified fluids as it will be shown in the Section 2.3. At very high Γ the profile will degenerate to a temperature jump at the IL bottom. From physical point of view, the depth of IL Δh should also decrease with Γ increasing, so we arrive at asymptotic case of a temperature jump ΔT in a layer of zero depth, – an approximation widely used in modeling the turbulent entrainment in stratified fluids (so-called "zero-jump" approximation).

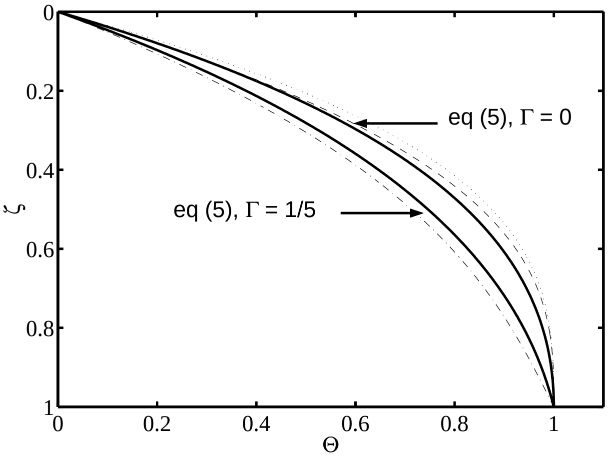

Figure 2.3: Dimensionless temperature profile; thick solid line – as it given by (2.29), thin lines – previously used approximations: dashed line – $\Gamma = 0$, $\vartheta = 8/3\zeta - 2\zeta^2 + \zeta^4/3$ (Kitaigorodski and Miropolski 1970); dotted line – $\Gamma = 0$, $\vartheta = 1-(1-\zeta)^3$ (Arsenyev and Felsenbaum 1977); dash-dotted line – $\Gamma = 1/5$, $\vartheta = 2\zeta - 6/5\zeta^2 + 1/5\zeta^4$ (Linden, 1975)

The formula can be achieved from the heat transfer equation in the following way. Assuming linear dependence of the water density on temperature, equation (2.9) can be rewritten in terms of buoyancy

$$b = -g(\varrho - \varrho_0)/\varrho_0, \tag{2.30}$$

where $g = 9.81$ m/s^2 is the gravity acceleration and ϱ_0 is the reference density.

Taking into account aforementioned simplifications, equation in the co-ordinates (2.3) takes the form:

$$(\zeta - 1)\frac{\mathrm{d}\vartheta}{\mathrm{d}\zeta} = \frac{\mathrm{d}\Phi}{\mathrm{d}\zeta}. \tag{2.31}$$

Here $\Phi = \langle b'w' \rangle / (\Delta b \mathrm{d}h/\mathrm{d}t)$ is the dimensionless buoyancy flux. The buoyancy flux profile corresponding to the solution of the ordinary differential equation can be found as:

$$\Phi = \frac{2-\Gamma}{(\Gamma-1)^2} + \frac{\mathrm{d}\vartheta/\mathrm{d}\zeta}{(\Gamma-1)^2}\left[1 + \zeta\Gamma - \zeta - \frac{\zeta\left(\Gamma^2+\Gamma-2\right)}{1+\zeta\Gamma-\zeta}\right], \tag{2.32}$$

which expression reduces in case of $\Gamma = 0$ to:

$$\Phi = 2 - \frac{\mathrm{d}\vartheta}{\mathrm{d}\zeta}\left(\zeta^2+1\right)/(\zeta-1). \tag{2.33}$$

Reverting to dimensional variables, one gets (the co-ordinates origin is moved to the upper thermocline boundary h, excluding D from the equation):

$$\langle b'w' \rangle = (\Delta h - z)^{-1}\frac{\mathrm{d}h}{\mathrm{d}t}\left[2\Delta b(\Delta h - z) + N^2(\Delta h^2 + z^2)\right], \tag{2.34}$$

where N^2 is the squared Brunt-Väisälä frequency:

$$N^2 = \frac{1}{b_0}\frac{\mathrm{d}b(z)}{\mathrm{d}z}.$$

The expression in square brackets of (2.34) is the potential energy on the level z. The same expression for the potential energy in IL was derived by Kantha (1977) from dimensional considerations when investigating internal wave generation during thermocline deepening.

The expression (2.34) clarifies the physical meaning of the self-similar buoyancy flux profile. According to it, the turbulent buoyancy flux at the depth *z* is equal to time changing of potential energy at *z* due to "compression" of the thermocline with the buoyancy jump across it being constant. In Fig. 2.4 dimensionless profiles of buoyancy (or temperature), buoyancy flux and

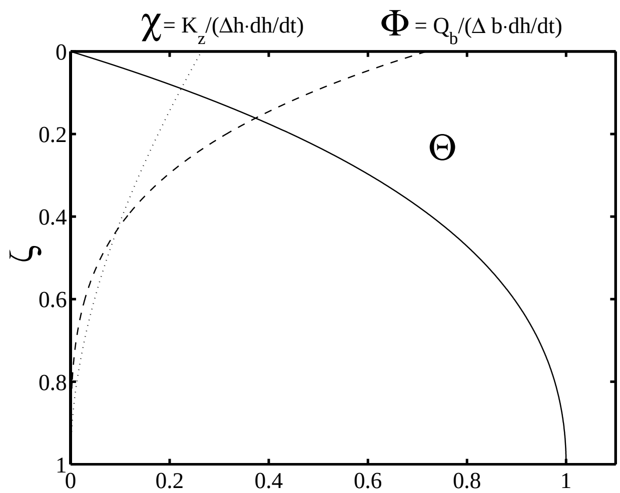

Figure 2.4: Vertical profiles of dimensionless temperature ϑ, heat (or buoyancy) flux Φ and vertical diffusivity χ corresponding the self-similar representation (2.29, 2.33).

diffusion coefficient $\chi = \Phi\left(\mathrm{d}\vartheta/\mathrm{d}\zeta\right)^{-1}$, are drawn. The profiles reveal the typical features of turbulent entrainment in stratified fluid.

The fact that the present entrainment model accounts for stratification in the entrained fluid, extends its applicability on a wider spectrum of geophysical processes. In couple with the assumption of fully-mixed upper layer, the parameterization describes vertical distribution of main physical characteristics across the whole turbulized fluid column, that can serve as a basis for a one-dimensional model of temperature evolution in a lake or in surface layers of the ocean and the atmosphere.

The reliability of the proposed parameterization for various geophysical situations is demonstrated in the following section. Spatial scales vary there from few meters in shallow lakes to tens of kilometers in the atmosphere of Mars allowing us to verify the validity of the proposed scaling.

2.3 Thermocline Development in Natural Conditions. Comparison with the Proposed Model

While the information about temperature distribution is easy available, direct measurements of vertical heat flux in the thermocline are difficult to perform. In natural conditions such measurements are often influenced by essentially three-dimensional small-scale processes, which disagree with one-dimensional assumption used here. The disagreement does not mean an inconsistency of the one-dimensional approach; the approach is regarded as the asymptotical solution, the real distributions tends to at larger time scales. In following, heat flux profiles are estimated, where possible, from available information using some simplifications.

2.3.1 Oceanic upper layer

Development of the seasonal thermocline in the ocean was numerously investigated, in particular with application of the thermocline self-similarity hypothesis. Field data on vertical temperature distribution in upper ocean layers were analyzed in terms of co-ordinates (2.3) e.g. in (Miropolsky *et al.* , 1970; Reshetova & Chalikov, 1977; Efimov & Tsarenko, 1980). Observations data were compared with parameterizations (2.5), (2.6) which in their turn are very close to the function given by (2.29) with $\Gamma = 0$. The comparison had shown good agreement between observed and modeled profiles. Since the conclusion can be extended on the present model, the analysis is not replicated here and can be found in the cited papers. It should be only mentioned, that all authors cited here used data collected in the central Pacific, where the main thermocline does not exist, i.e. there is no temperature gradient below the seasonal thermocline. In these conditions no examination can be made about Γ influence on the shape of temperature profile in the interfacial layer.

Measurements in the central part of the Baltic Sea were used by Tamsalu & Myrberg (1998) for testing the self-similarity approach in application to the thermocline problem. The temperature structure is very similar here to that observed in the open ocean (Fig. 2.5, left panel). The temperature gradient at the thermocline's bottom is also absent here, and, not surprisingly, the temperature structure agrees well with the parameterization (2.29). In addition to the temperature data, the authors report the vertical heat flux estimations based on CTD (conductivity-temperature-depth) measurements. The values are reported in dimensionless form based on the same co-ordinates (2.3), but no estimations of the entrainment velocity$\dot{h}$ is given as well as no dimensional values of the heat flux are reported, that does not allow us to evaluate the relation $\dot{h}\Delta T/Q(h)$. Therefore, the expression (2.33) is re-scaled with regard to the surface heat flux

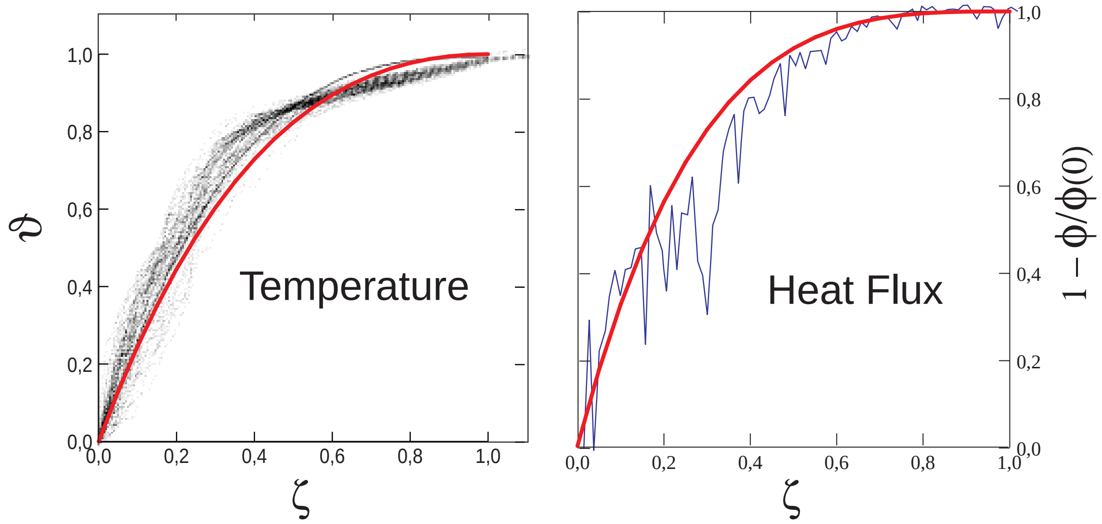

Figure 2.5: Dimensionless profiles of water temperature (left) and vertical heat flux (right) in Baltic Sea. The figure is adapted from (Tamsalu and Myrberg 1998). Model representations (2.29), (2.33) are drawn over the measured profiles (red lines)

$Q(h)$ in order to be adequate to the scaling used in the cited paper. The estimations agrees fairly good with the heat flux parameterization (2.33), as it is demonstrated in the right panel of Fig. 2.5.

2.3.2 Data from laboratory experiments

The only example, where direct heat flux measurements were made in conditions close to one-dimensional, is laboratory modeling of turbulent entrainment. The heat flux representation was tested against results of laboratory modeling on entrainment in stratified fluid (Deardorff, 1979). The profiles for different underlying stratification are drawn in Fig. 2.6 in terms of dimensionless variables ζ and Φ. The accordance with experimental data is rather quantitative. Nonetheless, in case of neutral stratification under the interfacial layer (case E1 in Fig. 2.6), the solution predicts well the value of buoyancy flux at the top of thermocline as $-[\exp(1)-2]\,\Delta b\;\mathrm{d}h/\mathrm{d}t$. Uncertainties in heat flux estimation appearing in other cases could result from the fact that the measured values are taken at the initial stage of the experiment, when entrainment process has not stationary nature. In this case, the 1st term in the equation cannot be neglected and the assumption about fixedness of the lower pycnocline border is not valid.

2.3.3 Atmospheric convective boundary layer

The density structure of the surface boundary layer in the atmosphere is very similar to that of the oceanic upper layer. Solar heating of the surface results in convection, which develops on background of stable temperature stratification formed during night cooling. Hence the process has diurnal time scale in contrast to seasonal scales in the ocean and to the synoptic ones in shallow lakes. The spatial dimensions of the convective layer are about several kilometers, that is much larger in its turn than in water. Another distinctive feature of the convection in the atmosphere is existence of the stably stratified inversion layer capping the CBL from above. As long as the convection entrains the air from above, the interfacial layer between the CBL and the

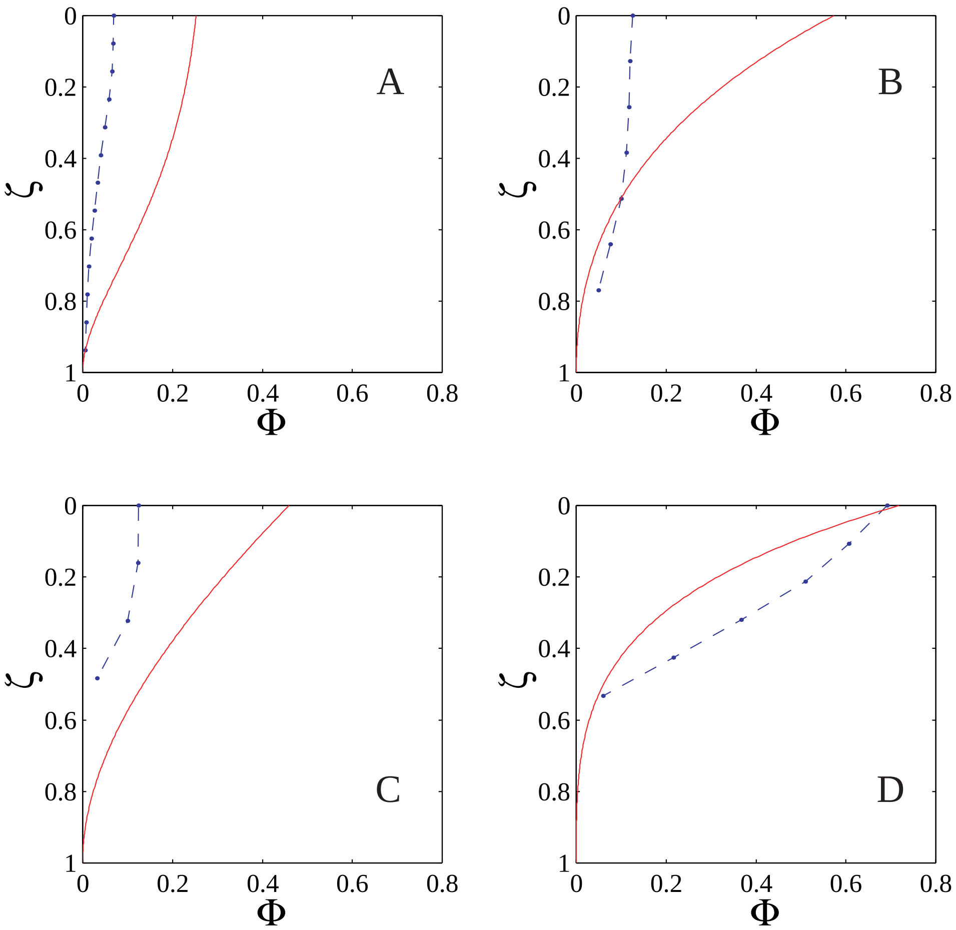

Figure 2.6: Dimensionless heat flux distribution within the pycnocline based on data from laboratory experiments of Deardorff (1979). Dashed lines with dots are measured values, solid lines are buoyancy flux profiles as they found from (2.32). Four plots present cases with different stratification under the entrainment layer Γ. Plot **A**: $\Gamma = 3.5$ (case A3 in the Deardorrf paper); plot **B**: $\Gamma = 0.6$ (case B3); plot **C**: $\Gamma = 1.3$ (case C3); plot **D**: $\Gamma = 0$ (case E1).

inversion layer is formed, similar to the thermocline in the ocean. Unlike the seasonal thermocline, a density gradient always exists at the boundary between the IL and the inversion layer, i.e. Γ differs substantially from zero. A number of parameterized models for the atmospheric CBL were proposed. The IL is parameterized in these models usually as a zero-order temperature jump (Lilly, 1968) or by using of linear approximation of the real temperature profile (e.g. Betts 1974; Gryning & Batchvarova 1994). A polynomial approximation of the temperature structure in the IL was proposed by (Fedorovich & Mironov, 1995) and is described above in section 2.1 (Eq. 2.18). However, the approximation is unable to describe the temperature distribution at high values of the Γ (it produces negative values of the dimensionless temperature ϑ, which are unrealistic from physical point of view: the density inside the IL cannot be higher than in the fluid below).

The solution (2.28), (2.32) describes adequately the IL behavior in the whole range of Γ variability and can be directly applied to modeling of the atmospheric entrainment layer. In order to demonstrate it, the solution is compared with data from radiosonde air temperature measurements. The data were collected during the First International ISLSCP Field Experiment (FIFE) (Strebel *et al.* , 1994).

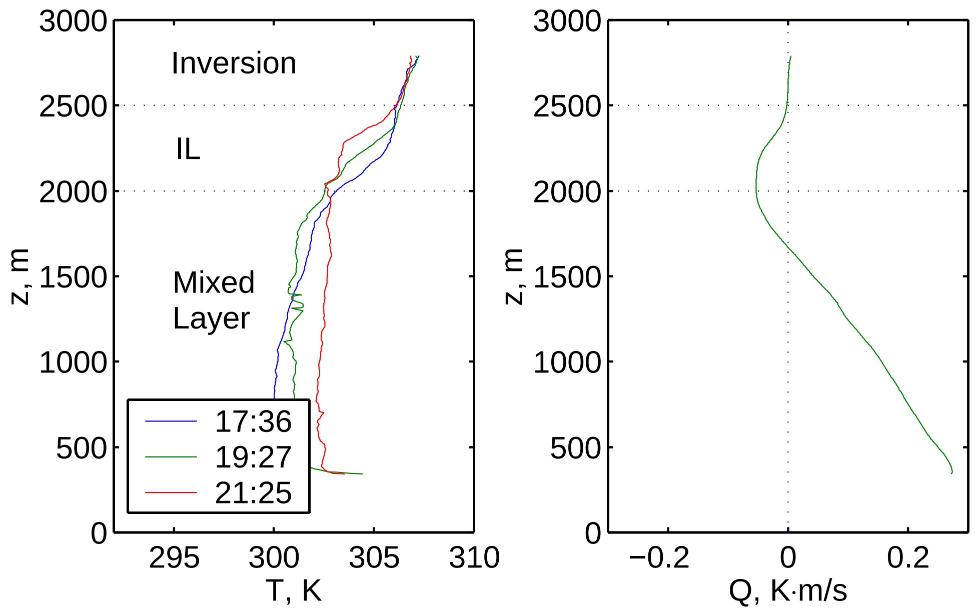

Figure 2.7: Radiosonde data collected during FIFE Experiment, 11 Aug. 1989. **Left panel:** Three potential temperature profiles in late afternoon; **right panel:** averaged upward temperature flux estimated from the air temperature time evolution.

Profiles of potential temperature in the atmosphere were measured by means of intensive radiosoundings conducted in northeastern Kansas in the late summer 1989. The profiles are shown in the left panel of Fig. 2.7, representing the convective boundary layer structure at the end of daytime heating. They reveal the typical structure of the CBL with well-developed mixed layer at the surface and the stable inversion layer above. The interfacial layer developing at the top of mixed layer is about 500 m. deep and has the structure similar to the oceanic thermocline. The vertical heat flux estimation (right panel in Fig. 2.7) is made on the basis of 1-dimensional equation (2.22) using successive temperature profiles for calculating the flux divergence and assuming the turbulent flux to be zero above the IL (Chorley *et al.* , 1975).

When scaled using co-ordinates (2.3) with account of the average temperature gradient in the inversion layer (Fig. 2.8), the temperature and heat flux profiles agree fairly well with the parameterized solution (2.28) and (2.32). The slight disagreement between the observed and modeled shapes of the heat flux profile can be referred to uncertainties in the flux estimation method from temperature profiles.

Nevertheless, the theory gives the correct value of Φ at the top of the IL (at $\zeta = 0$) and describes the overall structure of the heat flux inside the IL. It allows us to draw the conclusion about adequacy of the present model in application to the atmospheric CBL description and, more commonly, about generality of the scales ζ, ϑ and Γ for 1-dim description of turbulent entrainment in stratified media.

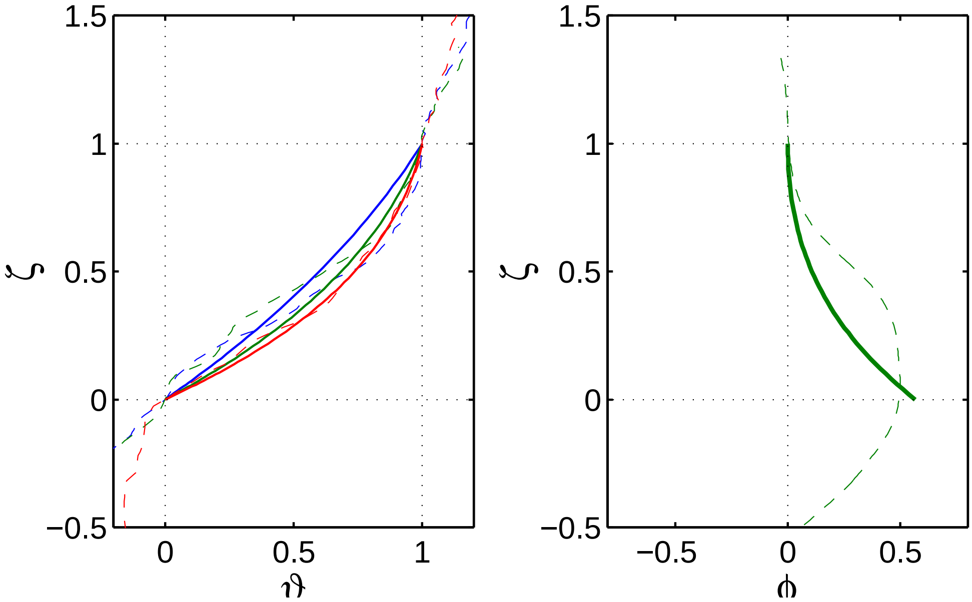

Figure 2.8: **Left panel**: dimensionless representation of air temperature; **right panel**: heat flux in IL. Dashed lines are observational data from Fig. 2.7, solid lines represent corresponding model profiles calculated with Eqs. (2.28), (2.32).

2.3.4 CBL in the Mars atmosphere

An interesting example of the interfacial layer formation, illustrating versatility of the achieved solution, show data of the Mars atmosphere sounding acquired during the Mars Global Surveyor experiment (MGS) (Hinson *et al.* , 1999). The daytime boundary layer developing above the Mars surface is very similar to that existing in the Earth atmosphere but has different temperature and spatial scales. Potential temperature profiles typical for the Mars atmosphere are shown in Fig. 2.9. A strong stable stratification develops here during the night, which stratification

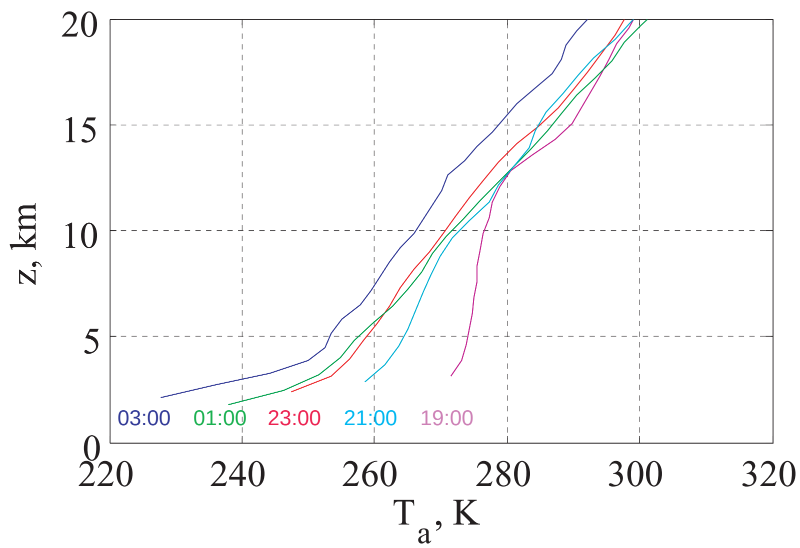

Figure 2.9: Potential temperature profiles over the Mars surface in early summer 1998 at mid-latitudes (southern hemisphere). MGS data from the NASA's planetary data system.

achieves the surface (03:00 curve in Fig. 2.9), while daytime surface heating forms convectively mixed layer analogous to the CBL in the Earth atmosphere, but more than 10 km. deep (19:00 curve in Fig. 2.9). Time scale of this process is the local day, which is close in duration to the

Earth day (24 hours 38 min). A distinctive feature of this layer is the strongly stratified inversion

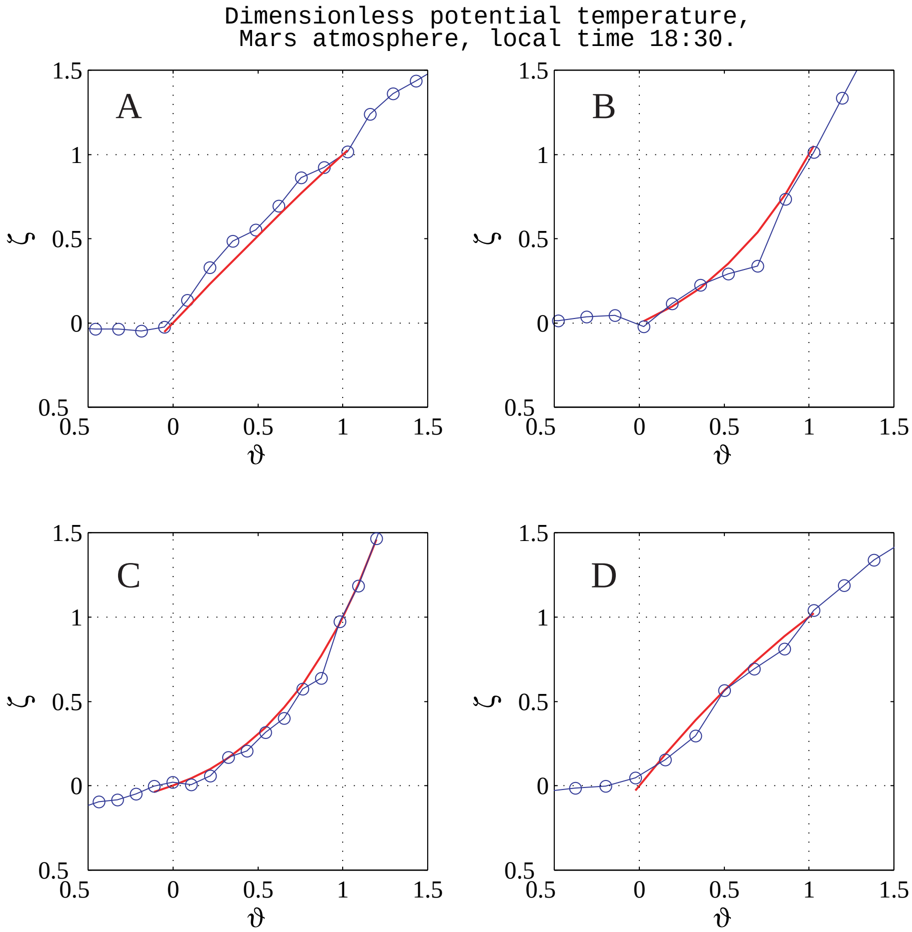

Figure 2.10: Dimensionless potential temperature profiles in the lower part of the Mars atmosphere. Data collected during summer months by MGS. Local time 18:00–19:00. Four plots present cases with different mean temperature gradients over the entrainment layer Γ. Red lines are profiles calculated with (2.28)

layer adjoining the well-mixed boundary layer from above. The vertical temperature gradient in this layer varies with latitude and is usually much higher than the gradient in the inversion layer of the Earth atmosphere. The shape of the temperature profile in the interfacial layer ϑ depends strongly on this gradient and cannot be described by any function of the co-ordinate ζ only. This variety of the IL structure is demonstrated in Fig. 2.10, where the sounding data are presented in the dimensionless co-ordinates (2.3). The four temperature profiles were achieved in the same evening hours, when the CBL is fully developed, but they differ noticeably in their structure. However, if one takes into account the stratification above the IL and includes it in form of the dimensionless gradient Γ into equation (2.28), the agreement between the observed profiles and the proposed parameterization (red solid curves in Fig. 2.10) becomes decisive.

Among all examples of the mixed layer development in natural conditions, the CBL of the Mars atmosphere has the largest spatial scales and the strongest background temperature gradients. The fact, that the equation (2.28) reproduces it structure adequately, argues the solution to be quasi-universal for one-dimensional thermocline modeling.

2.3.5 The thermocline in fresh-water lakes

The seasonal thermocline in lakes has similar structure and formation mechanisms as that in the ocean. In many cases, there is no observable stratification in the non-turbulent layer below the thermocline, that allowed many investigators to apply directly polynomial approximations similar to (2.6) to its modeling (see e.g. Mironov *et al.* 1991; Golosov & Kirillin 2000). It suggests the present model in zero-gradient form (Eq. 2.29) also to simulate the thermocline structure in the right way. Temperature measurements in dimictic lakes support this suggestion. Figure 2.11 demonstrates data of such measurements in four North-American lakes presented in

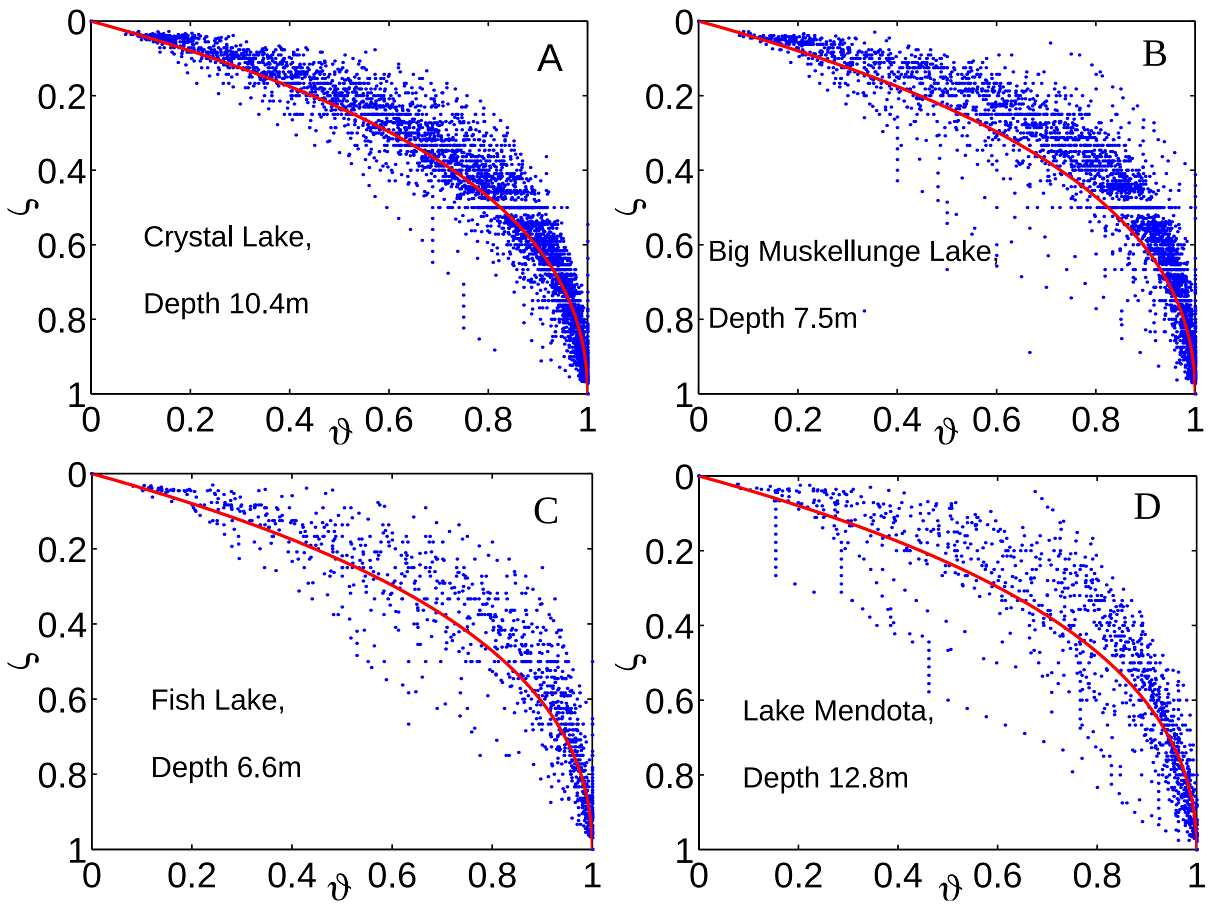

Figure 2.11: Dimensionless temperature profiles in the thermocline in four North-American lakes. **Panel A**: Crystal Lake (89°37′W 46°00′N); **panel B**: Big Muskellunge Lake (89°37′W 46°01′N); **panel C**: Fish Lake (89°39′W 43°17′N); **panel D**: Lake Mendota (89°24′W 43°06′N). Mean depths are given in the figures. The thermocline base was determined as the depth, where $\partial T/\partial z = 0$.

non-dimensional form according to (2.3).

The *essence* of self-similarity idea consist in universality of the temperature profile in dimensionless co-ordinates. Hence, all measurement points should group around the self-similarity curve, independent on the real temperature profiles. The figure demonstrates this fact, where data points, collected during more than 20 years, delineate the curve very close in shape to that given by Eq. (2.29). The data were collected by the North Temperate Lakes site of the Long Term Ecological Research Network (LTER, `http://lternet.edu/`). All lakes are dimictic, i.e. seasonal thermocline exists here during the whole summer heating period between spring and autumn overturns. As the temperature gradient below the thermocline vanishes, all profiles tend to collapse at one universal curve, which curve is very close to that given by Eq. (2.29). The agreement of observed temperature profiles with the parameterization is better for deeper lakes, (Crystal Lake panel A in 2.11 and Big Miskellunge Lake, panel B), though profiles in the Lake Mendota have less universal shape. The apparent explanation for that, is the horizontal inhomogeneity. The Lake Mendota has the largest surface area (3938 Ha) and highly developed shoreline. For comparison, the Crystal lake with similar mean depth has the surface area of 36.7 Ha and low shoreline development, providing horizontal homogeneity and consequently, the good agreement with the theory.

2.3.6 A polymictic lake – the Lake Müggelsee

Series of vertical temperature distribution measurements were performed during the summer 2000 in the Lake Müggelsee located near Berlin, Germany. The observations data were processed in terms of co-ordinates (2.3) (Kirillin, 2001b). In many typical situations, bottom boundary mixing destroys the vertical temperature gradient below the thermocline and the temperature profile agrees well with that, given by (2.28). In case of significant stratification at the bottom, the formula reproduces the temperature profile deformation fairly good (Fig. 2.12, left). The representativity of the expression is demonstrated by the dependence of the integral shape factor $C_b = \int_0^1 \vartheta \mathrm{d}\zeta$ on the background stratification Γ (Fig. 2.12, right), which dependence is adequately described by the solution in the whole range of the Γ variability.

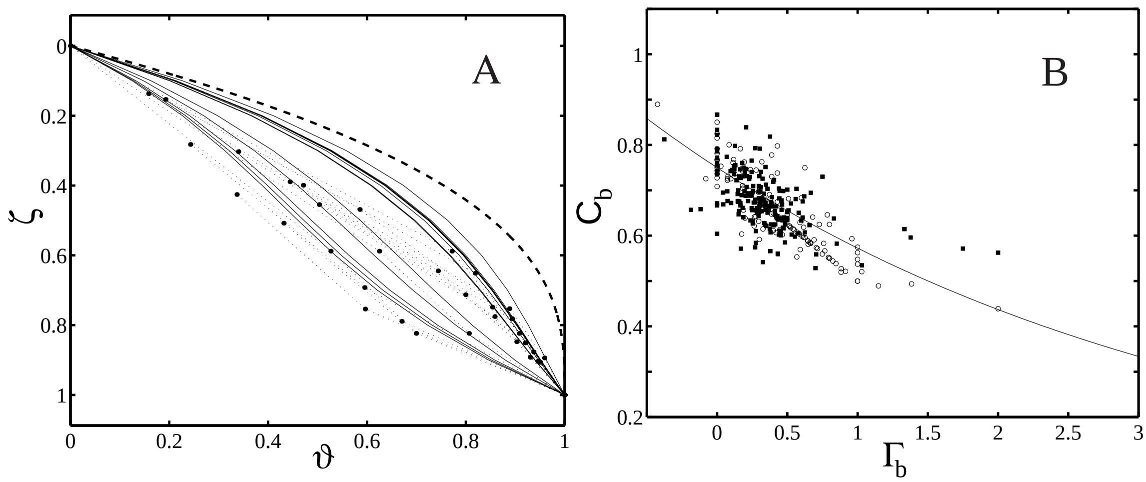

Figure 2.12: Comparison of the self-similar solution with observations data from the Lake Müggelsee. **Panel A**: Dimensionless temperature profiles for the case of strong bottom temperature gradient; points with dashed lines are measurements, solid lines – computed with (2.28) dotted line – asymptotic profile from (2.29). **Panel B**: Variability of the integral shape factor C_b (see text for definition) depending on the bottom temperature gradient in the Lake Müggelsee. Points are data from weekly temperature profiles collected during 1979-1996. Line represents C_b give by the present solution.

Chapter 3

The 1-dim model of lake temperature evolution TeMix

The model of the thermocline, introduced in the chapter 2 can serve as a basis for 1-dimensional model of temperature evolution in a lake. In couple with mixed layer approach the thermocline's model gives a integral (bulk) description of the entire water column subjected to turbulent mixing. It allows us to avoid introducing small-scale turbulence parameters such as the eddy diffusion coefficient, which are difficult to estimate and have often ambiguous physical meaning. Of course, parameterizing the multi-scale turbulent motions by means of lake-scale variables excludes many processes from consideration and makes the model rather rough. However, the integrated approach has some apparent advantages: transparent physics underlying the model parameterizations ensure their versatility and make the model not a predictive tool only but also a reference for information about physical mechanisms governing real processes; besides, the method assure minimum of computations making bulk models an attractive alternative for implication in applied tasks critical for computer capacities.

The following model derivation adopts general ideas underlying the version 2 of the TeMix model (Mironov *et al.* , 1991). Conserving the calculation algorithm for the air-lake fluxes, the model of the water column is re-derived here using results described above. The polynomial representation of the thermocline profile from TeMix2 (2.21) have been rejected to take advantage of the current thermocline model (chapter 2). In addition, the entrainment equation is derived more carefully with taking care of the vertically distributed absorption of the solar radiation. Implementation of this new entrainment equation in TeMix2 results in sufficient improvement of the model predictions as it demonstrated in chapter 4. No sequential number to this research version of the model and it is referred to below as TeMix.

3.1 Problem's statement. Basic concepts

After Kraus & Turner (1967), one-dimensional mixed-layer models were numerously utilized as a method for analysis and prediction of vertical density structure of the natural fluids. A number of bulk-models have been proposed based on upper mixed layer concept in application to the open ocean (Kraus & Turner, 1967; Denman, 1973), to the atmosphere (Ball, 1960; Batchvarova & Gryning, 1991) and to lakes (Tucker & Green, 1977; Spigel *et al.* , 1986).

A number of 1-dimensional models were developed for lake and reservoir dynamics simulation (Imberger & Patterson, 1981, DYRESM model), (Jirka *et al.* , 1978; Jirka & Watanabe, 1980, MITEMP model). Being an attractive alternative to eddy coefficient models, they need, however, additional hypotheses describing the temperature evolution below the mixed layer. The Fickian description of vertical turbulent exchange is invoked here by most of authors again (see e.g. review in Octavio *et al.* 1977). The value of the eddy coefficient is assumed usually in this case to be greater than the molecular diffusivity but constant with depth or semi-empirical dependence of K on stratification is introduced.

3.1.1 Governing equations and general assumptions

The thermocline model developed in chapter 2 complements the mixed layer approximation (2.1) to the representation fully parameterized in vertical direction (Fig. 3.1), excluding the eddy coefficient from consideration.

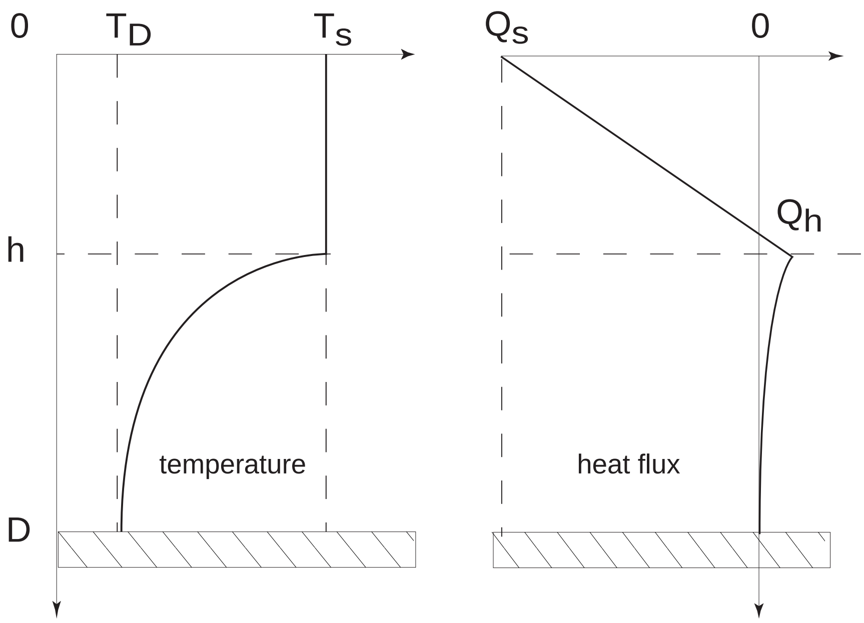

Figure 3.1: The parameterized representation of the temperature (left) and of the vertical heat flux (right) profiles in a lake.

The evolution of the temperature profile in a lake is described by the heat transfer equation:

$$\frac{\partial T}{\partial t} = -\frac{\partial Q}{\partial z} - \frac{\partial I}{\partial z} + \varkappa \frac{\partial^2 T}{\partial z^2}, \tag{3.1}$$

where: $Q \equiv \left\langle \widetilde{w}\widetilde{T} \right\rangle$ is the vertical turbulent temperature flux;

I is the kinematic flux of solar radiation (i.e. the radiation heat flux divided by the reference density, $\varrho_0 = 10^3$ kg·m^{-3}, and specific heat of water at constant pressure, $c_p = 4.218 \cdot 10^3$ J · kg^{-1}·K^{-1});

$\varkappa = 1.4 \cdot 10^{-7}$m^2·s^{-1} is the molecular temperature conductivity.

Last term in (3.1) describes the molecular heat transfer and is negligibly small in most of the natural conditions[1], so we exclude it from further consideration. Bulk modeling approach consists of integrating (3.1) along the vertical axis on the basis of some physically sound assumptions about vertical profiles of the variables T, Q and I.

To summarize general assumptions underlying subsequent model derivations:

[1]A special case, where $\varkappa$ is important, takes place in ice-covered lakes when strongly stratified layer with no turbulence is formed under the ice cover, see chapter 5.

i. Horizontal variations in all characteristics are neglected.

ii. Water density is assumed to be a function of water temperature only, that is close to reality for most of fresh-water lakes.

iii. Temperature changes associated with dissipation and with changes in salinity are neglected.

iv. Within the thermocline the temperature distribution obeys the equation (2.28), whereas the temperature of the UML is a function of time only.

With the assumption (*iv*), the temperature profile is written as

$$T = \begin{cases} T_s & \text{at} \quad 0 \le z \le h \\ T_s - (T_s - T_D)\vartheta(\zeta, \Gamma) & \text{at} \quad h \le z \le D \end{cases} . \tag{3.2}$$

The temperature distribution (3.2) is fully parameterized in vertical direction allowing us to integrate equation (3.1).

A simple state equation of fresh water corresponding to the assumption (*ii*) is:

$$\varrho = \varrho_0[1 - \alpha_T/2(T(t,z) - T_0)], \tag{3.3}$$

where: ϱ_0 – maximum water density, which corresponds to the temperature T_0;
$\alpha_T = \alpha_0(T(t,z) - T_0)$ – the thermal expansion coefficient for fresh water.

The following values of constants in (3.3) are adopted: $\varrho_0 = 999.9757 \approx 10^3$ kg·m^{-3}, $T_0 = 276.9817 \approx 277$ K, and $\alpha_0 = 1.6509 \cdot 10^{-5}$ K^{-2}. The above estimates provide the best fit to the UNESCO equation of state in the temperature range from 273 K to 293 K at atmospheric pressure. (Fofonoff & Millard, 1983). According to Eq. (3.3), the thermal expansion coefficient α_T and the buoyancy parameter β depend on the water temperature, $\beta(T) = g\alpha_T(T) = g\alpha_0(T - T_0)$, where $g = 9.81$ m·s^{-2} is the acceleration due to gravity.

Using the buoyancy definition (2.30), the vertical buoyancy flux is:

$$B = \beta Q$$

and the buoyancy transport is given by:

$$\frac{\partial b}{\partial t} = -\frac{\partial B}{\partial z} - g\alpha_T \frac{\partial I}{\partial z}. \tag{3.4}$$

The mixed layer approach closely related to the turbulent entrainment concept (Turner, 1986). The entrainment equation links the movement of UML bottom h with turbulent mixing in a water body, and is derived on the basis of assumptions specific for certain physical conditions from the equation of the turbulent kinetic energy $e = \langle \widetilde{w} \rangle /2$ evolution. The last one can be written in one-dimensional form as follows (Kraus, 1972):

$$\frac{\partial e}{\partial t} = \underbrace{\langle \widetilde{w}\widetilde{u} \rangle \frac{\partial U}{\partial z}}_{\mathrm{I}} + \frac{\partial}{\partial z}[\underbrace{\langle \widetilde{w}\widetilde{e} \rangle}_{\mathrm{II}} + \underbrace{\varrho_0^{-1} \langle \widetilde{w}\widetilde{p} \rangle}_{\mathrm{III}}] - \underbrace{B}_{\mathrm{IV}} - \underbrace{\epsilon}_{\mathrm{V}} \tag{3.5}$$
$$\mathrm{I} + (\mathrm{II} + \mathrm{III}) - \mathrm{IV} - \mathrm{V}$$

Individual terms on the right hand side of the equation (3.5) have the following meaning: the work of the stress $\langle \widetilde{w}\widetilde{u} \rangle$ on the mean shearing flow, the convergence of the turbulent vertical flux

(II), turbulent pressure fluctuations (III), rate of working of the buoyancy force (IV) and the rate of viscous dissipation of turbulence energy (V).

The partial differential equations set (3.1), (3.4), (3.5), when complemented by appropriate boundary conditions, determines the problem of heat transport in the co-ordinates t an z. In spirit of the bulk modeling approach, we reduce the system of the three *partial* differential equations to a system of *ordinary* differential equations for *parameters* $T_s(t)$, $T_D(t)$, and $h(t)$, where the explicit dependence of the problem on the vertical co-ordinate z is excluded through the parameterization (3.2).

3.1.2 Boundary conditions

Heat flux at the lake surface Q_s, downward flux from the thermocline Q_D and the surface momentum flux $\langle\widetilde{u}\widetilde{w}\rangle_S$ form the boundary conditions for the problem. The heat flux through the lake surface is contributed by different mechanisms; the principal ones are absorption of solar radiation, sensible air-water heat exchange and latent heat flux driven by evaporation. The flux boundary condition at the surface can be written in general form as:

$$Q_s = (1 - A)I_R + H + LE + R, \tag{3.6}$$

where: I_R – incoming short-wave solar radiation;
A – surface albedo;
H – sensible heat exchange at the air-lake boundary;
LE – latent heat loss during evaporation;
R – total long-wave radiation of the atmosphere and of the lake.

The terms of (3.6) are complicated functions of atmospheric conditions. In the present model we adopt the algorithm of sensible and latent fluxes calculation from (Mironov, 1991) based on bulk parameterizations accounting stratification in the lower atmosphere. The methods of long-wave radiative fluxes calculation are used described in (GGO manual, 1982), whereas short-wave insolation is supposed to be measured directly at the lake surface or at the next meteorological station.

The momentum flux,

$$\langle\widetilde{u}\widetilde{w}\rangle_S = \tau/\varrho_0 = u_*^2, \tag{3.7}$$

is the source of the mechanical energy contributing mixed layer deepening and is defined by the surface wind stress τ. The characteristic u_* is known as the friction velocity.

At the bottom of the thermocline the turbulent heat flux is zero by definition, that means:

$$\frac{\partial T_D}{\partial t} = -\frac{\partial I(D)}{\partial z}, \tag{3.8}$$

The equation (3.8) is not valid when the thermocline extends to the lake bottom. Turbulence in bottom boundary layer causes heat exchange with sediments, which can be much more significant than the amount of solar radiation reaching the bottom. The bottom heat flux Q_D should be included in this case into boundary conditions of the model.

The general structure of the model with corresponding boundary conditions is shown in the Fig. 3.2.

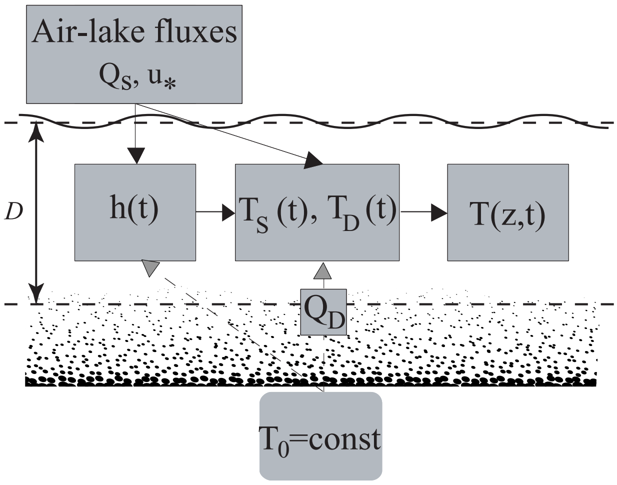

Figure 3.2: External energy fluxes influencing lake temperature and main blocks of the temperature model.

3.2 Model equations

3.2.1 The radiative heat flux

In order to integrate (3.1) in vertical direction, the function $I(z)$ should be specified. It is known, that monochromatic light is absorbed in water by the exponential *Beer* law (Jerlov, 1976):

$$I_\lambda(z) = I_\lambda(0)\ \mathrm{e}^{-\gamma(\lambda)\mathrm{z}}, \tag{3.9}$$

where γ is the extinction coefficient for a given wavelength λ. With sufficient accuracy the extinction law for solar light can be written as:

$$I(z) = \int I_\lambda(0)\mathrm{e}^{-\gamma(\lambda)z}\mathrm{d}\lambda \approx I(0)\sum_n a_n \mathrm{e}^{-\gamma(\lambda_n)z}, \tag{3.10}$$

where the number of wavelength bands in the sum on the r.h.s is chosen according to desirable accuracy of the integral approximation. Assumption of constant γ for the whole daylight spectrum is often used in physical applications despite the extinction variability can influence noticeably modeling results (Orlov, 1996; Hocking & Straškraba, 1999). The derivation of the model equations below is made in assumption of I to be a predetermined function of depth.

In calculations the simplest one-band approximation is used,

$$I(z) = I_0\ \mathrm{e}^{-\gamma\mathrm{z}}, \tag{3.11}$$

with I_0 defined as $(1-A)I_R$ (see Eq. 3.6).

More sophisticated parameterizations for the light distribution can be easily integrated into the model if they are justified by available observational data.

3.2.2 The integral heat budget

Entire water column Integrating (3.1) from the lake surface to the bottom one gets the equation for the vertically averaged temperature evolution:

$$\frac{\partial \overline{T}}{\partial t} = \frac{1}{D}\frac{\partial}{\partial t}\int_0^D T(z,t)\mathrm{d}z = \frac{\big(Q_s + I_0\big) - \big(Q_D + I(D)\big)}{D}, \tag{3.12}$$

The mean temperature $\overline{T}$ is defined according to (3.2) as:

$$\overline{T} = T_s - (1 - h/H)\,(T_s - T_D)\int_0^1 \vartheta \mathrm{d}\zeta, \tag{3.13}$$

where the dimensionless integral is found from (2.28):

$$\int_0^1 \vartheta \mathrm{d}\zeta = \frac{\Gamma - 2}{(\Gamma - 1)^2} + \frac{\mathrm{e}^{1-\Gamma}}{(\Gamma - 1)^2}. \tag{3.14}$$

From (3.12) and (3.13) we can express $\mathrm{d}T_s/\mathrm{d}t$:

$$\frac{\mathrm{d}T_s}{\mathrm{d}t} = \left[\frac{\mathrm{d}C_T}{\mathrm{d}t}\Delta T \Delta h + \dot{h} C_T \Delta T + \frac{\mathrm{d}T_D}{\mathrm{d}t} C_T \Delta h - \Delta Q\right] / (C_T \Delta h - D), \tag{3.15}$$

where:

$$\Delta T = T_s - T_D, \qquad \Delta Q = \big(Q_s + I_0\big) - \big(Q_D + I(D)\big),$$
$$\Delta h = D - h, \qquad C_T = \int_0^1 \vartheta \mathrm{d}\zeta = \frac{\mathrm{e}^{1-\Gamma} + \Gamma - 2}{(\Gamma - 1)^2}.$$

Upper mixed layer The assumption that the temperature of the mixed layer T_s is independent of z co-ordinate allows easily integrating (3.1) over the mixed layer depth and achieving the equation of the mixed layer temperature evolution:

$$\frac{\mathrm{d}T_s}{\mathrm{d}t} = \frac{\big(Q_s + I_0\big) - \big(Q_h + I(h)\big)}{h}. \tag{3.16}$$

Integrating (3.1) from the surface to a depth z', and again from the surface to the depth h we achieve with account of (3.16) the expression for the turbulent heat flux profile in the UML:

$$Q(z) = \left(1 - \frac{z}{h}\right)(Q_s + I_0) + \frac{z}{h}\Big(Q_h + I(h)\Big) - I(z). \tag{3.17}$$

Stratified layer The turbulent heat exchange inside the stratified layer below the UML is assumed to comply with the thermocline model described in chapter 2. This implies the lower thermocline's boundary coincide approximately with the lake's bottom. Generally, the condition is satisfied in most of stratified lakes except very deep ones. Then, the equation (3.1) can be written as (see Eq. 2.28)

$$Q = (T_s - T_D)\Phi\,(\zeta, \Gamma)\,\mathcal{H}\Big(\dot{h}\Big) \qquad \text{at} \quad h \le z \le D, \tag{3.18}$$

where dimensionless function Φ is

$$\Phi(\zeta, \Gamma) = \frac{2 - \Gamma}{(\Gamma - 1)^2} + \frac{\mathrm{d}\vartheta/\mathrm{d}\zeta}{(\Gamma - 1)^2}\left[1 + \zeta\Gamma - \zeta - \frac{\zeta(\Gamma^2 + \Gamma - 2)}{1 + \zeta\Gamma - \zeta}\right], \tag{3.19}$$

and $\mathcal{H}()$ is the Heaviside-like step function defined as follows:

$$\mathcal{H}(x) = \begin{cases} 0 & \text{if } x \le 0, \\ x & \text{if } x > 0. \end{cases} \tag{3.20}$$

The function $\mathcal{H}\left(\dot{h}\right)$ reveals the fact that the turbulent heat flux exists in the stratified layer only during UML deepening, when there is a turbulence energy source at the UML base.

Integrating (3.1) with regard to the vertical co-ordinate z from h to some depth z' and again from h to D, we arrive:

$$\frac{\Delta h^2}{2}\frac{\mathrm{d}T_s}{\mathrm{d}t} - \frac{\mathrm{d}C_{TT}}{\mathrm{d}t}\Delta h^2\Delta T + 2C_{TT}\Delta h\Delta T\dot{h} - C_{TT}\Delta h^2\left(\frac{\mathrm{d}T_s}{\mathrm{d}t} - \frac{\mathrm{d}T_D}{\mathrm{d}t}\right) = C_Q\Delta h\Delta T\mathcal{H}(\dot{h}) - \Delta h I(h) + \int_h^D I(z)\mathrm{d}z, \quad (3.21)$$

where,

$$C_{TT} = \int_0^1 \mathrm{d}\xi\int_0^\xi \vartheta(\zeta)\mathrm{d}\zeta = \frac{\Gamma-3}{(\Gamma-1)^3} + \frac{(\Gamma+1)}{(\Gamma-1)^3}\mathrm{e}^{1-\Gamma},$$
$$C_Q = \int_0^1 \Phi(\zeta)\mathrm{d}\zeta = \frac{\Gamma^2-5G+8}{(\Gamma-1)^3} - \frac{(\Gamma+3)}{(\Gamma-1)^3}\mathrm{e}^{1-\Gamma}. \quad (3.22)$$

Substituting (3.15) in (3.21) yields the ordinary differential equation for the bottom temperature T_D:

$$\frac{\mathrm{d}T_D}{\mathrm{d}t} = \Big\{(Q_s - Q_D)\Delta h(1-2C_{TT}) + \frac{\mathrm{d}h}{\mathrm{d}t}\Delta T\Big[2C_Q(C_T\Delta h - D) - \Delta h C_T(1+2C_{TT}) + 4C_{TT}D\Big] + \frac{\mathrm{d}C_T}{\mathrm{d}t}\Delta T\Delta h^2(1-2C_{TT}) + \frac{\mathrm{d}C_{TT}}{\mathrm{d}t}2\Delta T\Big[h^2C_T + D^2(C_T-1) + hD(1-2C_T)\Big]\Big\}/(\Delta h^2 C_T - 2\Delta h D C_{TT}). \quad (3.23)$$

Now we have two ordinary differential equations (3.15) and (3.23) and three unknowns T_s, T_D and h. An equation for mixed layer depth h (the entrainment equation) is needed to close the problem.

3.2.3 The entrainment equation

The entrainment equation can be achieved from the TKE budget in the UML. As first approximation, let us assume following Niiler & Kraus (1977) the TKE budget be in equilibrium with external forces. Alternatively, certain scaling hypotheses can be applied to time rate of change of the TKE, as it was done e. g. in (Spigel *et al.* , 1986; Zilitinkevich, 1987). Such scaling is considered based on TKE similarity hypothesis in Chapter 5 while modeling radiatively-driven convective mixing below the temperature of maximum temperature (see Section 5.2.2). However, there exist generally two TKE generation mechanisms, which we have to parameterize in the present model: convection driven by negative surface buoyancy flux and shear stress at the UML boundaries. The interaction of these mechanisms is rather complicated and has no adequate description yet. In this case, a parameterization is possible only through essential simplifications and introducing additional terms scarcely follows in better model predictions. Then, integrating

(3.5) from the lake surface to the UML base h yields,

$$0 = \int_0^h \langle\widetilde{w}\widetilde{u}\rangle \frac{\partial U}{\partial z} \mathrm{d}z + \widetilde{w}(e + \frac{\widetilde{p}}{\varrho_0})\Big|_0^h - \int_0^h B\mathrm{d}z - \int_0^h \epsilon \mathrm{d}z. \tag{3.24}$$

Buoyancy flux derivation. Integrating (3.17) from 0 to h yields the integral buoyancy flux within the UML (the term B in Eq. 3.24):

$$\int_0^h B\mathrm{d}z = \frac{hB_h}{2} + \frac{h}{2}\left[B_s + \beta\left(I_0 + I(h) - \frac{2}{h}\int_0^h I(z)\mathrm{d}z\right)\right] = \frac{hB_h}{2} + \frac{w_{*R}^3}{2}. \tag{3.25}$$

Here, B_s and B_h are the turbulent buoyancy fluxes across the UML boundaries and w_{*R} is the convective velocity scale analogous to the Deardorff (1970a) convective scale extended to take into account the radiation absorption within the mixed layer. The last equation represents the rate of change of the potential energy within the UML on account of buoyancy forces.

In classical mixed layer models, the layer below the UML, where the turbulence develops on background of strong density stratification, is parameterized either as density jump of zero depth ("zero-order jump" approach, Kraus & Turner 1967; Lilly 1968; Zilitinkevich 1991) or by means of linear approximation for vertical profiles of physical properties ("first-order jump" approach, see e.g. Betts 1974; Spigel *et al.* 1986). For zero-order jump approximation, the buoyancy flux at the UML base Q_h is written as:

$$B_h = \begin{cases} \Delta b\dot{h} & \text{if } \dot{h} > 0 \\ 0 & \text{if } \dot{h} \le 0 \end{cases},$$

or using our notation,

$$B_h = \mathcal{H}\left(\dot{h}\right) \Delta_0 b,$$

where $\Delta_0 b$ is the buoyancy jump below the UML and the function $\mathcal{H}\left(\dot{h}\right)$ has the same meaning as in Eq. (3.18).

The parameterization of the turbulence within the stratified layer developed in Chapter 2 allows us to define the turbulent flux condition at the UML base as

$$B_h - \widetilde{w}(e + \varrho_0^{-1}\widetilde{p})\big|_{z=h} = \Delta b\,\mathcal{H}\left(\dot{h}\right)\,\Phi(\zeta, \vartheta, \Gamma), \tag{3.26}$$

where Δb is the overall buoyancy difference across the stratified layer and the dimensionless function Φ is defined by Eq. (2.32).

Shear TKE generation. When dealing with shear generation term (the first term on r.h.s in Eq. 3.24), it is common to assume it be proportional the external TKE input from the atmosphere u_*^3 (Kraus & Turner, 1967; Niiler & Kraus, 1977; Spigel *et al.* , 1986). The background physical mechanism can be treated as follows: the mean velocity shear $\partial U/\partial z$ exists at the surface in relatively thin layer of depth δ and at the UML bottom, while the rest of the mixed layer moves uniformly, like a slab. If the momentum flux within the layer δ is set as near constant, one achieves, with account of the boundary condition (3.7):

$$\int_0^\delta \langle\widetilde{w}\widetilde{u}\rangle \frac{\partial U}{\partial z}\mathrm{d}z = \langle\widetilde{w}\widetilde{u}\rangle_S \int_0^\delta \frac{\partial U}{\partial z}\mathrm{d}z = u_*^2(U_\delta - U_0), \tag{3.27}$$

where velocity jump $(U_\delta - U_0)$ is parameterized using of the bulk formula:

$$(U_\delta - U_0) = C u_*. \tag{3.28}$$

The shear stress generation at the thermocline bottom as well as TKE flux at the surface $\widetilde{w}(q/2+\varrho_0^{-1}\widetilde{p})\big|_{z=0}$ assumed in their turn be proportional to the TKE generation at the surface.

Thus, we arrive the simplest TKE budget equation accounting of the wind driven shear turbulence on background of convective mixing:

$$\Delta b\,\mathcal{H}\!\left(\dot{h}\right)\;\Phi(\zeta,\vartheta,\Gamma) = -w_{*R}^3/h + 2(m' u_*^3/h - \bar{\epsilon}), \tag{3.29}$$

where m' is an empirical constant and $\bar{\epsilon}$ is a mean TKE dissipation rate within the UML.

TKE dissipation rate. For parameterization of the dissipation term in Eq. (3.29) two ways are usually followed. The first one assumes the dissipation be proportional to the sum of generation terms (Kraus & Turner, 1967; Niiler & Kraus, 1977). The other way consists of derivation an expression for $\bar{\epsilon}$ from dimensional analysis. The expression

$$\bar{\epsilon} \propto \bar{e}^{3/2}/h, \tag{3.30}$$

where $\bar{e}$ is the mean TKE inside the mixed layer, was introduced by Mahrt & Lenschow (1976) in application to convectively mixed atmospheric CBL. It was later used by Spigel *et al.* (1986) for modeling the diurnal mixed layer in lakes. A usage of the dimensional analysis implies similarity of the modeled process in relation to the scales used as independent variables. The convective mixing is a large-scale process encompassing the whole UML, so the mixed layer depth h is the decisive scale of mixing by convective cells. On the other hand, a validity of h as a scaling variable for wind mixing is rather questionable. The similarity hypothesis for the TKE and dissipation rate profiles within the UML will be used in Chapter 5 when dealing with purely convective mixing in ice-covered lakes. Yet in the present model the Niiler & Kraus (1977) formulation is preferred, as incorporating "*just about all that can be said with any confidence about the underlying physical processes*" (Niiler & Kraus, 1977). Thus, we can rewrite (3.29) as

$$\Delta b\,\mathcal{H}\!\left(\dot{h}\right)\;\Phi(\zeta,\vartheta,\Gamma) = \frac{-w_{*R}^3 + C_0\left[\mathcal{H}(w_*^3) + \mathcal{H}(w_R^3)\right] + C_* u_*^3}{h}, \tag{3.31}$$

with new "combined" empirical coefficients C_0 and C_* including the energy sink on account of viscous dissipation (see Niiler & Kraus 1977 for details). The term on C_0 is written in the particular form with the convective velocity scale w_{*R} divided into two parts: the one specified by the surface buoyancy flux (Deardorff velocity scale w_*) and that from heating by penetrating radiation w_R:

$$\begin{gathered} w_{*R} = w_* + w_R; \qquad\qquad w_*^3 = h B_s; \\ w_R^3 = h\beta\left(I_0 + I(h) - \frac{2}{h}\int_0^h I(z)\,\mathrm{d}z\right). \end{gathered} \tag{3.32}$$

It reflects the fact, that both of them can be either positive or negative appearing respectively as a source or a sink of the TKE. While the radiative heat flux is never negative, the corresponding buoyancy flux changes his sign in fresh water lakes through the buoyancy parameter β if temperature drops below the maximum density value. The surface cooling has in its turn stabilizing effect in these conditions and do not contribute turbulence energy generation, that excludes w_* from the dissipation rate parameters.

Particular cases of the UML development. Depending on prevailing sources and sinks of the TKE, different terms in Eq. (3.31) become crucial for the mixed layer evolution. Below some asymptotic cases are considered.

Strong surface cooling. If the air temperature is much lower than that of lake surface, strong convective mixing develops overshooting wind driven mixing. The situation is typical for summer nights. The winds are usually very weak over the lake surface on account of night breeze and there is no solar radiation, so the surface flux convection is the only mixing mechanism. Excluding u_* and radiative term from Eq. (3.31) one gets,

$$\dot{h} = -\frac{C_1 B_s}{\Delta b\, \Phi(\zeta, \Gamma)}, \tag{3.33}$$

where $C_1 = (1 - C_0)$, which expression specifies the entrainment flux as a constant fraction of the surface buoyancy flux:

$$B_h/B_s = \text{const.}$$

Entrainment equation in this simplest form was originally deduced for modeling of the atmospheric boundary layer (Betts, 1973; Carson, 1973; Tennekes, 1973). As it follows from (3.33), the entrainment always present in this case leading to unlimited increasing of the UML depth. In reality, the entrainment decelerates on account of the growing stratification below the UML, Δb and can be arrested by the lake bottom in shallow lakes.

Surface cooling balanced by radiative heating If in addition to surface cooling there is solar radiation penetrating into the upper layers of a lake, it will restrain the convection and the equilibrium will be established at some UML depth h_{eq}, at which the entrainment cannot further develop. Thus, the l.h.s of (3.31) turns into zero and the equilibrium depth is determined as,

$$h_{eq} = \frac{2\int_0^h I(z)\mathrm{d}z}{C_0 Q_s + (I_0 + I(h))}. \tag{3.34}$$

This situation is rather rare in small lakes since the air temperature is usually higher than that of the lake surface during the insolation periods on account of heat exchange with surrounding land. However, such equilibrium is typical for the oceanic upper layer (Soloviev, 1979; Soloviev & Vershinskii, 1982) and was firstly modeled by Kraus & Rooth (1961). A non-stationary mixed layer model was developed by Mironov & Karlin (1989), who also demonstrated the relevance of (3.34) for h_{eq} estimation in contrast to frequently used "thermal compensation depth" (Woods, 1980) – the thickness of the water column absorbing radiation sufficient to compensate the heat loss at the surface.

Destabilizing by radiative heating Another regime of buoyancy-driven mixing exists only in fresh waters at temperatures less than the maximum density value. As it has been mentioned above, the penetrating solar radiation plays destabilizing role in this situation. The peculiarity of the convection process in this case is that the instability source is not concentrated at the boundary but distributed vertically over the absorbing layer. Two natural examples of this regime are convective mixing in melting water over the sea ice and the spring convection in ice-covered lakes. In the first case, the relatively thin layer of water develops on the ice surface during spring melting; the temperature at the bottom of this layer is fixed at the freezing point, while the rest of the water column warms up by solar radiation absorption. Since the absorption is vertically distributed with upper layers gaining more heat, the instability occurs leading to intensive vertical mixing. This mixing supplies the ice-water interface with an additional heat accelerating significantly the melting process; the contribution of the convection should be taken into account for adequate prediction of ice conditions in polar seas (Townsend, 1964).

In late winter at moderate and polar latitudes, when the snow cover over the lake ice disappears, the amount of the solar radiation penetrating the ice increases significantly resulting in convective mixing similar to that described above. The entrainment rate can be derived in this case from (3.31) with neglecting of the heat flux from water to ice, as:

$$\dot{h}\,\Delta b\,\Phi(\zeta,\vartheta,\Gamma) = -C_1\left[\beta\left(I_0 + I(h) - \frac{2}{h}\int_0^h I(z)\mathrm{d}z\right)\right] = -C_1 w_R^3/h. \tag{3.35}$$

The convection of this kind can present in polar lakes during the most of the year, determining, among the temperature structure, the chemical and biological conditions in a lake (Hawes, 1983; Matthews & Heaney, 1987; Kelley, 1997). In addition, the regime provides the ideal example for studying convectively-driven mixing in natural conditions in absence of shear turbulence. In chapter 5 a particular analysis of the radiatively-driven convection is performed by means of non-stationary mixed-layer model and by comparison of modeling results with observational data from different sources.

Wind mixing in the stable UML If buoyancy flux at the lake surface is positive, it will oppose the mixed layer deepening until an equilibrium state between wind-driven mixing and stabilizing buoyancy flux will establish at some UML depth h_{eq}. If there is no wind, this depth is identically zero, the water column is fully stratified and Eq. (3.31) has no sence. Otherwise, Eq. (3.31) takes the form:

$$0 = -\left[B_s + \beta\left(I_0 + I(h_{eq}) - \frac{2}{h_{eq}}\int_0^{h_{eq}} I(z)\mathrm{d}z\right)\right] + C_*\frac{u_*^3}{h_{eq}}. \tag{3.36}$$

Assuming the whole amount of the solar radiation be absorbed within the mixed layer, the expression for the equilibrium depth becomes,

$$h_{eq} = -C_*\frac{u_*^3}{B_s} = -C_* L_*, \tag{3.37}$$

where L_* is the Monin-Obukhov (MO) length scale. Kitaigorodski (1960) was the first who proposed the MO scale as a measure for wind-mixed layer in the ocean. It can be seen, that as soon as the buoyancy difference Δb on l.h.s. of (3.31) was excluded from consideration, h_eq not more depends on the lake stratification. Moreover, if the surface flux B_s is close to zero, the UML depth tends to infinity even on weak winds. This behavior is the direct consequence of scaling of shear mixing terms in the TKE budget (3.24) on the surface friction velocity u_*. Such scaling does not take into account the local character of the wind induced turbulence (Nieuwstadt & Duynkerke, 1996). Zilitinkevich & Mironov (1996) proposed an alternate derivation of h_{eq} from Eq. (3.24) based on parameterization of the mean velocity profile in the UML using stability correction function concept as it formulated by Hinze (1959). The correction function was chosen in such a way, that the resulting expression for the equilibrium depth combines the MO length with other two length scales characterizing the UML deepening. The first one is the

Ekman length scale characterizing the UML depth in absence of the buoyancy flux (Rossby & Montgomery, 1935):

$$L_f = u_*/f, \tag{3.38}$$

where, $f = 2\Omega \sin\varphi$ is the Coriolis parameter,
$\Omega = 7.29 \cdot 10^{-5} 1/\mathrm{s}$, is the angular frequency of the Earth rotation,
φ is the lake's latitude.
The second length scale represents dependence of h_{eq} on the underlying stratification (Kitaigorodskii & Joffre, 1988):

$$L_N = u_*/N, \tag{3.39}$$

where N is the Brunt-Väisälä frequencybelow the UML:

$$N = \sqrt{\frac{1}{\varrho}\frac{\mathrm{d}\varrho}{\mathrm{d}z}}. \tag{3.40}$$

The resulting equation for h_{eq} is (Zilitinkevich & Mironov, 1996, Eq. 26):

$$\left(\frac{f h_{eq}}{C_n u_*}\right)^2 + \frac{h_{eq}}{C_s L} + \frac{N h_{eq}}{C_i u_*} = 1; \tag{3.41}$$

here the coefficients are:

$$C_n = 0.5;\ C_s = 10;\ C_i = 20.$$

The question about the value of N to be used in (3.41) is open. Physically motivated ones can be both the average value in the thermocline $\overline{N} = 1/(D-h)\int_h^D N\mathrm{d}z$ and the value just below the mixed layer $N_h = N|_{z=h+0}$. As a rule, the second value is the largest one in the thermocline, so we use it. Substituting (3.2) in (3.3), differentiating the latter on z and using (3.40), we can write

$$N_h = \sqrt{\frac{\alpha_T(T_s - T_D)(T_s - T_0)}{1 - \alpha_T/2(T_s - T_0)^2}\left.\frac{\mathrm{d}\vartheta}{\mathrm{d}\zeta}\right|_{\zeta=0}}. \tag{3.42}$$

The ϑ derivative can be easily found as a function of Γ differentiating (2.28) on ζ and substituting $\zeta = 0$ into result.

Convective UML deepening on background of wind mixing Equation (3.41) represents an equilibrium mixed layer depth, i.e. the depth the layer can achieve in case of permanent constant positive surface heat flux. An expression for time changing of wind-driven mixed layer depth can be written as following relaxation equation (Nieuwstadt & Duynkerke 1996, Nieuwstadt & Tennekes 1981):

$$\frac{\mathrm{d}h}{\mathrm{d}t} = \frac{h_s - h}{\tau_*}. \tag{3.43}$$

here, h_s is the equilibrium depth as it is found from (3.41).

There are different estimations for the time scale τ_* in Eq. (3.43). These are, e.g.

i. The Coriolis scale $\tau_* \sim 1/f$

ii. Combination of the Monin-Obukhov length scale and of the shear velocity $\tau_* \sim L/u_* = u_*^2/(\beta Q_s)$

iii. Normalized heating rate $\tau_* \sim \Delta T(\mathrm{d}T_s/\mathrm{d}t)^{-1}$

The typical estimations of these time scales for temperate lakes not exceed one day. Thus, we can assume the wind-mixed layer be adjusted to the h_{eq} value within the daily time step of the model.

Convective mixing develops relatively slow in relation to the wind mixing. so we should solve a differential equation (3.31) for $\dot{h}$ as a function of surface heat flux and wind. However, at small negative values of the surface heat flux, the entrainment equation in form (3.31) will lead to infinite growth of the UML depth h. This unrealistic situation is a consequence of using the UML depth as a length scale for local wind-driven turbulence. In order to take into account the local character of wind mixing, the entrainment equation for negative surface heat flux is written in following form:

$$\dot{h} = \left\{ \frac{-C_1 w_*^3 + w_R^3}{h} + \frac{C_* u_*^3}{h} F_h\left(h_{eq} - h\right) \right\} \left\{ \Delta b \Phi(\zeta, \vartheta, \Gamma) \right\}^{-1}, \tag{3.44}$$

where h_eq is defined by Eq. (3.41) and F_h is the Heaviside function defined as:

$$F_h\left(x\right) = \begin{cases} 1 & \text{at} \quad x \geq 0 \\ 0 & \text{at} \quad x < 0 \end{cases} \tag{3.45}$$

A number of estimations for constants C_1 and C_2 was made based on results of laboratory modeling, observational data and large eddy simulations (see e.g. Spigel *et al.* 1986; Zilitinkevich 1987, 1991; Kreiman & Kirillin 1998 for reviews). Here we accept the values proposed by Zilitinkevich (1991):

$$C_1 = 0.2 \quad C_* = 5$$

3.2.4 Basin's depth limited mixed layer

During periods of strong surface mixing the mixed layer depth can achieve the lake's bottom. On each time step the condition $h < D$ have to be checked. If the condition does not hold true, the lake supposed to be fully mixed vertically:

$$\left. \begin{array}{c} h = D \\ T_D = T_s \end{array} \right\} \ \text{if} \quad h \geq D. \tag{3.46}$$

Now the equations system is closed. The peculiarity of the algorithm consist of determining on every time step which equation for h should be used depending on the surface heat flux direction. If $Q_s > 0$ the system of two ODE's (3.23) and (3.15) should be solved in couple with algebraic equation (3.41) assuming $\dot{h} = 0$; if $Q_s < 0$ the problem consists of three ODE's (3.23), (3.15) and (3.44). The surface heat flux is calculated in its turn using the T_s at previous time step.

3.3 Algorithm realization

3.3.1 Input data

Input information can be organized into following two groups:

External information The first group includes:

- Basin characteristics
  - The average lake depth D.
  - Latitude φ, which used in the Coriolis acceleration estimation.
- Meteorological time series, which include:
  - *Incoming solar radiation.*

    If the radiation is measured over the water surface or over the land, additional information about the albedo of water surface should be provided. The model includes the Payne (1972) algorithm for albedo calculation based on atmospheric transmittance data.
  - *Wind speed.*
  - *Air temperature.*
  - *Air humidity.*

    The above three variables are used for estimation of turbulent momentum and heat fluxes at the surface. The algorithm is based on hypothesis of self-similarity of wind, humidity and temperature profiles in boundary layer, so the elevation of measurements point above the lake surface should be provided in order to reconstruct the characteristics profiles over the lake.
  - *Cloudiness*.

    The algorithm of long-wave radiation evaluation provides the possibility of calculation of radiation emission by clouds with account of vertical cloudiness distribution.
- The heat flux at the water-sediments interface Q_D.

  The value of Q_D can be an external parameter or can be calculated using the algorithm described in (Golosov & Kreiman, 1992). The value of the temperature gradient at the bottom Γ is derived then from the bottom heat flux as:

$$\Gamma = \frac{Q_D}{K_D}(D-h), \tag{3.47}$$

  and the expression for time derivative is, correspondingly

$$\frac{\mathrm{d}\Gamma}{\mathrm{d}t} = \left[\frac{\mathrm{d}Q_D}{\mathrm{d}t}\Delta h - Q_D\frac{\mathrm{d}h}{\mathrm{d}t}\right]/K_D, \tag{3.48}$$

  where K_D is a characteristic value of the heat diffusion coefficient at the water-sediments interface, which depends on sediments properties.
- Initial values of the surface temperature T_s,bottom temperature T_D and mixed layer depth h.

  The values are to be derived from available observational data, a reasonable guess can be adopted alternatively.

Parameters of the calculation The second group consists of:

- Time step dt.

  Since diurnal averaging underlies the model philosophy, the time step is supposed to be not less than 24 hours. Depending on required accuracy and available input data, a larger value can be chosen.

- The time frame of calculations.

  The start and stop moments have to be specified, that gives, in couple with the time step, the dimensions of the output arrays.

A simple graphical user interface was developed for the model using MATLAB® programming environment. The appearance of the input window is shown in Fig. 3.3.

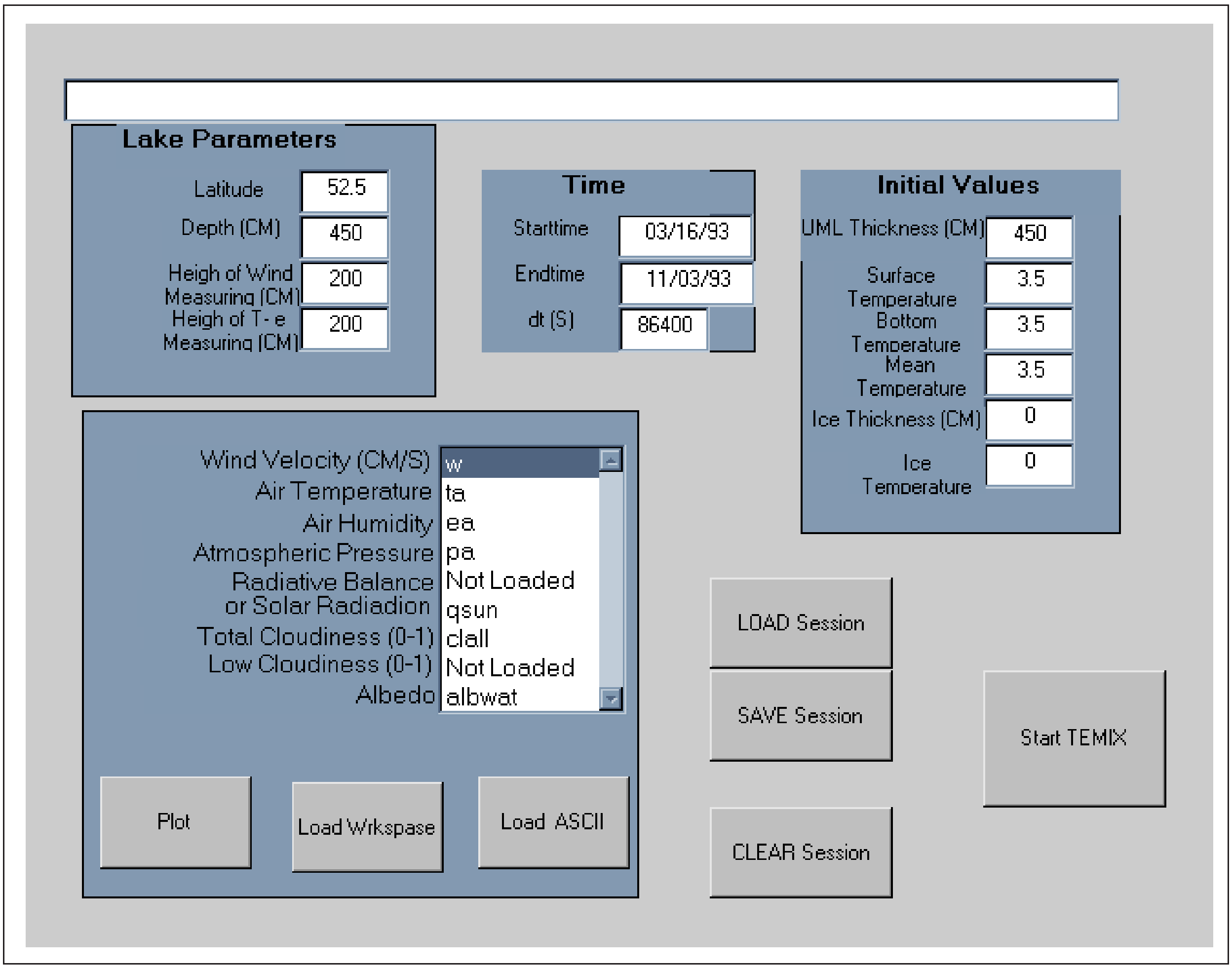

Figure 3.3: `TeMix` input window.

3.3.2 Calculation

Calculations are organized inside a time loop. The structure is subdivided into following logical blocks:

***ODE solver* subroutine** A subroutine performing one of the standard algorithms of ordinary differential equations system solution. Currently the simplest one-step Newton algorithm is used. Other methods (e.g. one of the Runge-Kutta methods) can be also implemented.

The program takes as input the array of function values $X(m)$ at previous time step, the main time step dt and a reference to subroutine-function which calculate the array of derivatives $\mathrm{d}X/\mathrm{d}t$. The return value is X at new time step.

***derivatives* subroutine** The block, where model equations are solved. It is called by ODE solver. In our case, the equations set varies during calculations depending on the Q_s sign. Thus, the subroutine receives an additional parameter-flag in order to define which equations set should be solved.

a set of subroutines for self-similarity functions calculation The dimensionless funcltions ϑ and Φ as well as their integrals and derivatives present in the model equations. All of them depend on time through the dimensionless bottom gradient Γ (2.28).

Differentiating (3.14) and (3.22) with regard to t and using (3.48) one gets expressions for $\mathrm{d}C_T/\mathrm{d}t$ and $\mathrm{d}C_{TT}/\mathrm{d}t$, which are then substituted in (3.15) and (3.23).

3.3.3 Output

The output includes 1xN arrays of T_s, T_D, Γ and h. The vertical temperature profile at any given time can be then reconstructed using Eqs. (2.28) and (3.2).

Chapter 4

Application of the `TeMix` model to the Lake Müggelsee

4.1 Site description and data set

The Lake Müggelsee is a shallow polymictic lake located in the eastern part of Berlin, with co-ordinates $52^o26'N$ and $13^o39'E$ (Fig. 4.1). The mean depth of the lake is 4.9 m. and the maximum one is about 8 m. Owing to its location the lake undergoes a significant anthropogenic impact due to urbanization of surrounding area and river Spree basin. During the last century significant changes in ecological state of the lake were indicated, resulted in essential increasing of plankton and seston contents in lake water (Behrendt *et al.* , 1990). Since 1978 regular monitoring of the the Lake Müggelsee ecosystem has being performed by Institute of Water Ecology and Inland Fisheries, Berlin (Driescher *et al.* , 1993). The monitoring includes meteorological observations at the station **m1**, located at the institute's pier near the northern shore of the lake (Fig. 4.1). The observations consist of hourly readings of the solar radiation, near-surface air temperature, humidity and wind vector as well as water temperature measured at 0.5 m. beneath the surface. In addition, the subsurface short-wave radiation is measured at two depth levels allowing estimation of the light extinction in the lake water. Vertical temperature profiles are collected weekly at the deepest point of the lake (depth ≈8 m, station **m7**, Fig. 4.1). The meteorological conditions over the lake are characterized by relatively weak winds. The wind speed probability distribution is close to lognormal and about 70% of wind speeds are less than 4 m/s, (Fig. 4.2). The distribution of the local wind directions is characterized by strong predominance of south-west winds drawing up along the main axis of the lake that is conditioned by the surrounding landscape (Fig. 4.3). Thus, the general wind mixing conditions at the air-lake interface can be treated as having the constant fetch, favoring application of the 1-dim model to the lake. The morphometry of the lake is also in a good agreement with the one-dimensional assumption: the pan-like shape of the lake (see hypsographic curve in Driescher *et al.* 1993) allows approximating it by a parallelepiped that excludes lake area variations with depth from consideration.

Another factor potentially destroying the one-dimensional structure in the lake is the inflow of River Spree. Considering difference in the heat content between the river and lake waters, one can distinguish a certain regularity in its seasonal variations. This is illustrated in Fig. 4.4 using temperature data of 1993. A notable difference in the temperatures exists in spring and autumn periods, before and after of the summer stratification. In spring, river waters are apparently warmer than those of the lake, and own, therefore, positive buoyancy. That will lead to spreading

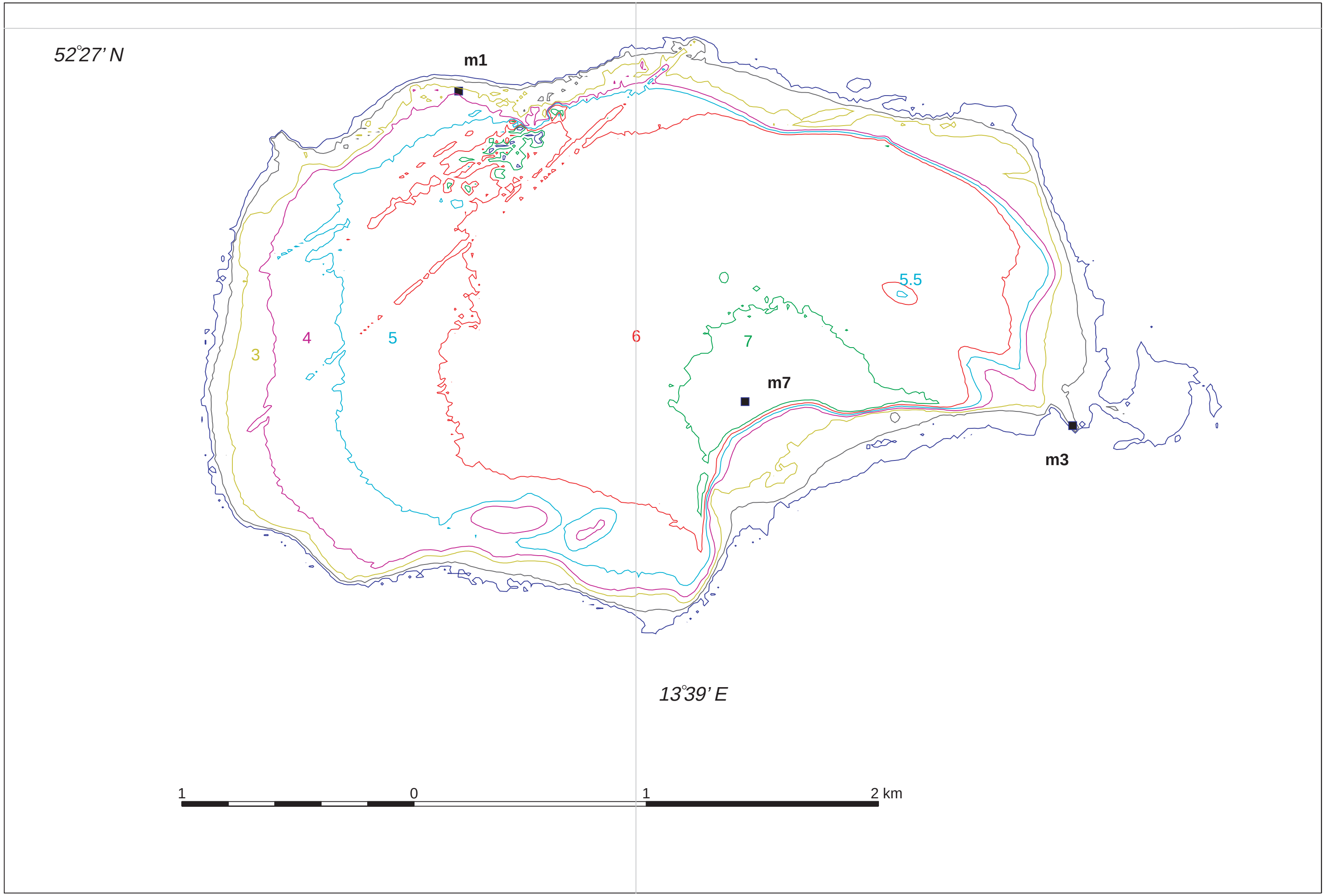

Figure 4.1: The Lake Müggelsee study site and measurement points location. **m1**: Meteorological station of the Institute of Freshwater Ecology and Inland Fisheries (meteoparameters, water temperature and transparency measured hourly). **m3**: The river Spree inflow (water temperature and discharge measured weekly). **m7**: The deepest (8 m) point (water temperature and chemical components measured weekly.)

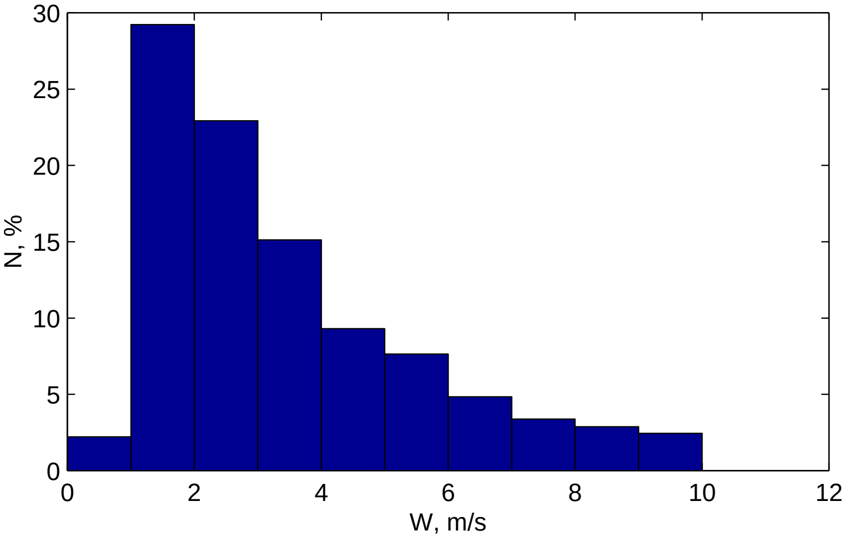

Figure 4.2: Wind histogram built on data from the the Lake Müggelsee meteorological station **m1** for the period 1979-1996.

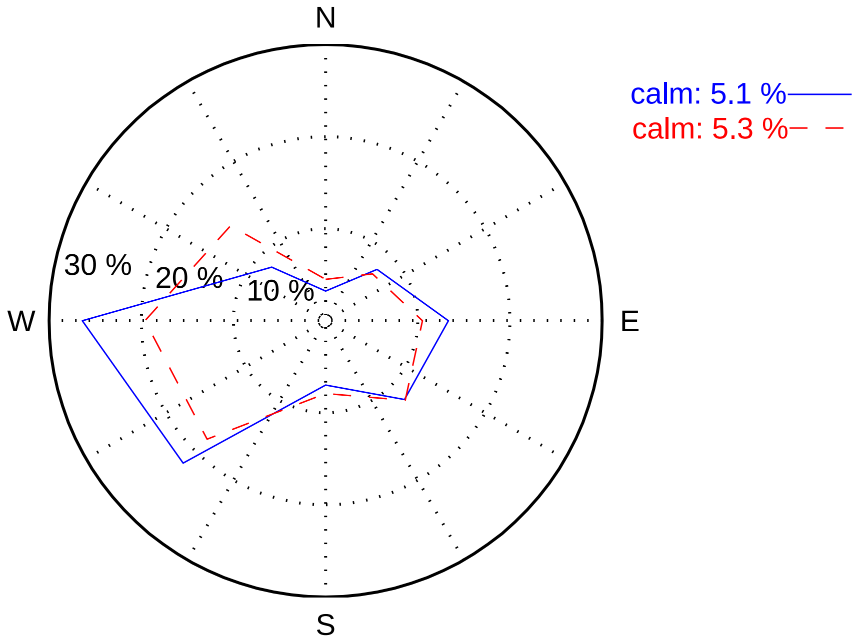

Figure 4.3: Wind rose for the Lake Müggelsee: solid line - data from the Müggelsee meteorological station **m1** for 1979-96, dashed line - climatic data for the Berlin area from (Kohl 1969).

of the river jet over the lake surface without significant influence on the vertical structure. During autumn cooling, the colder and denser should plunge in a stratified lake to a depth with the same density and spread further along the isopycnal surfaces. As it was shown in Section 1.2, effect of this plunging on the vertical structure of a lake can be estimated from balancing density gradient and inertial forces, expressed by the internal Froude Number Fr (1.5) and the modified Wedderburn Number $\tilde{W}$ (1.6). Using typical values for the River Spree discharge 4-22m^3/s with average value 9m^3/s, Fr lies in range 0.01-0.04 and $\tilde{W}$ is about 20-50. The fact that the Froude Number is much less than one indicates the density perturbations to be localized in the vicinity of the inflow, and large Wedderburn Numbers allow us to say that the one-dimensional assumption can be applied to the lake to a good accuracy. During the summer, the temperature of the inflow do not differ from that at the lake surface more than by 1°C and is typically higher. It allows concluding that the river input in the lake heat budget is minimal in summer. In spring and autumn, the river influence should be generally taken into account, although the one-dimensional approximations remains valid here. The simplest way of accounting the heat inflow from the river

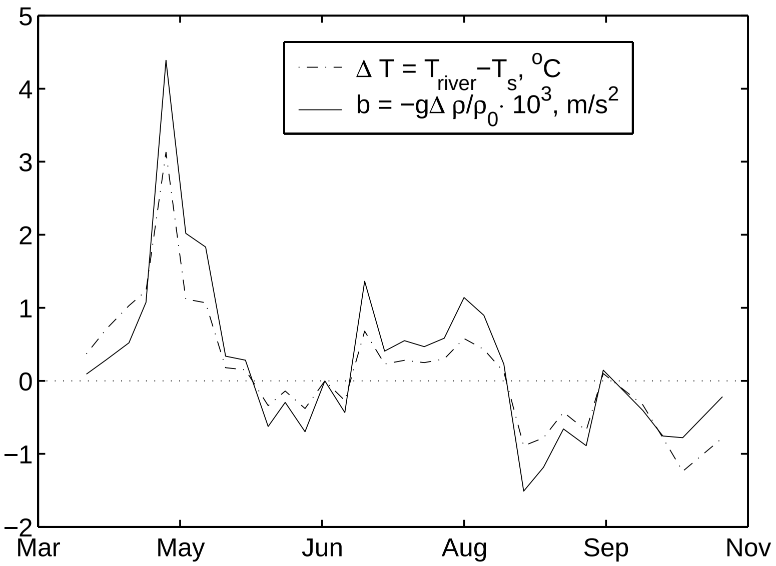

Figure 4.4: Temperature jump ΔT between the river inflow (measurements point **m3** in Fig. 4.1) and lake surface water (measurements point **m7**), and corresponding buoyancy b of the river plume, 1993.

consists in addition of the river-conditioned heat flux to the flux at the surface Q_s.

Calculations of the lake temperature evolution were performed using `TeMix` model for summer heating periods of 1980-1999. For estimation of the heat fluxes at the lake surface, data from the meteorological station **m1** were used. The time span for calculations is chosen based on available measurements data and covers the heating periods from April till November of each year that allows tracing the thermocline formation and destroy in summer. During the cold period of year the lake is entirely mixed in vertical direction that would simplify the model to solving the only one equation (3.12). Such simple one-equation models give generally good results for well-mixed temperate lakes (see e.g. Ljungemyr *et al.* 1996) and are of minor interest in scope of the current study.

The air temperature, air humidity and wind speed readings at 2 m. over the lake surface were used for calculation of the sensible and latent heat fluxes and of the friction velocity. The sensible heat flux and momentum flux across the air-lake interface were calculated following the procedure described in (Mironov, 1991). The algorithm includes calculation of the sensible and latent heat fluxes from the measurements of air temperature, air humidity and wind speed at a given height together with the water surface temperature taken from model predictions at the previous time step. The short-wave solar radiation measured directly over the lake surface was transformed in subsurface values by subtraction of the reflected part. Albedo of the water surface was calculated from atmospheric transmittance (the ratio of measured insolation to the no-atmosphere insolation) using the method described in (Payne, 1972). In addition, the solar radiation data from the standard meteorological observations at the Potsdam meteorological station (52.38°N,13.52°E) were used for verification of the local observations.

The emission of the long-wave radiation by the water and by the atmosphere was estimated from the air temperature and air humidity measurements at the **m1** station and the water temperature values predicted by the model using the bulk algorithm described in (GGO manual 1982, see also Fung *et al.* 1984). Information about the cloud conditions is not collected at the lake station and was adopted from the Extended Edited Cloud Reports (Hahn & Warren, 1999), allowing estimation of the long-wave radiation emission by cloud cover.

4.2 Prediction of the surface temperature and stratification occurrences

The initial model calculations were performed with the solar radiation data from the lake meteorological station **m1** (see Fig. 4.1). The model results exhibited in this case a regularity in the prediction error: when the model predicted the surface temperatures in 1990-1999 fairly well and errors had rather random nature, the temperature estimations for 1980-1989 had a systematic positive bias, achieving few degrees in magnitude. In order to verify the input information quality, the incoming solar radiation values measured at the **m1** station were compared with those from the Potsdam meteorological station. The comparison clearly shows an overestimation of the insolation values by the sensor at the lake station in the eighties and a good agreement between the both data sources afterwards (Fig. 4.5). Correction of the model input by accepting the Pots-

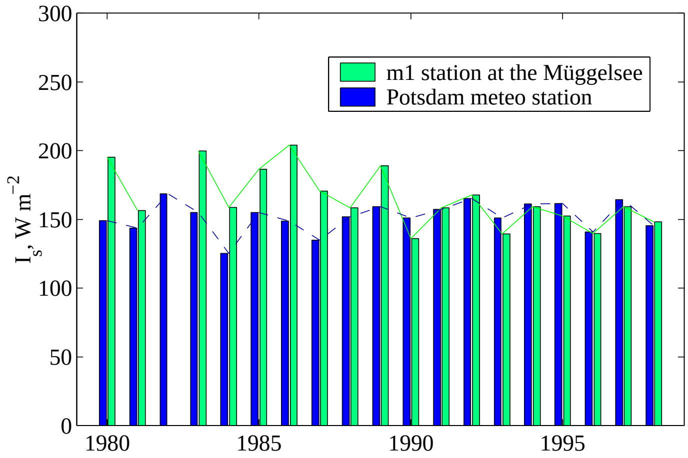

Figure 4.5: Incoming solar radiation I_0 measured over the lake at the **m1** point (green) and at the Potsdam meteorological station (blue) averaged over summer periods.

dam insolation values resulted in a reasonable agreement between the predicted temperatures and observations. An example of the surface temperature evaluation with different radiation inputs is shown in Fig. 4.6. The overestimation of radiation values by the sensor installed over the lake

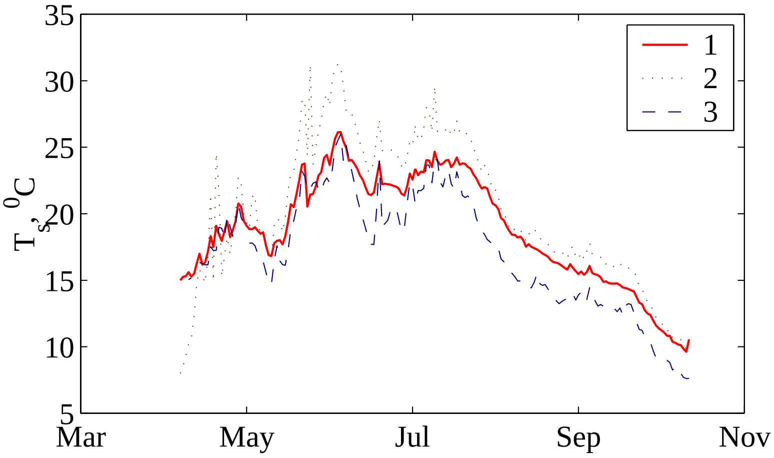

Figure 4.6: Surface temperature T_s evolution in 1986. 1,2 - T_s calculated: 1 - using I_0 from Potsdam , 2 - using I_0 from **m1**; 3 - T_s measured at **m1**.

surface was probably caused by additional short-wave radiation reflected by the water. In 1990 the construction of the measuring station was improved providing only the downward radiation be measured. As seen in Fig. 4.5, it resulted in decreasing of measured quantities that brought them in accordance with Potsdam measurements. For years after 1990, both solar radiation inputs lead to similar model output with slightly better prediction when direct measurements over the lake are used. (Fig. 4.7).

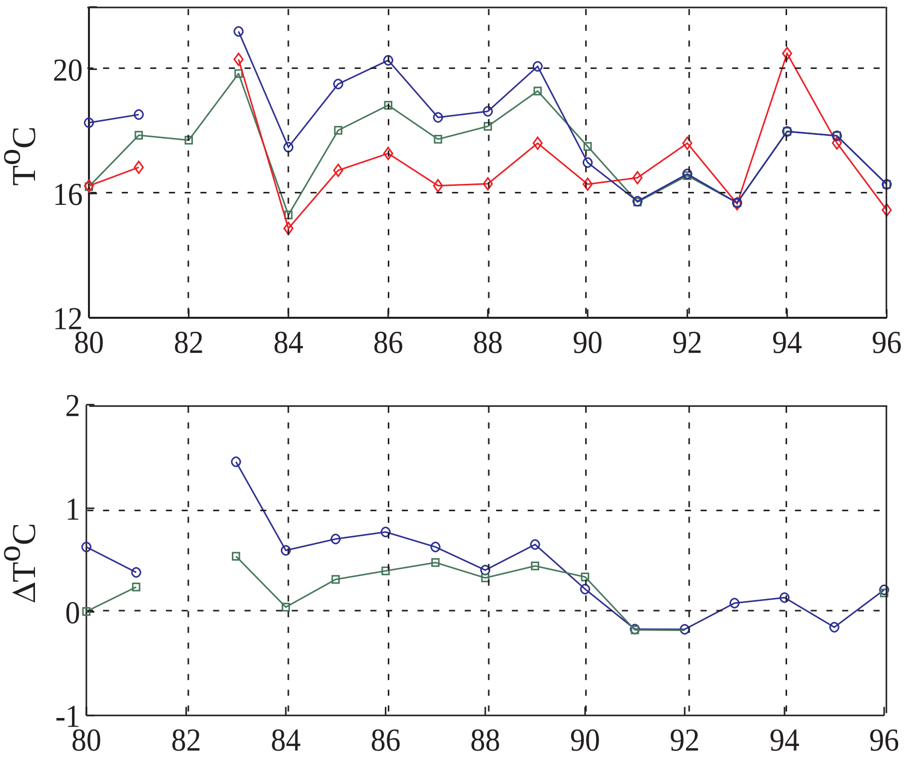

Figure 4.7: Surface temperature $\overline{T_s}$ (up) averaged over summer period and error in it's estimation $\overline{(T_s - T_{s\,\mathrm{mes}})}$ (middle). blue-circles: with solar radiation input from **m1**, green-squares: using Potsdam solar radiation data, red-diamonds: measured surface temperatures $T_{s\,\mathrm{mes}}$.

The small difference in measured radiation values at the two points and, as a result, in model predictions are caused apparently by the local cloudiness variability. Being more representative, the measurements data from the **m1** station was used as the model input for years 1990-1996, while the short-wave radiation data from the Potsdam station were adopted in calculations for 1980-1989.

This example illustrates a "feedback" between a lake dynamics model and observations. Modeling results provoked a revision of observations data and allowed uncovering uncertainties in the measurements. It speaks also to the advantage of the model's reliability: the model responds adequately to changes in the input data and predicts the real situation well if and only if the input is correct.

The general modeling results for all simulated years are shown in Figure 4.8. The year 1982 is excluded from consideration, since the were no meteorological observations performed at the lake station **m1** in this period.

In the figure three outputs T_S, T_D and h of the parameterized model are drawn in comparison to their observed values. These three parameters define the vertical temperature profile, which can be reconstructed for any moment of time using Eq. (3.2). As it was mentioned before, diurnal averaging of real processes is one of the essential assumptions underlying the model, so the model profiles can differ from instantaneous measured profiles without affecting, however, the model adequacy at larger time steps. The validity of the parameterized profile representation (3.2) was discussed in Section 2.3 and we concentrate here only on the parameters prediction.

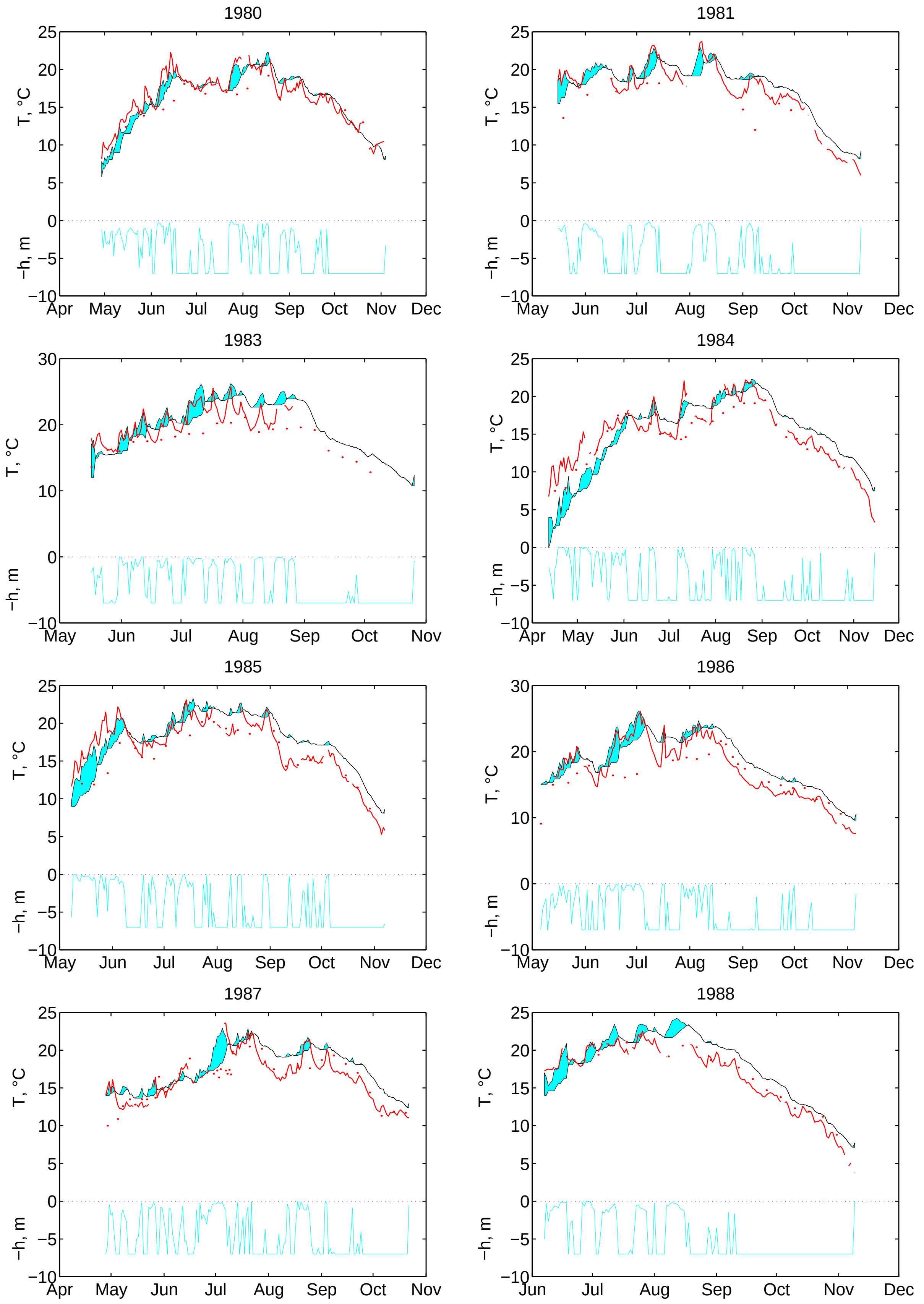

Figure 4.8: Results of the Lake Müggelsee thermal structure modeling. Red solid lines: measured surface temperature; red dotted lines: bottom temperature; black lines with filling areas represent the surface and bottom temperature values given by the model. Solid lines in lower part of plots show the UML depth.

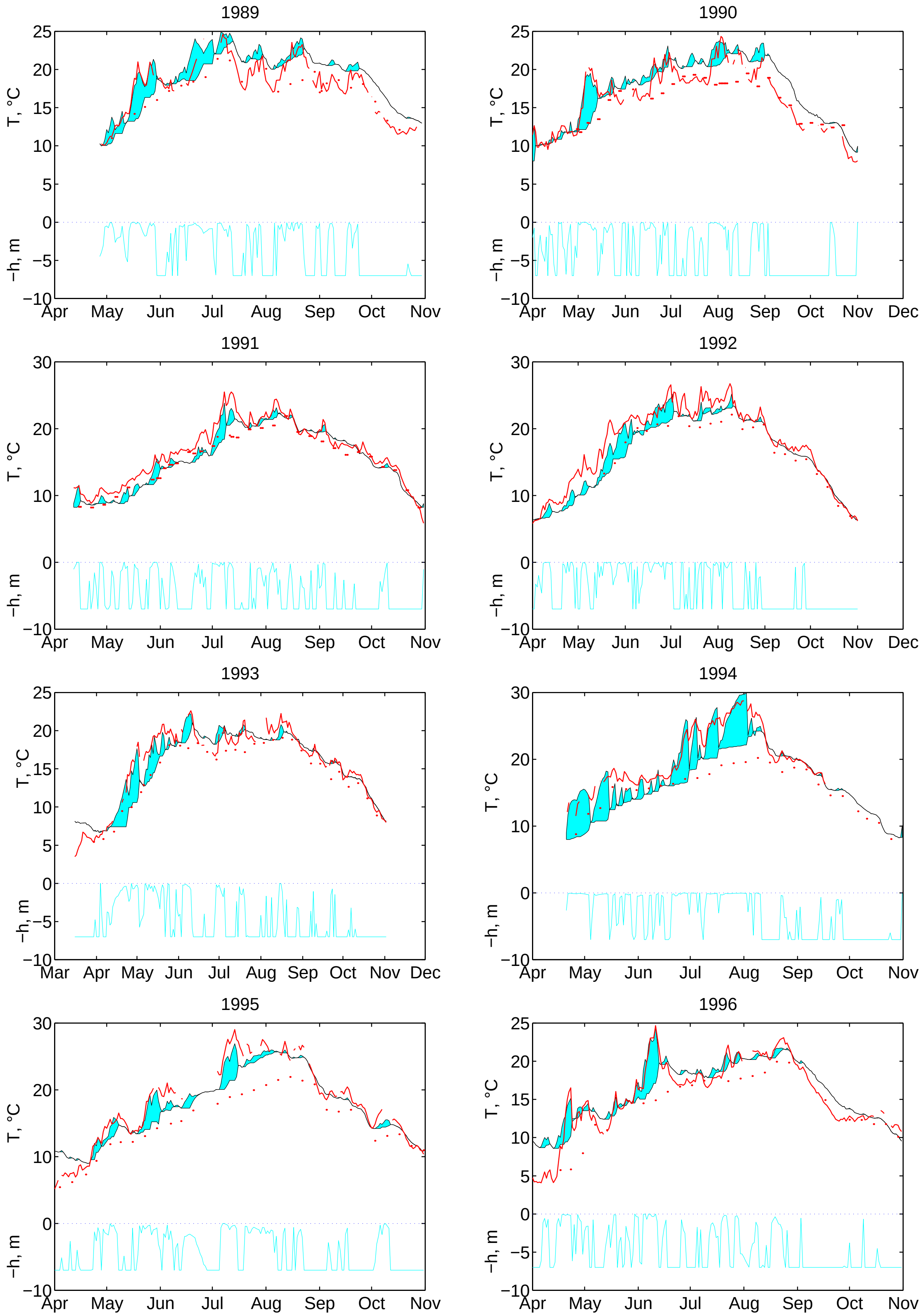

Figure 4.8: continued

Despite essential reductionism of the model, the simulation results are in good agreement with observations for all years. The model predicts well the temperature of the mixed layer as well as occurrence and destroying of the vertical stratification in the lake. The first result is important for possible integration of the model in modeling of atmosphere dynamics for estimation of the temperature and of the heat flux at the atmosphere's bottom. The information about the vertical stratification in a lake is essential in its turn for modeling of lake ecosystem components.

In some years (1984-1989) the model overestimates autumn temperatures during the whole autumn cooling period by 1-2°C. In other years, particularly in nineties, the agreement between predicted and measured temperatures is quite good. One possible reason of this disagreement can lie in neglecting of the river inflow influence, which can be important in autumn, as it was discussed in Section 4.1. On the other hand, the systematic error in eighties can result from uncertainties in measurements during this period, similar to that found in solar radiation measurements revealed above.

For relatively long stratified periods, the model tends to overestimate the near-bottom temperature (the plots for 1980, 1986, 1995 in Fig. 4.8). The disagreement is much less for large lakes but becomes more apparent when the model is applied to small shallow lakes, where the vertical stratification appears occasionally for several weeks. The similar overestimation was obtained with the previous version of the model when modeling temperatures in lakes Krasnoye, Russia and Windermere, Great Britain (S. Golosov, pers. comm.). Physically, that means an additional sink of the TKE in the water column, which is not taken into account by the model. Unlike the previous `TeMix` version, the current model entertains the vertically distributed absorption of the solar radiation, which results in dampening of the vertical mixing intensity and consequently in stronger vertical stratification. The remaining discrepancy between measured and predicted bottom temperatures can be ascribed to the TKE loss on account of internal seiches breaking in a stratified lake. Such breaking appears on sloping lake boundaries and leads to dissipation of the mixing energy here and as a result, to weaker mixing in deeper layers (Ivey & Nokes, 1989; Ostrovsky *et al.* , 1996). Apparently, the influence of sloping boundaries on the horizontally averaged temperature structure is stronger in small lakes. A parameterization of the TKE dissipation at the bottom slopes in frames of 1-dim approach will certainly improve the simulation of such strongly stratified cases. Furthermore, one should take into account that the observations presented here are performed at the deepest point of the lake and can be used only as a rough estimation of the lake-averaged bottom temperature, whereas real values can be significantly higher.

Figures 4.9 and 4.10 shows an example of the modeling results for the year 1993 in more detail. The calculated values of the surface temperatures (red line in Fig. 4.9) are very close to measured ones and the disagreement lies within confines of the horizontal variability in the water temperatures (the difference between data from the near-shore station **m1** and those from the deepest point of the lake **m7**, which difference does not exceed in its turn half a degree). The vertical temperature difference is also predicted fairly good (Fig. 4.10), even for the very short appearances of weak stratification in the end of September. The results support the general assumptions lying in background of the `TeMix` and demonstrate the model be a trustworthy tool for the lake surface temperature prediction.

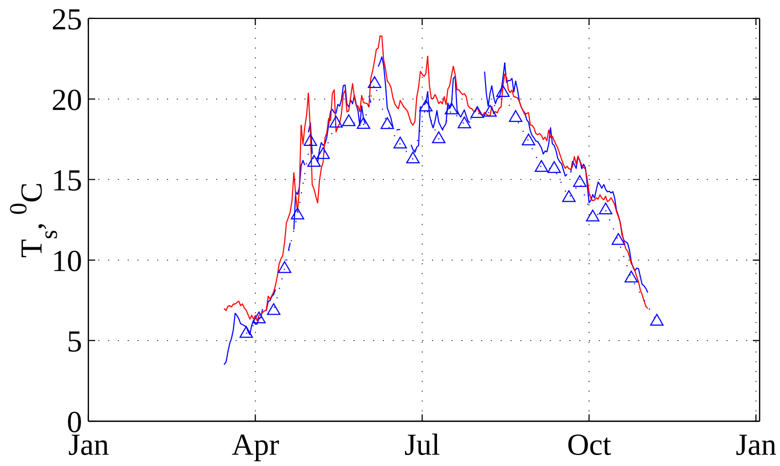

Figure 4.9: Surface temperature evolution in 1993 from IGB meteo station **m1** (solid blue line), from **m7** measurement point (blue dotted line and triangles) and that achieved with `TeMix` modeling (solid red line)

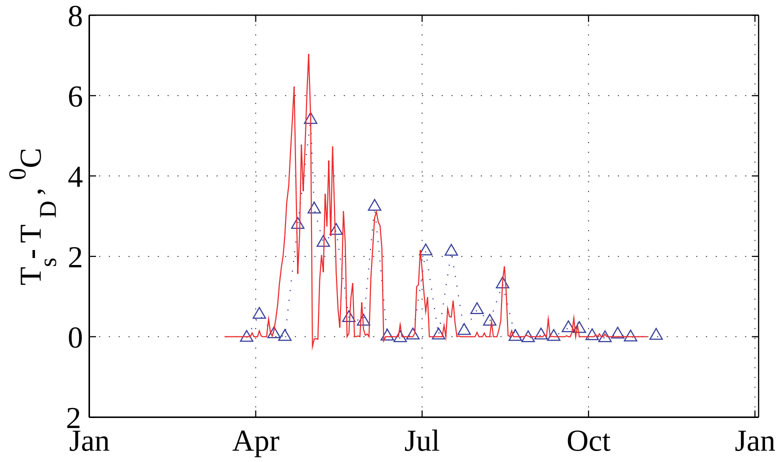

Figure 4.10: Surface-bottom temperature difference in 1993 at the deepest point **m7** (dotted blue line and triangles) and that achieved with `TeMix` modeling (solid red line)

4.3 Mixed layer depth prediction. Comparison with observations and with turbulence closure models

An important part of the model output is the upper mixed layer depth. It's value is a fundamental parameter characterizing the vertical structure of the lake and is used as appropriate length scale in ecological modeling. An example of the UML depth prediction by the model is shown in Figure 4.11. In order to examine the reliability the calculated value, gradients of the temperature and the oxygen concentration as they measured at the **m7** point are presented at the same figure as two-dimensional time-depth plots. The comparison with the O_2 concentration is performed here since this characteristic is more sensitive to mixing and gives often a better performance in the mixing layer definition (Behrendt *et al.* , 1993). An overall agreement can be seen at both plots, probably more distinct when compared with the oxygen distribution. It is relatively difficult, however, to estimate the validity of the model prediction for the UML depth on the available observations data. Vertical profiles of the water temperature and O_2 concentration were taken at **m7** only once a week, that does not allow to trace the UML evolution carefully. In order to evaluate the model additionally, the `TeMix` predictions were tested against the results of two-equation turbulence modeling.

Comparison of the bulk model `TeMix` performance with turbulence closure models is of apparent interest per se. The two-equations modeling approach in form of k-ϵ and Mellor-Yamada k-kL models have became to the moment a “standard” in modeling of vertical structure of natural water bodies. Ranking between simple but often coarse bulk models and more precise

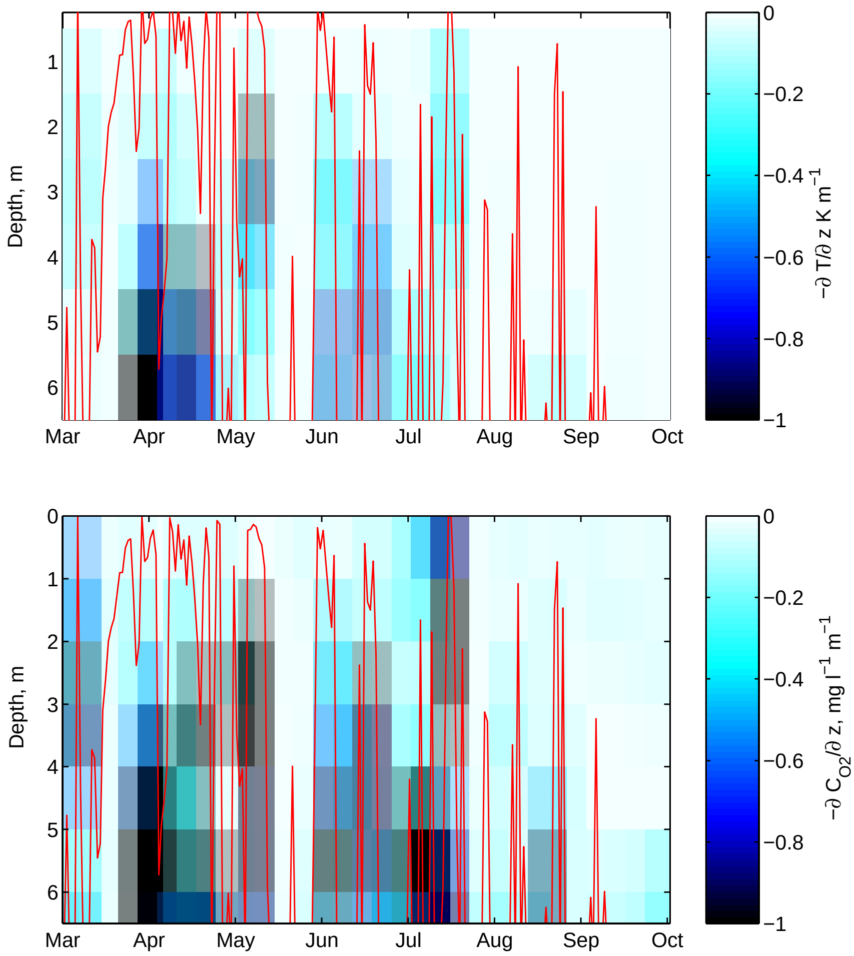

Figure 4.11: Measured temperature (up) and oxygen concentration (down) vertical gradients in comparison with the calculated mixed layer depth (solid line). Müggelsee, 1993

but computationally cumbersome methods such as large-eddy simulation (LES) and direct numerical simulation (DNS), the turbulence closure models are the most exploited compromise in engineering and research applications related to 1-d vertical modeling of geophysical turbulent flows. This kind of models is however not *a priori* a better choice for lake modeling than parameterized bulk-models. While using direct numerical solution of the differential TKE transport equation, the models involve eddy-diffusivity concept where stratification influence is modeled by means of so-called stability functions (see e.g. Burchard & Bolding 2001), which definition supposes essential arbitrariness and has often an obscure physical meaning. The relevance of the eddy-diffusivity coefficient concept is questionable by itself in application to stratified lakes, where the local shear turbulence is of minor importance compared with internal wave motions (Imberger, 1994).

The source code of the model GOTM (`http://www.gotm.net`) was adopted with minor modifications allowing its implementation on the PC platform. The code is aimed at two-equation turbulence modeling in both k-ϵ (Svensson, 1978) and Mellor-Yamada (Mellor & Yamada, 1974, 1982) variants with different parameterizations for the stability functions. Here, the second-moment closure is used proposed by Canuto *et al.* (2001), as providing the best overall performance for the mixed layer modeling (see comparison of different schemes in Burchard &

Bolding 2001 for further discussion).

An example of the surface temperature prediction by the k-ϵ and Mellor-Yamada (MY) two-equation models is shown in Fig. 4.12. Both k-ϵ and MY models predict the overall tendency in

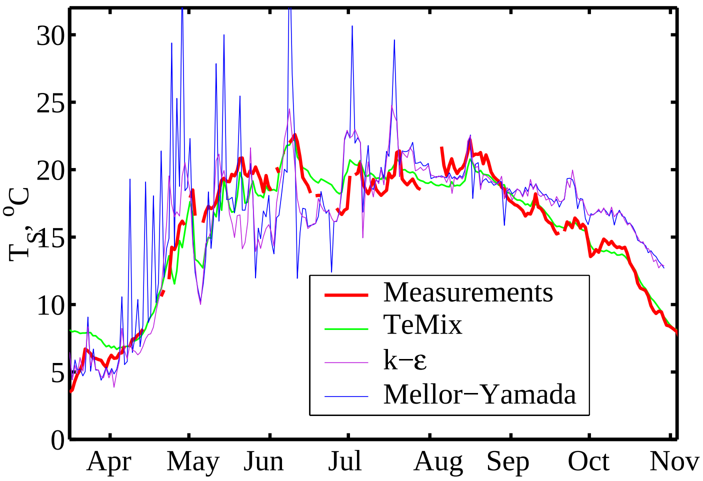

Figure 4.12: Surface temperature calculated with the k-ϵ model, the Mellor-Yamada level 2.5 model, and by the `TeMix` model compared with temperatures measured at the **m1** station, the Lake Müggelsee, 1993

the evolution of the surface temperatures. However, the small-scale oscillations achieving 10°C in amplitude are distinguished in the modeling results, especially for the MY model. In contrast, the `TeMix` results are free from such instability. Furthermore, the current model predicts correctly the autumn temperature at the lake surface after the stratification period, while the turbulence models overestimate it. This fact argues in favour of the `TeMix` algorithm as adequately reproducing the overall heat budget of a lake.

The vertical temperature gradients predicted by k-ϵ and MY models are compared with the UML depth in the Fig. 4.13 in the way analogous to that of the Fig. 4.11. Both k-ϵ and MY models produce similar vertical structure and the agreement with the UML prediction by `TeMix` is clearly distinguishable: the colored areas representing the stratified parts of the water column, are delineated by the mixed layer boundary with the good accuracy.

An alternative method of the UML depth determination from the k-ϵ model consist of associating it with some marginal value of the TKE production. In Figure 4.14 the areas with the TKE $\geq 10^{-5}$ m^2/s^2 as predicted by the k-ϵ model are compared to the mixed layer depth given by `TeMix`. The agreement between the two UML depth predictions is fair.

Thus, the bulk parameterization of the vertical turbulent transport underlying the `TeMix` algorithm accounts for the essential circumstances of the real vertical exchange omitting numerical complexity appropriate to the two-equational turbulence models. Furthermore, the bulk algorithm is free from numerical instability of the turbulence models. This instability results in unrealistic surface temperature estimations by k-ϵ and MY models on account of rapid surface heat flux oscillations which are in their turn typical for small lakes.

The interannual variability of the mixing regime given by the modeling results is compared in Figure 4.15 with the weekly temperature profiles from the **m7** measurements point.The predictions are in satisfactory agreement with observations within the limits of measurements accuracy. The peak in stratification continuance in 1982 is not predicted by the model, apparently on account of lack of measurements data. No meteorological observations were performed at the lake this year and the model simulation was based on meteorological data from the Potsdam station. In interannual variability a small trend to strengthening of stratification in nineties is predicted by the model and can also be distinguished in the observations. It can be caused by climatic

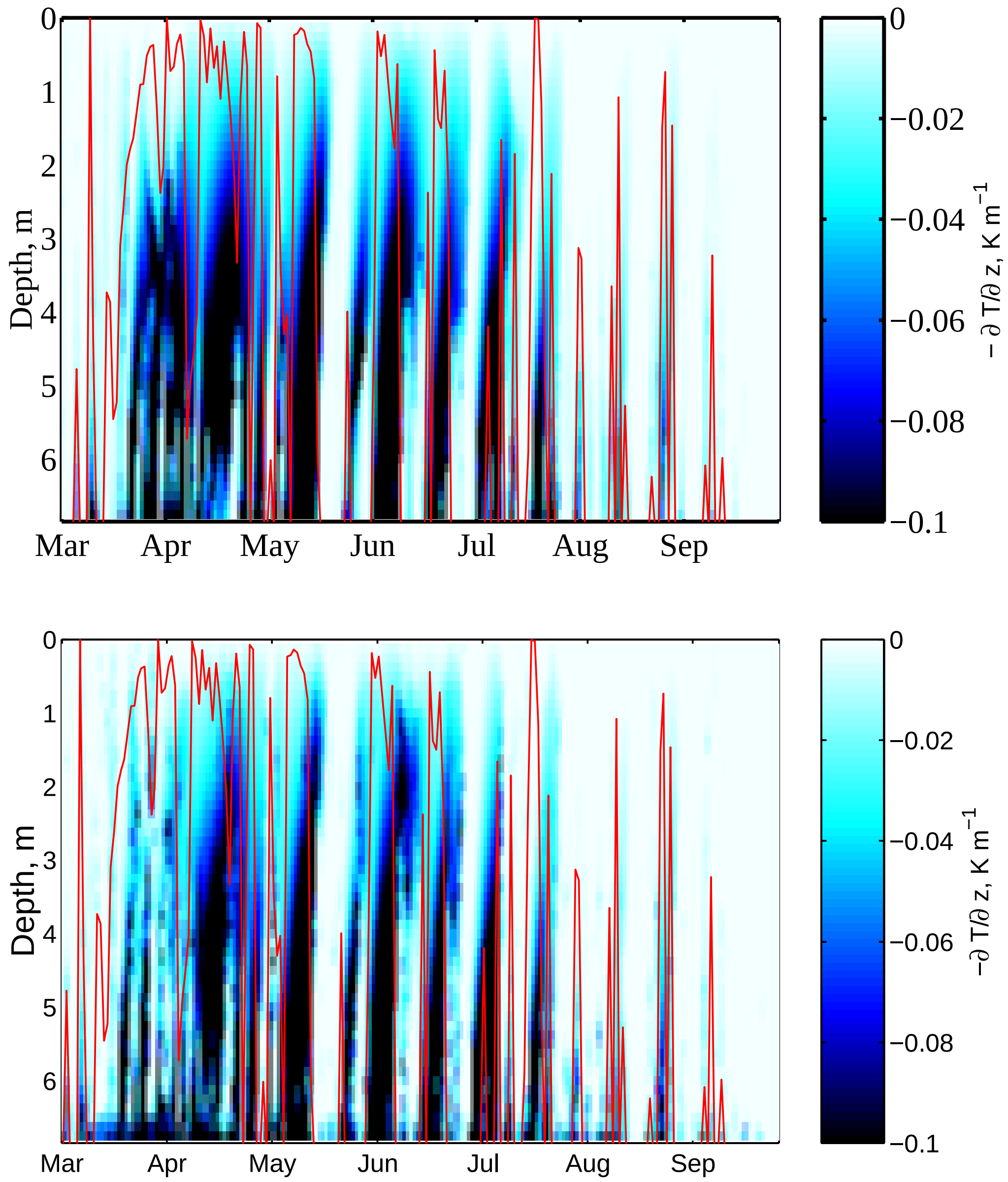

Figure 4.13: Temperature gradient calculated with k-ϵ (up) and Mellor-Yamada level 2.5 model (down) and mixed layer depth from `TeMix` (red line). Müggelsee, 1993

changes, but also alterations in water transparency driven by eutrophication can lead to changes in thermal regime of the lake. The effect of water transparency on temperatures in the Lake Müggelsee is considered in some detail in following section.

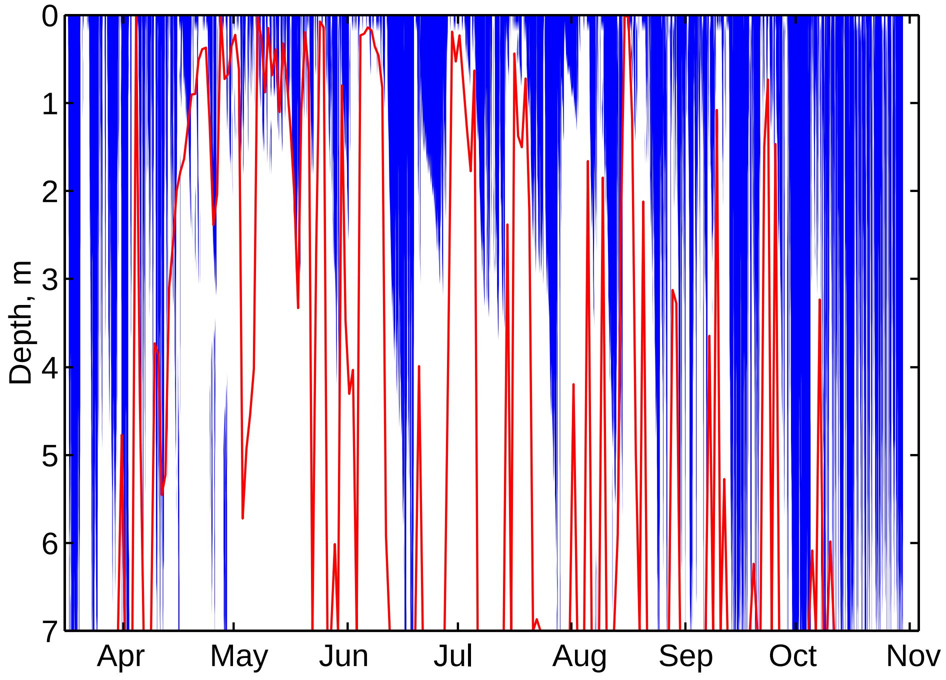

Figure 4.14: UML depth calculated with `TeMix` (**red line**) versus well-mixed regions (q $\geq 10^{-5}$ m^2/s^2) predicted by k-ϵ model (**filled areas**). The Lake Müggelsee, 1993.

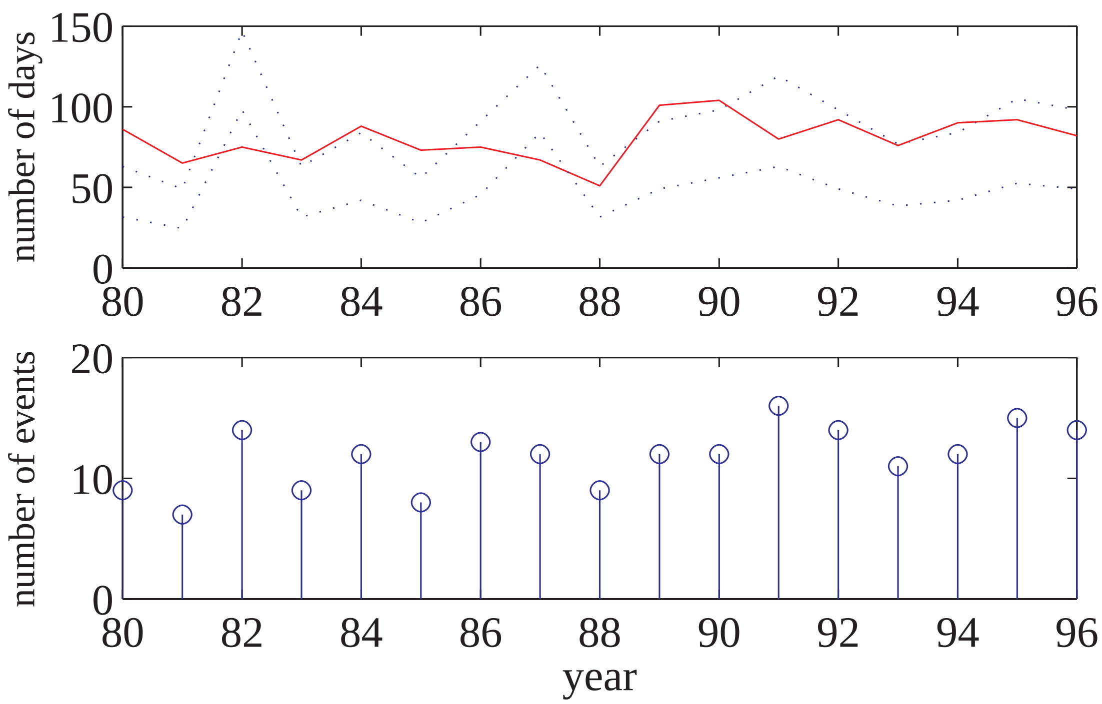

Figure 4.15: Prediction of the mixing regime in a polymictic lake. The number of days with temperature stratification (above): red line is the model prediction; blue dashed lines are the measurements at the deepest point (**m7**) with confidence range estimated as $\pm n\Delta t/2$ where n is the number of events (the plot below), $\Delta t = 1$ week is the measurements frequency.

4.4 Influence of the water transparency variability on temperature structure

The important feature differentiating the current model from the previous `TeMix` version (Mironov *et al.* , 1991) is accounting of the vertically distributed heat absorption within the UML. When modeling the temperature evolution in deep lakes [e.g. the Lake Ladoga (Mironov *et al.* , 1991) or lake Sevan (Rumiantsev *et al.* , 1986)], assuming all heat be absorbed at the surface produces satisfactory results. In shallow lakes, however, such assumption suggests leads to significant overestimation of the entrainment at the UML base (Fig. 4.16). Absorption of the short-wave so-

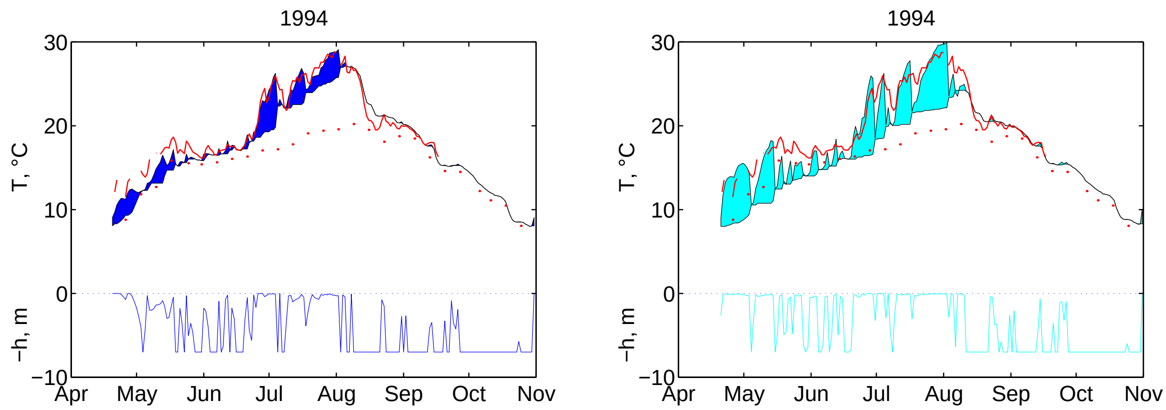

Figure 4.16: Simulation results for the summer period 1994 achieved with the old version of the `TeMix` model (**left**) and with that accounting the volumetric heat absorption inside the UML (**right**). Red solid line: measured surface temperature; red dotted line: bottom temperature; black lines with filling areas represent the surface and bottom temperature values given by the model.

lar radiation within the upper layer in oceans and lakes depends on optical properties of the water. This dependence was already included in the mixed layer model formulation of Kraus & Turner (1967) in form of the one-band exponential decay law (3.11). Dake & Harleman (1969) and later Zimmerman *et al.* (1981) emphasized the role of the water transparency in vertical thermal structure of different lakes. Most of studies dedicated to the light absorption by lake water paid the primary attention to its role in the diurnal variability of the surface temperatures (Soloviev, 1979; Woods, 1980; Price *et al.* , 1986) and to different parameterizations of the radiation decay law (Simpson & Dickey, 1981; Orlov, 1996; Hocking & Straškraba, 1999). The calculations performed here for the Lake Müggelsee made use of simplest parameterization (3.11) with a constant value of the extinction coefficient γ for each year. The main idea underlying the current model consist of adequate representation of the lake thermal structure involving a minimal set of easily available input data and a simple numerical algorithm. Therefore, it seems not relevant to introduce more sophisticated light extinction parameterizations, as the information about the dependence of γ on wavelength in particular lakes is often unknown. On the other hand, the water transparency influences not only the diurnal temperature cycle but also the biological productivity (Prézelin *et al.* , 1991) which controls in its turn the transparency of upper layers of a lake. Such feedback can result in water temperature oscillations with time scales longer than diurnal ones, conditioned by variations in the plankton biomass.

The data collected at the lake Müggelsee include the daylight attenuation measurements at the **m1** station with one hour sampling frequency. The measurements allow us to clarify the influence of the light extinction variability within a summer season on the lake water temperature.

The summer periods 1993-1999 was chosen for the analysis as having a minimum number of missed data. Remaining gaps were filled by using of linear interpolation. Time evolution of the main characteristics governing the heat exchange at the lake-atmosphere interface are shown in Fig. 4.17. Surface temperatures achieve their maximum in the beginning of August, while

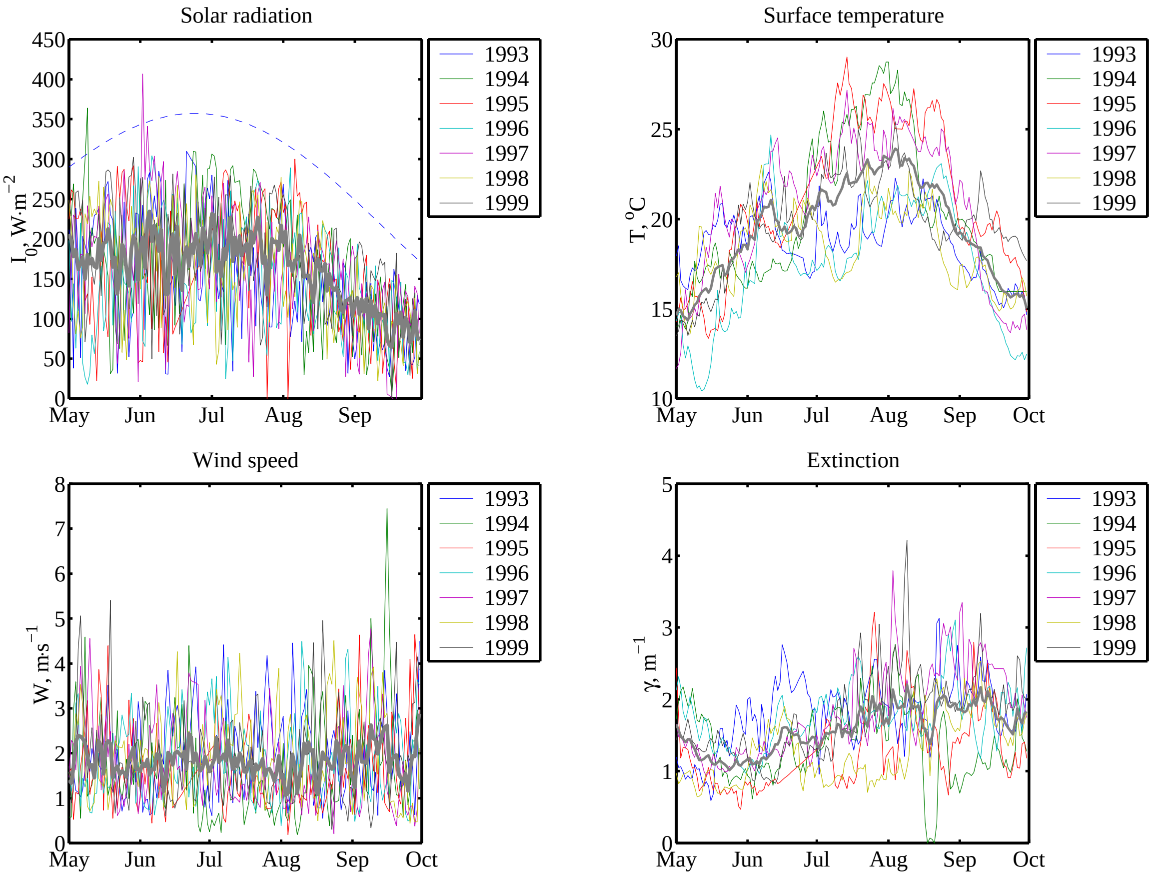

Figure 4.17: Time series of characteristics measured at the Lake Müggelsee meteorological station: Measured insolation, water surface temperature, wind speed and extinction coefficient. Thick grey line in all panels shows the average values for 1993-1999. Dashed line in the left upper graph is the "clear-sly insolation" for the given latitude.

the strongest insolation takes place over the late June (the period of the solstice). Absorption of the solar radiation by the atmosphere and clouds can be estimated from comparison of the measured radiation values with the clear-sky insolation for the current geographical position (blue dashed line in Fig. 4.17). The wind speeds are generally low tending to increase in the autumn. Warming of the lake water in the end of July is followed by extremely high values of the extinction coefficient (3–5 m^{-1}) and high frequencies in its variability.

Under conditions of low wind speed, the primary contribution in the surface temperature variability makes the process of solar radiation absorption. Figure 4.18 demonstrates the cross-spectral characteristics of this process. The figure reproduces the coherence spectrum and the phase angle evaluated for the variable pairs $I_0 \leftrightarrow T_s$ and $\gamma \leftrightarrow T_s$ (for estimation algorithm see Emery & Thomson 2001). One can see the high coherence between I_0 and T_s at frequencies corresponding to diurnal and semidiurnal oscillations; the phase angle is positive in the whole range of frequencies with significant coherence, indicating the lead of the radiation variability

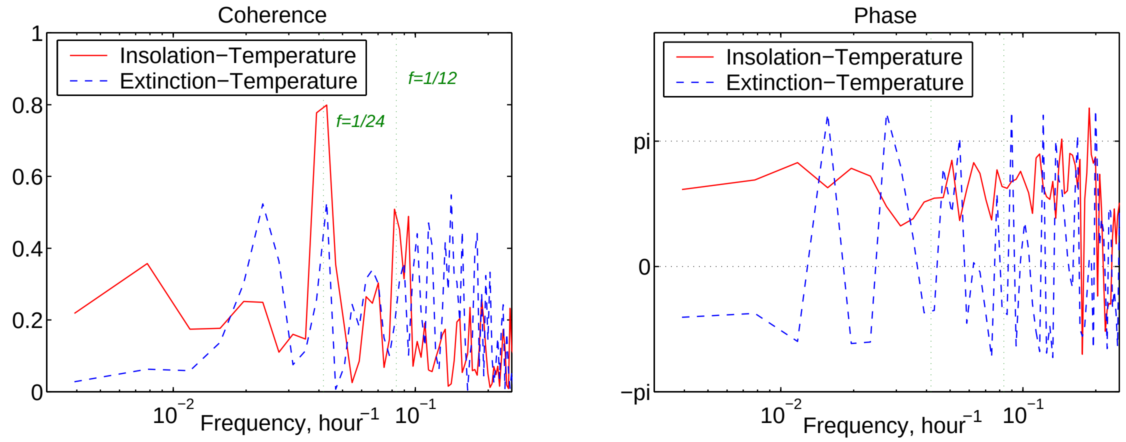

Figure 4.18: Coherence spectrum (**left**) and phase angle (**right**). Solid red line: between incoming solar radiation I_0 and surface temperature T_s; blue dashed line: between light extinction γ and surface temperature T_s. Green vertical lines correspond to the diurnal and semidiurnal oscillations.

relative to that of the water temperature. The interrelation between the water transparency and the temperature (blue dashed lines in Fig. 4.18) has more complicated nature. The coherence maximum at diurnal frequency thought exist but is much weaker than in the I_0/T_s coherence spectrum. A sufficient part of the energy is concentrated in low frequency range with a peak at 2-3 days periodicity.

Additional information about the surface temperature variability in relation to the forcing mechanisms represent the cross-correlation graphs averaged over the years 1993-1999 in the right panel of Fig. 4.19. Both the solar radiation and the wind speed are correlated with the tem-

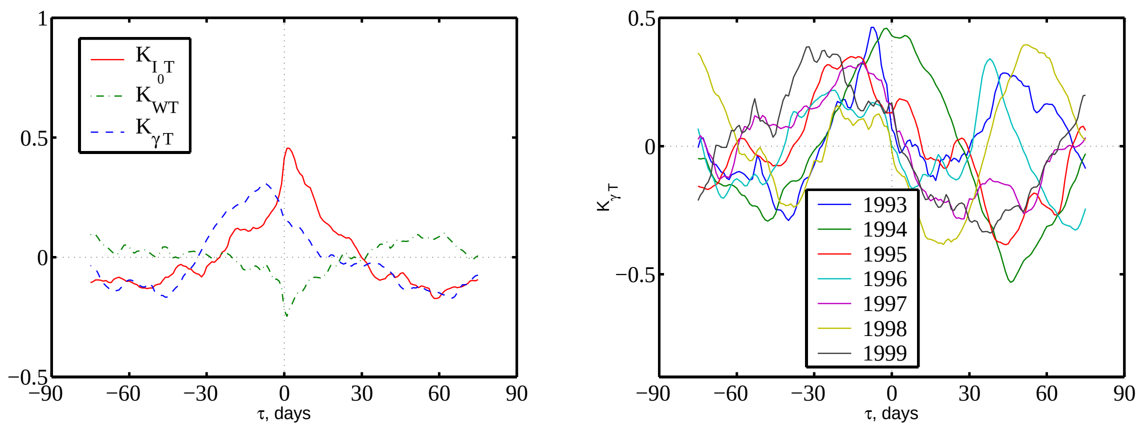

Figure 4.19: **Left panel**: Average cross-correlation for 1993-1999 between external forcing and surface temperature; I_0 vs. T_s (red solid line), W vs. T_s (green dash-dotted line), γ vs. T_s (blue dotted line). **Right panel**: cross-correlation between γ and T_s for each year.

perature at zero time lag, whereas no significant time-shifted correlation presents. The concurrent values of the water transparency and of the surface temperature have in its turn no remarkable correlation. The maximum correlation is observed at negative zero lag of several days order. It indicates the dependence of the water transparency on the surface temperatures: surface heating is apparently followed by increasing biological production and consequently by higher values of the extinction coefficient. No backward influence of the water transparency on the surface temperature is found: the correlation values at positive lags are close to zero.

The cross-correlation of the surface temperature with the solar radiation and that with the wind speed not differ significantly from year to year being close to the average curves on the left panel of Fig. 4.19. The interaction between T_s and water transparency demonstrates more diversity, as it seen in the right panel of Fig. 4.19. While most of the curves show nearly the same behavior with the correlation maximum at negative time lags, the maximum correlation in 1994 exists on positive time lags that suggests T_s oscillations be influenced by variations of γ. This variability can be caused by alterations in mixing regime in the lake. The lake-averaged balance between the two main mechanisms governing the near-surface mixing, solar heating and wind, can be expressed in terms of velocity scales w_R and u_* (see Eq. 3.31), where h in expression for w_R is replaced by the mean lake depth D. The ratio of these velocity scales will exhibit the balance between the shear TKE production and buoyancy-driven stabilization. Figure 4.20 shows this ratio averaged over summer periods. One can easily note the predominance of

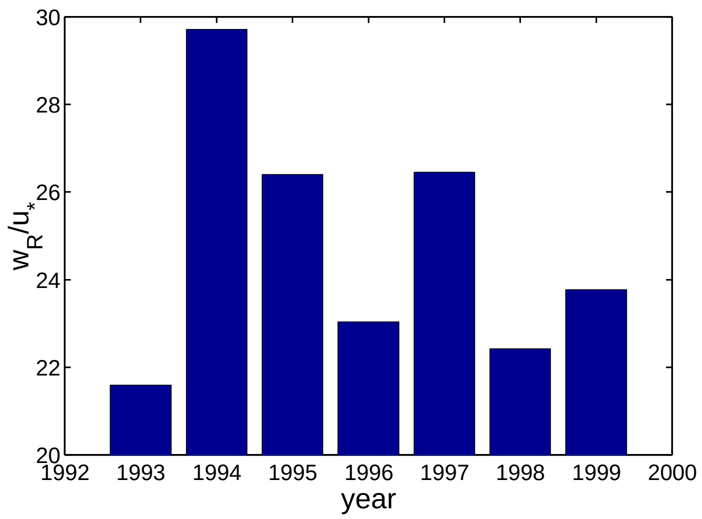

Figure 4.20: Ratio between radiation velocity scale w_R and friction velocity u_* averaged over summer periods, 1993-1999.

buoyancy forces over wind mixing in 1994. Thus, the low mixing conditions existing in this year provide the water temperatures be influenced by water transparency variability as it indicated by the cross-correlation curve in Fig. 4.19. This result gives evidence of a feedback between lake temperature and light conditions within the upper layers and suggests possible influence of lake eutrophication on water temperature: increasing plankton production is followed by stronger light extinction in lake and as a consequence in changes of the surface temperatures. As the current analysis shows, this mechanism is usually suppressed by wind mixing, but can appear important in conditions of low wind speed as it was in the Lake Müggelsee in 1994.

The predominance of stratification on account of radiatively-driven heating over the wind mixing in 1994 explains also the significant improvement of the `TeMix` predictions for this year after taking into account vertically distributed heat absorption (Fig. 4.16). Thus, the light conditions can influence noticeably the temperature structure at low winds and should be taken into consideration when modeling the vertical structure of shallow lakes. The special case represent lakes at temperatures lower than maximum density value. In this situation the radiative heating leads to destabilizing of the water column followed by convective mixing. The radiatively-driven convection is practically the only mixing mechanism in ice-covered lakes, where no wind mixing exists. This type of convection is considered in more details in following chapter using the mixed-layer approach.

Chapter 5

Radiatively-Driven Convection in Ice-Covered Lakes

Observations in ice-covered lakes (Barnes & Hobbie, 1960; Farmer, 1975; Petrov & Sutyrin, 1984; Bengtsson, 1996; Malm *et al.* , 1997a,b; Matthews, 1988; Terzhevik *et al.* , 2000) indicate that in late spring, when the snow cover above the ice disappears, a considerable part of the water column is well mixed and vertically homogeneous with respect to temperature. The homogenization was shown to occur due to convection caused by absorption of short wave solar radiation that penetrates the ice. The mechanism of TKE generation by absorption of solar radiation was briefly examined in chapter 3. Here, we consider the regime of convection driven by radiation heating in some detail. Data from observations in a number of temperate and polar lakes are summarized and discussed. A mixed-layer model is applied to simulate the mixed layer deepening. The model utilizes the mixed-layer scaling and turbulence kinetic energy (TKE) budget to derive an entrainment equation , and parameterizes the evolving temperature profile with zero-order jump approach. A stationary solution to the heat transfer equation is applied to describe the structure of the stably stratified layer separating a convectively mixed layer from the lower surface of the ice. Model predictions are compared with observational data, and entrainment regimes characteristic of convection in ice-covered fresh-water lakes are analyzed. The mixed-layer model is then extended to account for salinity effects. Although the salt concentration is very low in most temperate and polar lakes, it has important dynamical consequences when the temperature is close to that of maximum density.

Apart from its prominence as a particular class of naturally occurring convection, an understanding of radiatively driven convection during spring in ice-covered lakes is required for accurate interpretation and prediction of chemical and biological processes in lakes. For example, convective motions help suspend non-motile phytoplankton species in the surface layer, enhancing their growth (Baker, 1967; Matthews & Heaney, 1987; Kelley, 1997; Granin *et al.* , 1999a,b). In those lakes where convection is absent, motile species dominate due to their ability to position themselves in optimal light and nutrient environments (Hawes, 1983). Finally, the absence of mean shear ensures that convection beneath ice provides an ideal test case for turbulence models.

5.1 A Brief Overview of Previous Studies

Water heating by radiation penetrating the ice was mentioned by Forel (1901) as the mechanism accelerating ice melting in late spring. He did not consider the possibility of convective mixing development in ice-covered lakes, though he reported non-freezing holes of free water observed in the lake *Lac de Joux*, that suggests inhomogeneity of heat distribution in lake water under the ice. Later, Birge (1910) indicated that solar heating of the water under ice may cause convection. Considering melting of the underside of the ice, he conjectured that " . . . if the temperature rose above 4°C, convection currents might be set up which would subtract heat from the ice." He did not explicitly mention, however, that solar heating can cause convection even if the entire water column is below the temperature of maximum density.

Götzinger (1909) had presented in his paper a few photographs of melt holes in lake ice, similar to those described by Forel. He called them "Dampflöher" (steam holes). Götzinger did not attribute explicitly these holes to the differential melting of the underside of the ice caused by convective overturning of the water under the ice. However, one of these photographs demonstrates well-defined cell-like patterns on the ice cover, indicating their convective nature. The photograph is reproduced in the Fig. 5.1 and represents most likely the first implicit report of convection in ice-covered lakes. Later, photographs of shallow ice-covered ponds revealing

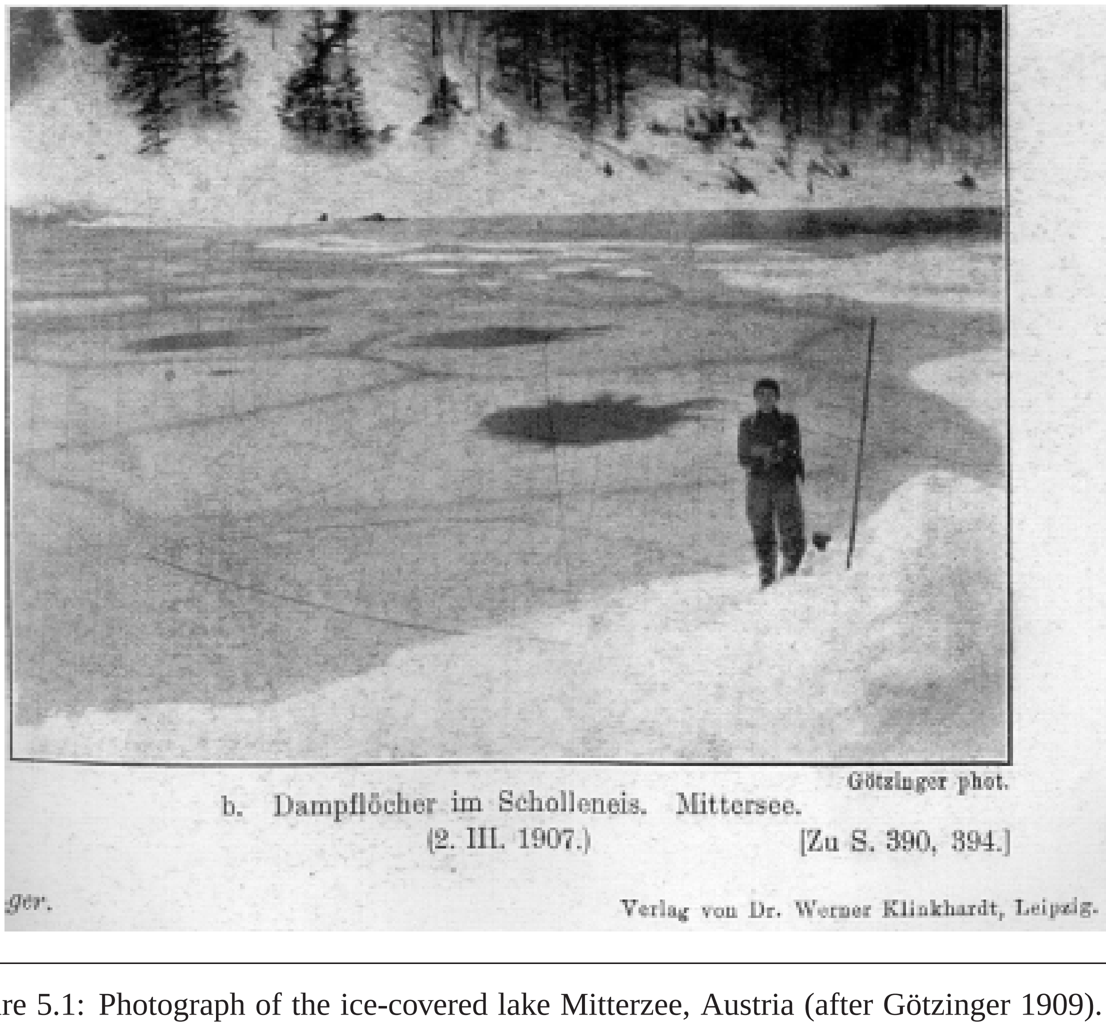

Figure 5.1: Photograph of the ice-covered lake Mitterzee, Austria (after Götzinger 1909). The author reported non-freezing "steam holes" (Dampflöcher) existing in the lake ice. One can see in the photograph, that the holes lie inside hexagonal structures similar to the Rayleigh-Bénard convective cells.

cell-like patterns were reported by Brunt (1946), Woodcock & Riley (1947), Neumann (1958), Woodcock (1965), Zwart (1976), Katsaros (1981, 1983) and Woodcock & Lukas (1983). A summary of the observations and discussion on different mechanisms responsible to generation of convective mixing under ice are given in (Mironov *et al.* , 2002).

The first systematic observations of radiatively driven convection in an ice-covered freshwater lake were reported by Farmer (1975). Detailed temperature measurements were taken in Lake Babine, Canada, between 1 February and 13 May 1973, using thermistor chains and an electronic bathythermograph. These revealed the temporal evolution of thermal structure, including initiation of instability, the properties of the upper boundary layer, convective motions within the mixed layer, the generation of internal waves at the base of the mixed layer and the evolving temperature step produced by penetration of the convective layer into the stable fluid beneath. Farmer (1975) developed a time dependent mixed layer model that accounted for the distributed buoyancy source and was matched to a stable boundary layer solution beneath the ice. In this study the theory was extended to allow for the effect of pressure on the temperature of maximum density, which is 0.02 $\mathrm{K \cdot b^{-1}}$ and can become quite important in deeper lakes.

The diurnal cycle of convection in an ice-covered lake was considered by Petrov & Sutyrin (1984). These authors used observational data and a mixed-layer model to analyze various regimes of mixed layer deepening and considered the role of entrainment in determining the rate of mixed layer growth. They also considered the Rayleigh number criterion for the onset of convection and found that a very small negative temperature gradient is sufficient to induce overturn in ice-covered lakes.

Detailed observations of convection under the ice were taken during consecutive field companies in 1994, 1995 and 1999 in two small and shallow lakes, Lake Vendyurskoe and Lake Rindozero in Karelia, north-western Russia (Bengtsson *et al.* , 1995; Bengtsson, 1996; Malm *et al.* , 1996, 1997a,b; Terzhevik *et al.* , 2000). Highly resolved temperature and salinity profiles were acquired together with direct measurements of solar radiation flux at the ice-water interface. During the spring 1999 (Terzhevik *et al.* , 2000) direct measurements of temperature microstructure were acquired within the convective layer beneath the ice leading to estimates of the turbulence kinetic energy dissipation rate. The temperature in the bottom layer at a number of locations was observed to exceed the temperature of maximum density of fresh water. Convective overturning was not detected, however, due to the stabilizing effect of salinity. Although observed values of salinity in Karelian lakes were very low, the dynamical effect of salinity stratification appeared to be significant as the water temperature was close to the temperature of maximum density.

A number of numerical modeling studies of convection in ice-covered lakes have been performed to date. Following Farmer (1975), several authors used mixed-layer models (e. g. Petrov & Sutyrin 1984; Bengtsson 1996; Mironov & Terzhevik 2000). A level model based on the heat transfer equation and a convective adjustment procedure was used by Matthews & Heaney (1987). A two-dimensional non-hydrostatic model with a k-ϵ sub-grid scale closure was applied by Pushistov & Ievlev (2000) to simulate the flow structures and the mixed-layer deepening. A large-eddy simulation model was applied by Mironov *et al.* (2001) to simulate radiatively-driven convection in ice-covered lakes.

The present study extends previous studies to consider the vertical temperature structure during radiatively-driven spring convection in ice-covered lakes in framework of the mixed layer approach. The mixed-layer scaling is developed that accounts for the vertically distributed character of the radiation heating. The scaling and similarity hypothesis for the convectively mixed layer (Zilitinkevich & Deardorff, 1974) are used to derive an entrainment equation. The similarity constants in this equation are not tuned to better fit data from measurements in a particular lake during a particular convective episode. They are evaluated independently, by comparing the entrainment laws predicted by the model with data from measurements, and by comparing the scaling relations for the TKE and its dissipation rate with data from measurements and from large-eddy simulations. In this way we avoid "tuning", which may improve an agreement with a limited amount of data and is sometimes justified, but should generally be avoided as it greatly reduces the predictive capacity of a physical model (Randall & Wielicki, 1997). A mixed-layer model that rests on the four-layer self-similar parameterization of the evolving temperature profile and involves salinity effects near the maximum density temperature is applied to simulate the mixed layer deepening in a number of temperate and polar lakes.

5.2 The Mixed Layer Model

5.2.1 The Heat Budget

The observed temperature profiles representative of the period of penetrative convection suggest that four layers can be distinguished (Fig. 5.2). In a comparatively thin surface layer just beneath the ice, the temperature increases from the freezing point at the ice-water interface to the value characteristic of the bulk of the convectively mixed layer. Convective motions in the mixed layer effectively homogenize its properties in the vertical. The temperature in the bulk of this layer is nearly constant with depth. An entrainment layer at the bottom of the mixed layer is characterized by a sharp temperature increase with respect to depth. The kinetic energy of thermals is expended there for entraining denser fluid from below, into the mixed layer. A stably stratified quiescent layer lies beneath the entrainment layer. Temperature changes in the quiescent layer occur due to the absorption of solar radiation and molecular heat conduction. As the solar heating proceeds, the depth and the temperature of the mixed layer increase. Remarkably, the evolving temperature profile preserves its four-layer structure. This permits the use of a self-similar parametric representation of the temperature profile.

Motivated by the empirical evidence, we adopt the following parameterization of the temperature profile during penetrative convection (Mironov & Terzhevik, 2000):

$$T = \begin{cases} T_s & \text{at } 0 \le z \le \delta \\ T_m & \text{at } \delta \le z < h \\ T_q & \text{at } h < z \le D. \end{cases} \tag{5.1}$$

Here, z is depth; t is time; $\delta(t)$ is the depth of the surface layer beneath the ice; $T_s(t,z)$ is the surface layer temperature; $h(t)$ is the depth to the lower boundary of the mixed layer whose temperature is $T_m(t)$; D is the depth to the bottom; and $T_q(t,z)$ is the temperature in the quiescent layer below the entrainment layer that is approximated by the zero-order temperature jump.

The Surface Layer

As the temperature, T, at the ice-water interface is fixed at the freezing point, T_f, there is always a thin layer just below the ice where the temperature increases rapidly with depth (see Fig. 5.2). Turbulence in this layer is mostly suppressed by the stable density stratification, and the heat transfer equation (3.1) can be rewritten as:

$$\frac{\partial T}{\partial t} = \varkappa \frac{\partial^2 T}{\partial z^2} - \frac{\partial I}{\partial z}, \tag{5.2}$$

Assuming the heat transfer process in the surface layer be quasi-stationary, Eq. (5.2) can be solved analytically. With $\partial T/\partial t = 0$, the solution to Eq. (5.2) describing the temperature $T_s(t,z)$

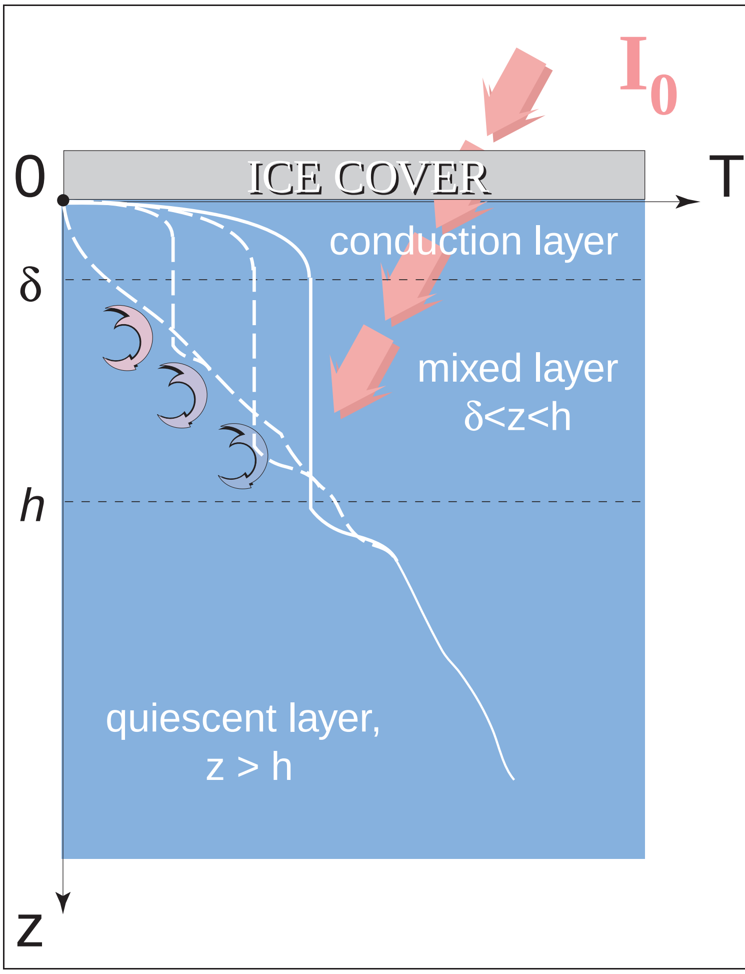

Figure 5.2: Mixed layer development during radiatively driven convection in ice-covered lakes and four-layered parameterization of the temperature profile.

in the surface layer reads

$$T_s = T_f + \frac{z}{\delta}(T_m - T_f) + \varkappa^{-1}\left(\int_0^z I dz' - \frac{z}{\delta}\int_0^\delta I dz'\right). \tag{5.3}$$

Strictly speaking, the solution to Eq. (5.2) obtained with the molecular temperature conductivity $\varkappa$ cannot be extended down to the depth of the mixed layer top δ. The reason is that there is a transition zone between the turbulent mixed layer and non-turbulent layer in the near vicinity of the ice, where the temperature conductivity considerably exceeds its molecular value. However, these peculiarities of the transition zone are ignored and the "molecular" solution is extended down to the mixed layer to match its temperature T_m. Equation (5.3) requires that the depth of the surface "conduction" layer be specified. The simplest way to determine δ is to use the condition of smooth matching for the temperature profile at the bottom of the surface layer, i.e. $\partial T/\partial z = 0$ at $z = \delta$. This gives

$$\varkappa(T_m - T_f) + \delta I(\delta) - \int_0^\delta I dz = 0. \tag{5.4}$$

The above parameterization of the surface layer was proposed by Barnes & Hobbie (1960).

In Figure 5.3, empirical data on the temperature profile in the surface layer are presented in dimensionless form as

$$\Theta = \frac{T_s - T_f}{T_m - T_f} \qquad \text{versus} \qquad \xi = \frac{\int_0^z I dz' - zI(\delta)}{\int_0^\delta I dz - \delta I(\delta)}. \tag{5.5}$$

In these co-ordinates, the temperature profile given by Eqs. (5.3) and (5.4) is simply a diagonal of the square of side one. The depth of the surface layer, δ, is determined from Eqs. (5.4) and (3.10) with the estimates of T_m, I_0, a_i and γ_i taken from measurements. Most of the data presented in Figure 5.3 were taken around noon to ensure a sufficiently high I_0 that does not vary with time too rapidly. As seen from Figure 5.3, empirical data tend to group around the diagonal $\Theta = \xi$,

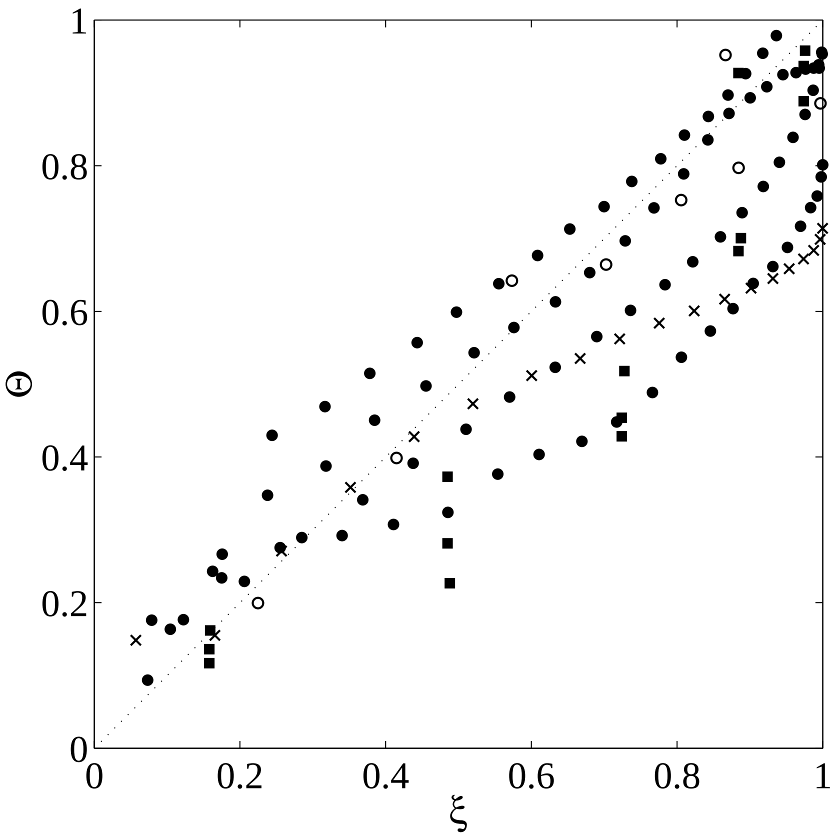

Figure 5.3: Dimensionless temperature in the surface conduction layer, $\Theta = [T_s - T_f]/[T_m - T_f]$, as function of dimensionless vertical co-ordinate, $\xi = \left[\int_0^z I dz' - zI(\delta)\right] / \left[\int_0^\delta I dz - \delta I(\delta)\right]$, where δ is determined from Eqs. (5.4) and (3.10). Open circles show data from Lake Peters, Alaska, taken on 16 May 1959 [*Barnes and Hobbie*, 1960], where a one-band approximation of the decay law with $\gamma = 0.3$ m^{-1} is used, and $I_0 = 4 \cdot 10^{-7}$ K·m·s^{-1}. Filled circles and filled squares show temperature-conductivity-depth profiles from measurements in Lake Vendyurskoe for the periods 21 – 22 April 1995 [*Malm* et. al 1996, 1997a, 1997b] and 19 – 22 April 1999 [*Terzhevik* et. al 2000]. For Lake Vendyurskoe, a two-band approximation Eq. (3.10) is used with $a_1 = 0.5$, $a_2 = 0.5$, $\gamma_1 = 2.7\,\mathrm{m}^{-1}$ and $\gamma_2 = 0.7\,\mathrm{m}^{-1}$; radiation heat flux at the ice-water interface, I_0, varies from $7.0 \cdot 10^{-6}$ K·m·s^{-1} to $1.5 \cdot 10^{-5}$ K·m·s^{-1}. Crosses are data from measurements in Lake Rindozero [*Malm* et. al 1996, 1997a, 1997b], taken on 19 April 1995, where $a_1 = 0.5$, $a_2 = 0.5$, $\gamma_1 = 7.1$ m^{-1}, $\gamma_2 = 1.5$ m^{-1} and $I_0 = 7.0 \cdot 10^{-6}$ K·m·s^{-1}.

although the surface radiation flux, the attenuation coefficients and the depth of the surface layer differ by more than an order of magnitude (e. g. δ is of order 0.2 m in Lake Vendyurskoe and is greater than 2 m in Lake Peters). The scatter of empirical data is substantial, particularly near the lower edge of the surface layer, $\Theta = \xi = 1$, indicating the effect of the mixed-layer turbulence. Notice also that the scatter of profiles taken during the 1999 field campaign is larger than the scatter of other data points. This is not surprising, however, as the 1999 measurements were performed in late spring, when the mixed-layer temperature was already close to the temperature of maximum density and the radiation heating was strong. In these conditions, the assumptions behind Eqs. (5.3) and (5.4) become more questionable. Notwithstanding these uncertainties, the overall performance of a simple solution given by Eqs. (5.3) and (5.4) is satisfactory.

Equations (5.3) and (5.4) yield the following expression:

$$Q_{wi} \equiv -\varkappa(\partial T_s/\partial z)_{z=0} = I(\delta) - I_0, \tag{5.6}$$

that can be used to compute the kinematic heat flux from water to ice.

The Quiescent Layer

The temperature in the quiescent layer below the entrainment layer should be found from the temperature transfer equation (5.2). To a good approximation, however, the effect of molecular heat transfer can be neglected. The temperature profile in the quiescent layer is then given by

$$T_q = T_{ini} + \int_0^t (-\partial I/\partial z)\, dt', \tag{5.7}$$

where $T_{ini}(z)$ is the initial temperature profile.

The Mixed Layer

In the mixed layer, the temperature transfer equation takes the form

$$\frac{\partial T}{\partial t} = -\frac{\partial Q}{\partial z} - \frac{\partial I}{\partial z}, \tag{5.8}$$

where Q is the vertical turbulent temperature flux (i.e. the heat flux divided by ϱ_0 and c_p). Since the mixed layer temperature is taken to be independent of depth, the molecular heat transfer is identically zero. Integrating Eq. (5.8) with due regard to Eq. (5.1) over the mixed layer, i.e. from $z = \delta$ to $z = h$, and using boundary condition $Q = 0$ at $z = \delta$, we obtain the following equation of the temperature budget in the mixed layer (cf. Eq. 3.16):

$$(h - \delta)\frac{dT_m}{dt} = -Q(h) + I(\delta) - I(h), \tag{5.9}$$

where $Q(h) = -\Delta T dh/dt$ is the temperature flux due to entrainment at the base of the mixed layer, and $\Delta T = T_q(h) - T_m$ is the zero-order temperature jump across the entrainment layer.

According to Eqs. (5.1), (5.8) and (5.9), the profile of the vertical turbulent temperature flux in the mixed layer is given by (cf. Eq. 3.17)

$$Q(z) = I(\delta)(1 - \varsigma) + [I(h) + Q(h)]\,\varsigma - I(z), \tag{5.10}$$

The profile differs from that given by Eq. (3.17) in replacing z/h by dimensionless vertical coordinate $\varsigma = (z - \delta)/(h - \delta)$ and by equating the turbulent flux to zero in the surface conduction layer and in the quiescent layer below the entrainment zone.

The mixed layer scaling Accounting bulk parameterization of temperature profile 5.1, the convective velocity scale (3.32) takes the form:

$$w_R = \left[-(h-\delta)B_R\right]^{1/3},$$

$$B_R = \beta[T(\delta)]I(\delta) + \beta[T(h)]I(h) - 2(h-\delta)^{-1}\int_\delta^h \beta(T)Idz. \tag{5.11}$$

The minus sign in the expression for w_R is introduced to ensure positive velocity scale, as at temperatures below the temperature of maximum density $\beta(T)$ is negative.

The physical meaning of the above scaling can be elucidated by analogy with the Deardorff (1970a,b) scaling. Consider a convective layer driven by the surface buoyancy flux. The quantity $w_*^3 \equiv hB_s$ is a measure of the generation rate of the turbulence kinetic energy in a layer of depth h by the buoyancy forces. This generation rate is the integral of the vertical buoyancy flux, the buoyancy production term in the TKE budget equation, over the convective layer. For the atmospheric convective boundary layer, for example, where the vertical buoyancy flux is to a good approximation linear, that integral is $\frac{1}{2}hB_s$. Similarly, the quantity $-\frac{1}{2}(h-\delta)B_R$ is nothing but the TKE generation rate in a layer of depth $h-\delta$ due to the radiation heating. This can be easily verified by integrating Eq. (5.10) over z from δ to h [and using a depth-constant buoyancy parameter $\beta = \beta(T_m)$]. In doing so, it is reasonable to neglect the buoyancy flux due to entrainment, $B(h)$. Since the entrainment process requires that the TKE be spent, $B(h)$ is not a measure of the TKE generation rate. The velocity scale $w_R' = \left(-\int_\delta^h Bdz\right)^{1/3}$, $B(z)$ being the vertical turbulent buoyancy flux, that unlike w_R includes the entrainment flux $B(h)$, was proposed by Farmer (1975) to estimate the velocity of convective motions in Lake Babine. Notice that when the ratio of $B(h)$ to B_R is small (which was the case in Lake Babine) the values of w_R and $2^{1/3}w_R'$ are numerically close to each other. One more example of geophysical flows where the energy considerations suggest the velocity scale very similar to w_R is convection in the atmospheric boundary layer capped by the stratocumulus clouds. A "generalized" convective velocity scale that accounts for the effect of radiative cooling near the top of the stratocumulus-capped convective boundary layer was introduced by (Deardorff, 1980) to scale data from three-dimensional numerical simulations.

Notice that the velocity scale w_R depends on the optical properties of water. A tempting possibility to simplify the scaling, Eq. (5.11), and to use the velocity scale $(-h\beta I_s)^{1/3}$ based on the surface value of the radiation flux should be discarded by the following simple reasoning. Clearly, if the water were perfectly transparent and did not absorb radiation, $I(z) = I_0$, convection would not have occurred no matter how large the radiation flux. In the opposite limit of very turbid water, where most of the radiation is absorbed in a thin layer just beneath the ice, the onset of convection depends of the strength of the initial stratification. If the water column is initially well-mixed and vertically homogeneous with respect to the temperature, convection will occur. If however the initial temperature gradient is sufficiently strong, convection will not occur. The absorption of most of the radiation just beneath the ice increases the temperature gradient there. Most of the accumulated heat is then returned back to the ice due to the enhanced molecular heat conduction, the temperature inversion is not developed, and the water column remains stably stratified. As Eq. (5.11) suggests, a simplified scale $C_s(-h\beta I_s)^{1/3}$, as used by (Kelley, 1997), that does not account for the optical properties of water is a reasonable first approximation of w_R only in the limit where the depth to the bottom of the CBL, h, far exceeds both the depth of the surface layer, δ, and the e-folding depth of the radiation flux, γ^{-1} in Eq. (3.10), and where the difference between $I(\delta)$ and I_0 is included in the dimensionless factor C_s.

Verification of the proposed scaling is made on data from direct temperature fluctuation measurements and from the LES of the radiatively-driven convection (Mironov *et al.* , 2002). Figure

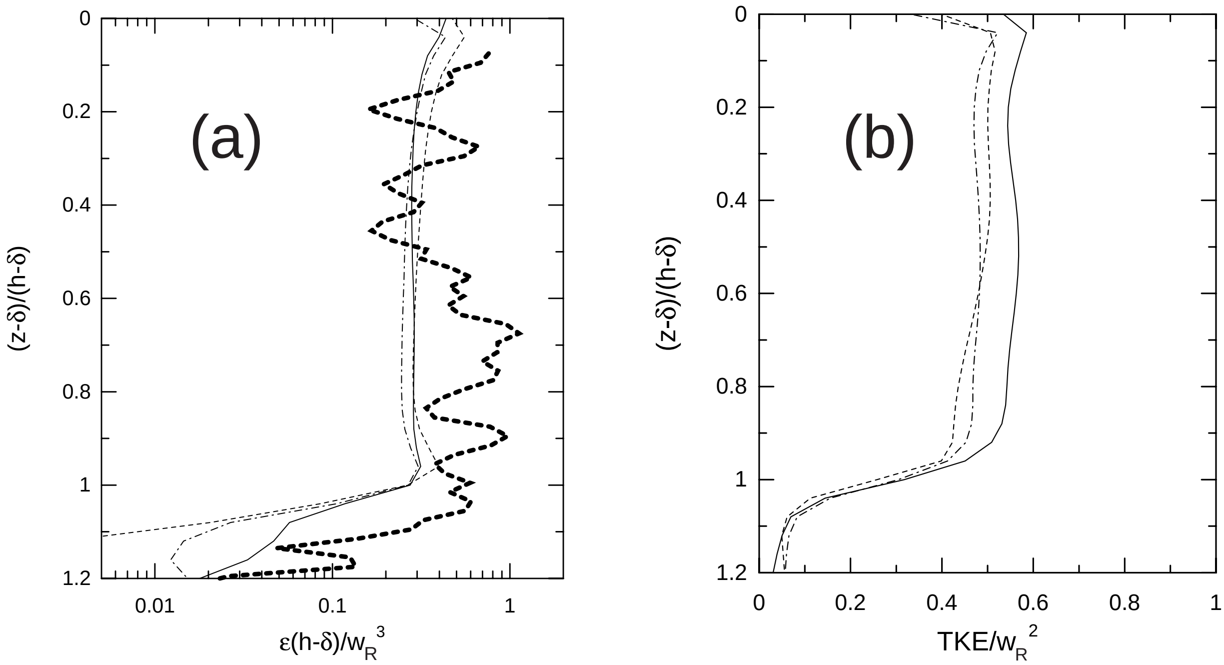

Figure 5.4: **(a):** Dimensionless TKE dissipation rate, $\epsilon(h-\delta)/w_R^3$, versus dimensionless depth, $(z-\delta)/(h-\delta)$. Heavy dotted curve shows measurements in Lake Vendyurskoe (*Jonas et. al, proposed to J. Geophys. Res.*). Thin curves show LES data for various simulations (Mironov *et al.* , 2002). **(b):** Dimensionless turbulence kinetic energy, TKE$/w_R^2$, versus dimensionless depth, $(z-\delta)/(h-\delta)$ on LES data (Mironov et. al 2001).

5.4a shows the TKE dissipation rate from LES study performed by Mironov *et al.* (2001) and that estimated from microstructure measurements (*Jonas et. al, proposed to J. Geophys. Res.*) using Batchelor (1959) method. Agreement between empirical and numerical data is fair. The dimensionless profiles show a clear tendency to group together, while the dimensional values of ϵ (not shown) differ by more than an order of magnitude between the simulations.Figure 5.4b shows the dimensionless TKE obtained from LES. Although the dimensional TKE values (not shown) differ significantly between the simulated cases, dimensionless TKE profiles group together nicely, thus supporting our mixed-layer scaling.

Some uncertainty in empirical data arises from diurnal changes of the radiation flux. Since the TKE dissipation rate does not immediately follow changes in forcing, an adjustment time on the order of a large-eddy turnover time is required, the TKE budget is not always in equilibrium. Averaging over a large number of profiles may well be required for these uncertainties to cancel out, whereas only eleven profiles are available to us.

5.2.2 The Entrainment Equation

For the horizontally homogeneous shear-free convective layer considered here, the TKE budget equation (3.24) reads

$$\frac{d}{dt}\left(\int_\delta^h e dz\right) = -\int_\delta^h \beta Q dz - \mathcal{F}_h - \int_\delta^h \epsilon dz, \tag{5.12}$$

where $\mathcal{F}_h$ is the vertical flux of energy at the bottom of the mixed layer. To arrive at Eq. (5.12), use has been made of boundary conditions $e = 0$ at $z = \delta$ and $z = h$ (strictly speaking, the lower boundary condition is established at the bottom of the entrainment zone, i.e. at $z = h + 0$), and the energy flux at $z = \delta$ has been neglected.

We utilize the quadratic state equation (3.3), which is the simplest equation of state that accounts for the fact that the temperature of maximum density of the fresh water exceeds its freezing point $T_f = 273$ K. Unless the water temperature lies beneath $T_0 = 277$ K, the buoyancy parameter β is negative and the term $\int_\delta^h \beta Q dz$ in (5.12) appears as the TKE source. For very deep lakes the effects of water compressibility should be also incorporated (Farmer & Carmack, 1981).

In order to parameterize the vertical profiles of e and ϵ, we make use of the scaling considered in section 5.2.1 above. Following numerous previous researchers (a summary is given by Zilitinkevich 1991), we employ the similarity hypothesis for the convectively mixed layer (Zilitinkevich & Deardorff, 1974). It states that the TKE and its dissipation rate, made dimensionless with the appropriate length and velocity scales, i.e. with $h - \delta$ and w_R, respectively, are universal functions of dimensionless depth $\varsigma = (z - \delta)/(h - \delta)$,

$$e = w_R^2 \Phi_e(\varsigma), \qquad \epsilon = (h - \delta)^{-1} w_R^3 \Phi_\epsilon(\varsigma), \tag{5.13}$$

where Φ_e and Φ_ϵ are dimensionless functions.

The energy flux at the bottom of the mixed layer, $\mathcal{F}_h$, is due to internal gravity waves that radiate energy into the stably stratified layer below. This flux is proportional to $N^3 A^2 \lambda$, where $N = (-\beta \partial T/\partial z)^{1/2}$ is the buoyancy frequency, and A and λ are the amplitude and length of the waves, respectively (see e. g. Thorpe 1973). Kantha (1977) assumed that A is of the order of the depth of the entrainment layer, while λ is of the order of the mixed-layer depth. Zilitinkevich (1987, 1991) took both A and λ to be proportional to the depth of the entrainment zone. Fedorovich & Mironov (1995) tested these two parameterizations against data from laboratory experiments. They found that the overall difference between the two parameterizations is rather small, although the Zilitinkevich (1987, 1991) parameterization performs slightly better. We adopt the following formulation:

$$\mathcal{F}_h = \frac{1}{2} C_w \overline{N}^3 \Delta h^3, \tag{5.14}$$

where $\overline{N}$ is the buoyancy frequency averaged over the quiescent layer $h < z \le D$, $\Delta h = h - h_0$ is the thickness of the layer where the vertical turbulent temperature flux is negative, and C_w is a dimensionless constant. The factor 1/2 on the right-hand side (r.h.s.) of the above expression anticipates the form of the subsequent result. Since the buoyancy frequency varies with depth at $z > h$, the layer-averaged N is taken as a characteristic value. The quantity $\Delta h = h - h_0$ is a crude approximation of the thickness of the entrainment layer. The zero-crossing depth of the vertical turbulent temperature flux, h_0, is determined by setting the r.h.s. of Eq. (5.10) to zero,

$$I(\delta)\left(1 - \frac{h_0 - \delta}{h - \delta}\right) + [I(h) + Q(h)]\,\frac{h_0 - \delta}{h - \delta} - I(h_0) = 0, \tag{5.15}$$

and solving for h_0.

Substitution of Eqs. (5.10), (5.13) and (5.14) into Eq. (5.12) and a little manipulation gives the entrainment equation that can be written in the form

$$(C_e + \mathrm{Ri}_\Delta)\mathrm{E}_h - C_e \mathrm{E}_\delta + C_w \mathrm{Ri}_N^{3/2} \left(\frac{\Delta h}{h - \delta}\right)^3 = C_\epsilon - \frac{2}{5} C_e \mathrm{De}. \tag{5.16}$$

Here, $\mathrm{E}_h = w_R^{-1} dh/dt$ is the dimensionless time-rate-of-change of the depth to the bottom of the mixed layer, the entrainment rate; $\mathrm{E}_\delta = w_R^{-1} d\delta/dt$ is the dimensionless time-rate-of-change of the depth of the surface layer; w_R is the convective velocity scale given by Eq. (5.11); $\mathrm{Ri}_\Delta = -w_R^{-2}(h-\delta)\Delta b$ is the Richardson number based on the buoyancy jump across the entrainment layer, $\Delta b = g a_T \left(T_m + \frac{1}{2}\Delta T - T_r\right)\Delta T$; $\mathrm{Ri}_N = w_R^{-2}(h-\delta)^2 \overline{N}^2$ is the Richardson number based on the buoyancy frequency in the quiescent layer below the mixed layer; and $\mathrm{De} = -w_R^{-4}(h-\delta)^2 dB_R/dt$ is the non-stationarity parameter (termed “the Deardorff number” by Zilitinkevich (1987), hence the notation De). Dimensionless constants C_ϵ and C_e are defined as

$$C_\epsilon = 1 - 2\int_0^1 \Phi_\epsilon(\varsigma) d\varsigma, \qquad C_e = \frac{10}{3}\int_0^1 \Phi_e(\varsigma) d\varsigma. \tag{5.17}$$

These constants should be evaluated either directly, by computing the integrals on the r.h.s. of Eq. (5.17) with $\Phi_\epsilon(\varsigma)$ and $\Phi_e(\varsigma)$ specified by the scaling relations (5.13), or indirectly, by comparing the entrainment law predicted by the model with data from measurements in natural and laboratory conditions. The estimates of $C_\epsilon = 0.2$ and $C_e = 0.8$ were recommended by Zilitinkevich (1987, 1991). They were obtained by both methods using laboratory, atmospheric and oceanic data from convective boundary layers driven by the surface buoyancy flux. These values were successfully used by Mironov & Karlin (1989) to simulate day-time convection in the upper ocean that is driven by the surface cooling but inhibited by the radiation heating. The estimate of $C_\epsilon = 0.2$ is fairly accurate. This value is commonly accepted and used in mixed-layer models of penetrative convection. It is consistent with the value of $C_\epsilon = 0.18$, with standard deviation of 0.087, determined over the upper 50 m of Lake Babine by Farmer & Carmack (1981), a calculation that included pressure effects. However, these authors also found that C_ϵ decreases rather rapidly at greater depths due to the pressure term. For Lake Babine, the pressure term reduced the work done in redistributing heat entrained at the mixed layer base relative to the work done in redistributing the same input absorbed by radiation near the surface, by 7% at 71.5 m, 34% at 100 m and 57% at 150 m. The pressure term must therefore always be included when scaling penetrative convection in lakes deeper than about 50 m.

The LES data presented in Figures 5.4 suggest slightly higher values of the dimensionless constants, but these are not in conflict with “conventional” estimates. In many entrainment regimes the mixed-layer growth is insensitive to the value of C_e, a result consistent with our solutions in section 5.3. The constant C_e becomes important when the TKE budget is strongly non-stationary, in which case an estimate based on the LES data would be inappropriate. An indirect estimate of order 1 based on observed CBL growth into a neutrally stratified fluid (in which case the entrainment equation reduces to $\mathrm{E}_h = C_\epsilon/C_e$) is preferred. Published estimates of the third constant of our model, C_w, are scarce. Using data from laboratory experiments, Fedorovich & Mironov (1995) found $C_w = 0.012 \approx 0.01$. We adopt this estimate.

5.2.3 Extension to the Case of Salt Water

When the lake temperature is in vicinity of the maximum density value, the dependence of its density on temperature $\partial\varrho/\partial T$ tends to zero and small salt concentrations existing in fresh-water lakes can influence the stability of the water column drastically. The mixed layer model described above is now generalized for the case of salt water where the salinity, S, affects the distribution of buoyancy. The salinity distribution is modeled in much the same way as the temperature distribution, i.e. through the use of a self-similar parametric representation of the profile of S.

We adopt the following parameterization for the profile of salinity that is similar to Eq. (5.1) for the temperature profile:

$$S = \begin{cases} S_s & \text{at } 0 \le z \le \delta \\ S_m & \text{at } \delta \le z < h \\ S_q & \text{at } h < z \le D. \end{cases} \tag{5.18}$$

Here, S_s, S_m and S_q are the salinities in the surface layer just below the ice, in the mixed layer and in the quiescent layer, respectively. The structure of the concentration field in the entrainment layer is approximated by the zero-order jump, $\Delta S = S_q(h) - S_m$.

Observations clearly indicate that salinity in the surface layer just beneath the ice significantly decreases after the onset of penetrative convection (Malm *et al.* , 1997a). The decrease occurs due to melting ice which releases water of lower salinity. The flux of salt due to melting ice can be estimated from the heat balance equation at the ice water interface,

$$\varrho c_p Q_{wi} + L_f M = 0, \tag{5.19}$$

where $L_f = 3.336 \cdot 10^5$ J·kg^{-1} is the latent heat of fusion, and M is the water mass flux, i.e. the amount of water released due to ice melting per a unit area in a unit time. The kinematic heat flux from water to ice, Q_{wi}, is given by Eq. (5.6). The heat flux from ice to water is neglected, although we note that if the ice is broken, the greatly increased ice-water surface area and near surface mixing leads to substantial cooling and thickening of the surface layer, temporarily overcoming the radiation induced instability and arresting convection for a few days (see Figure 6 in Farmer 1975). It is reasonable to assume that the incident solar radiation causes ice melting from above. The temperature at both the lower and upper ice boundaries is thus fixed at the freezing point T_f. We also assume that the temperature within the ice is not too different from T_f and varies only slightly with depth. Then, the heat flux through the ice that is proportional to the vertical temperature gradient is small and can safely be neglected, leading to the heat balance equation (5.19). The flux of salt at the underside of the ice, F_s, is given by

$$F_s = \varrho^{-1} M \left[S_i - S_s(0)\right], \tag{5.20}$$

where S_i and $S_s(0)$ are the salinities in the ice and in the water just beneath the ice, respectively.

The simplest model for the vertical salinity profile in the surface layer may be developed by assuming that (i) the turbulent flux of salt is zero throughout the surface layer (cf. the reasoning behind Eq. (5.3) for the temperature profile in the surface layer), and (ii) the molecular flux of salt decreases linearly from F_s at the ice-water interface to zero at the bottom of the surface layer, $-\mu\partial S/\partial z = F_s(1 - z/\delta)$, where $\mu = 5.0 \cdot 10^{-10}$ m^2·s^{-1} is the molecular diffusivity of salt in water (a value for main ions typical of lake waters, see Rodhe 1949 and Li & Gregory 1974). Then, the concentration profile that matches the mixed-layer concentration S_m is

$$S_s = S_m + \frac{F_s\delta}{2\mu}\left(1 - z/\delta\right)^2, \tag{5.21}$$

Notice that Eq. (5.21) ensures smooth matching of the mixed-layer concentration profile, i.e. $\partial S/\partial z = 0$ at $z = \delta$. The salinity in the water just beneath the ice is

$$S_s(0) = \frac{S_m + (M\delta/2\varrho\mu)S_i}{1 + (M\delta/2\varrho\mu)}. \tag{5.22}$$

Strictly speaking, the salinity profile in the surface layer should be found as a solution to the diffusion equation, $\partial S/\partial t = \mu\partial^2 S/\partial z^2$, subject to boundary conditions, $S = S_m$ at $z = \delta$

and $-\mu\partial S/\partial z = F_s$ at $z = 0$. However, a simpler problem may be considered instead if an approximate character of our model is taken into account. The salinity profile can be found as a solution to the stationary diffusion equation, $\mu\partial^2 S/\partial z^2 - F_s/\delta = 0$, where the effect of ice melting is represented as a depth-constant source term $-F_s/\delta$, subject to boundary conditions $S = S_m$ at $z = \delta$ and $S = S_s(0)$ at $z = 0$. The surface concentration $S_s(0)$ is then determined from the requirement of smooth matching of the mixed-layer concentration profile, $\partial S/\partial z = 0$ at $z = \delta$. It is easy to verify that the result is given by Eqs. (5.21) and (5.22).

The salinity of the mixed-layer should satisfy the transport equation in the form

$$\frac{\partial S}{\partial t} = -\frac{\partial F}{\partial z}, \tag{5.23}$$

where F is the vertical turbulent flux of S. Integrating Eq. (5.23) with due regard to Eq. (5.18) from $z = \delta$ to $z = h$, and using boundary condition $F = 0$ at $z = \delta$, we obtain the following equation of the salinity budget in the mixed layer:

$$(h-\delta)\frac{dS_m}{dt} = -F(h), \tag{5.24}$$

where $F(h) = -\Delta S dh/dt$ is the flux of S due to entrainment at the bottom of the mixed layer.

The salinity in the quiescent layer below the entrainment layer should be found from the solution to the diffusion equation. Salinity changes in the quiescent layer occur due to molecular diffusion only and are very slow. As a first approximation they may be neglected, and the salinity profile at $z > h$ may be kept fixed over the entire convection period,

$$S_q = S_{ini}, \tag{5.25}$$

where $S_{ini}(z)$ is the initial salinity profile.

The description of the salinity distribution is thus complete. Given an initial profile, evolution of the profile during the convective period can be found. However, as the salinity affects the buoyancy distribution, the following alterations should be made to the model equations.

The equation of state (3.3) should be amended to incorporate the salinity contribution to density. The simplest equation of state that accounts for this effect is

$$\varrho = \varrho_0 \left[1 - \frac{1}{2}a_T (T - T_r)^2 + a_S (S - S_r)\right], \tag{5.26}$$

where S_r is the reference salinity and $a_S = 7.93 \cdot 10^{-4}$ ppt^{-1} is an empirical coefficient optimized for temperature and salinity ranges of 273 K$<T<$278 K and 0<S<1. The buoyancy frequency (whose value averaged over the quiescent layer appears in the entrainment equation (5.16) through the Richardson number Ri_N) should include the effect of the salinity gradient, $N = [-ga_T (T - T_r)\,\partial T/\partial z + ga_S\partial S/\partial z]^{1/2}$.

Equation (5.15) for the zero-crossing depth of the vertical turbulent buoyancy flux should be replaced with

$$ga_T (T_m - T_r)\left[I(\delta)\left(1 - \frac{h_0-\delta}{h-\delta}\right) + I(h)\frac{h_0-\delta}{h-\delta} - I(h_0)\right] - \left(\Delta b\frac{dh}{dt}\right)\frac{h_0-\delta}{h-\delta} = 0, \tag{5.27}$$

where $\Delta b = ga_T\left(T_m + \frac{1}{2}\Delta T - T_r\right)\Delta T - ga_S\Delta S$ is the buoyancy jump across the entrainment layer. The buoyancy jump Δb also appears in Eq. (5.16) through the Richardson number Ri_Δ.

5.3 The Mixed Layer Deepening

Turning now to the discussion of the deepening of a convectively mixed layer, we use a mixed-layer model to simulate several convective episodes observed in lakes in the absence of salinity effects.

Several convective episodes have been simulated. These are the episodes described by *Malm et al.* (1996, 1997a, 1997b) for Lake Vendyurskoe, Russia, 21 – 23 April 1995, by Barnes & Hobbie (1960) for Lake Peters, USA, 16 May – 19 June 1959, by Schindler *et al.* (1974) for Lake Char, Canada, 1 – 15 June 1971, by Farmer (1975) for Lake Babine, Canada, 30 March – 30 April 1973 , and by *Malm et al.* (1996, 1997a, 1997b) for Lake Rindozero, Russia, 21 – 25 April 1995. We use the one-band and two-band approximations of the exponential decay law for solar radiation flux (Eq. 3.10).

We first focus on the most fully documented case of Lake Vendyurskoe. Using the estimate of I_0 derived from direct radiation measurements under the ice, together with the two-band approximation of the decay law with $a_1 = 0.5$, $a_2 = 0.5$, $\gamma_1 = 2.7$ m^{-1} and $\gamma_2 = 0.7$ m^{-1} (Malm *et al.* , 1996, 1997a), we compute the evolving temperature profile for the period 21 – 23 April 1995. As seen from Figures 5.5 and 5.6, although the model slightly underestimates mixed-layer depth and overestimates mixed-layer temperature towards the end of the period, predictions are in fair agreement with observations at station CS4-3 (station locations are shown in Figure 2 of Malm *et al.* 1997a). We emphasize that the constants C_ϵ, C_e and C_w in the entrainment equation, and the coefficients a_1, a_2, γ_1 and γ_2 in the radiation decay law, are estimated independently and not adjusted to improve the fit. We emphasize the close qualitative agreement between our

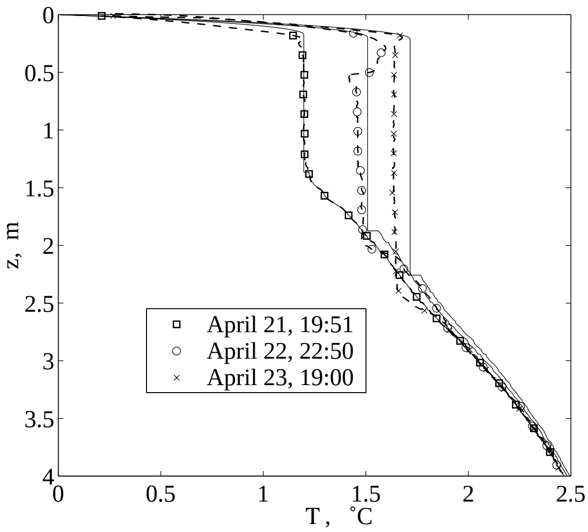

Figure 5.5: Successive temperature profiles in Lake Vendyurskoe, Karelia, Russia, 21 – 23 April 1995 (Malm et. al 1996, 1997a, 1997b). Solid curves: mixed-layer model. Curves with symbols: measured profiles. A two-band radiation decay law is used with $a_1 = 0.5$, $a_2 = 0.5$, $\gamma_1 = 2.7$ m^{-1} and $\gamma_2 = 0.7$ m^{-1} and a constant value of $I_0 = 7 \cdot 10^{-6}$ K·m·s^{-1}.

four-layer self-similar representation and the observed vertical temperature profile. Apart from a single profile on 24 April for which the upper part of the CBL exhibits an anomalous warming, the mixed layer is indeed well mixed. The temperature in the deeper quiescent layer slowly increases with time due to radiant heating beneath the mixed layer. Computed and measured values of the surface layer thickness, δ, are also in close accord. Although our surface layer model is simplified, it describes its depth and temperature quite accurately (see also the discussion in section 5.2.1). We note however, that a more sophisticated surface layer model would be required to describe effects of rapid variations in radiation flux.

Various terms in the entrainment equation (5.16) are shown in Figure 5.7 as functions of time. The leading-order terms are C_ϵ and $\mathrm{Ri}_\Delta \mathrm{E}_h$. The balance of these two terms,

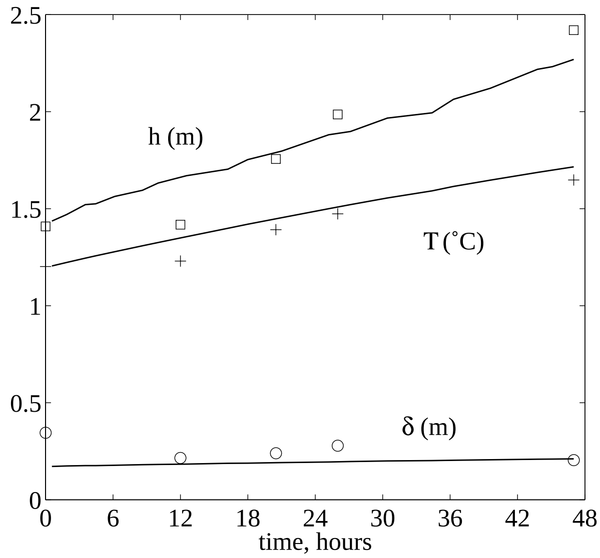

Figure 5.6: Model calculations of mixed depth, h, mixed layer temperature, θ_m, and surface layer depth, δ, in Lake Vendyurskoe 21 – 23 April 1995. Symbols are data from measurements of Malm et al. (1996, 1997a, 1997b).

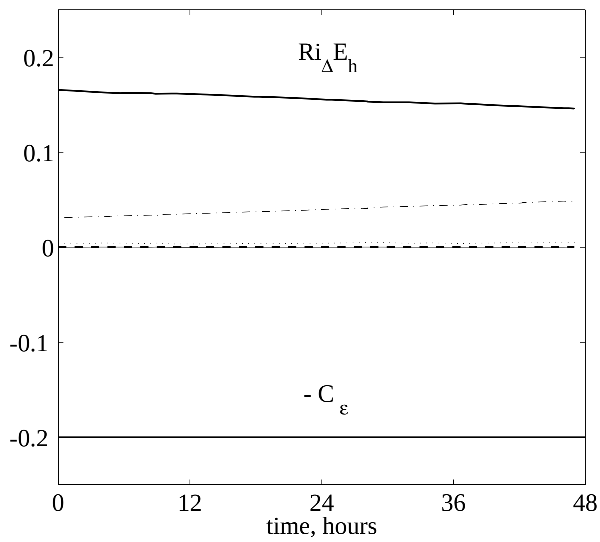

Figure 5.7: Terms in the entrainment equation (5.16) versus time for Lake Vendyurskoe 21 – 23 April 1995. Heavy solid curves show $-C_\epsilon$ and $\mathrm{Ri}_\Delta \mathrm{E}_h$ (curves are labeled), dot-dashed curve shows $C_w \mathrm{Ri}_N^{3/2} \left[\Delta h/(h-\delta)\right]^3$, dotted curve shows $C_e \mathrm{E}_h$, thin solid curve shows $\frac{2}{5} C_e \mathrm{De}$, and dashed curve shows $-C_e \mathrm{E}_\delta$.

$$\mathrm{Ri}_\Delta \frac{\mathrm{d}h}{\mathrm{d}t} = C_\epsilon w_R$$

represents the zero-jump approximation of the entrainment equation (3.35) derived in section 3.2.

Although considerably smaller, the term $C_w \mathrm{Ri}_N^{3/2} [\Delta h/(h-\delta)]^3$ is not negligible. The other terms are at least one and a half orders of magnitude smaller. This illustrates the similarity between convection beneath ice and conditions typical in the atmospheric convective boundary layer. To a first approximation, both environments are described by a simple relation $\mathrm{Ri}_\Delta \mathrm{E}_h = C_\epsilon$, i.e. by a constant entrainment coefficient $A = C_\epsilon$. The entrainment coefficient, which is a measure of entrainment efficiency, is usually defined as a negative of the ratio of the buoyancy flux due to entrainment, $B(h)$, to the surface buoyancy flux, B_s. For convection driven by radiation heating, it is natural to define the entrainment coefficient as $A = -B(h)/B_R$, which is just $\mathrm{Ri}_\Delta \mathrm{E}_h$. The regime of convection where $\mathrm{Ri}_\Delta \mathrm{E}_h = C_\epsilon$ is very accurately reproduced in two-layer laboratory experiments (see summary in Zilitinkevich 1991). Loss of energy through internal gravity wave radiation, described by the term $C_w \mathrm{Ri}_N^{3/2} [\Delta h/(h-\delta)]^3$, reduces the entrainment rate. Considering the "universal" character of the entrainment equation (5.16), i.e. the fact that it remains the same within the velocity and length scale definitions, shows that correct mixed-layer scaling is vital for modeling both of these convection regimes. Good agreement between model predictions and observations supports our choice of convective scales (5.11).

Notice that the terms $C_e\mathrm{E}_\delta$ and $\frac{2}{5}C_e\mathrm{De}$ in Eq. (5.16) that are negligible in our computation may be large for a rapidly varying radiation flux (e. g. if the diurnal variations of I_0 are considered). The term $C_e\mathrm{E}_h$, also negligible in our case, is the leading-order term (along with C_ϵ) in the convection regime where a mixed layer grows into a neutrally stratified quiescent layer. Then, the entrainment equation reduces to a simple relation $\mathrm{E}_h = C_\epsilon/C_e$. Petrov & Sutyrin (1984) showed that this regime of entrainment is encountered in ice-covered lakes during morning. It starts just after sunrise and lasts until the bottom of the mixed layer reaches the stably stratified interfacial zone formed by the end of the previous day. The term $C_e\mathrm{E}_h$ is not negligible at small times if $\Delta T = 0$ is taken as the initial condition (in our computation, $\Delta T = 0.02$ K at $t = 0$). This term remains important until the influence of initial conditions is negligible.

One more limiting regime of the mixed-layer deepening is the so-called encroachment, the regime with zero entrainment buoyancy flux. This regime was first analyzed by Zubov (1943). A model of radiatively-driven convection in an ice-covered lake based on the entrainment equation with $B(h) = 0$ was considered by Bengtsson (1996). As pointed out by Farmer (1975), whose entrainment equation accounts for encroachment as one of the limiting cases, a model with $B(h) = 0$ underestimates the rate of the mixed layer growth.

Figures 5.8, 5.9, 5.10 and 5.11 compare the modeled and measured vertical temperature profiles during convective episodes observed in Lake Peters 16 May – 19 June 1959 (Barnes & Hobbie, 1960), in Lake Char 1 – 15 June 1971 (Schindler *et al.* , 1974), in Lake Babine 30 March – 30 April 1973 (Farmer, 1975), and in Lake Rindozero 21 – 25 April 1995 (*Malm* et. al 1996, 1997a, 1997b), respectively. The empirical information available from the above four

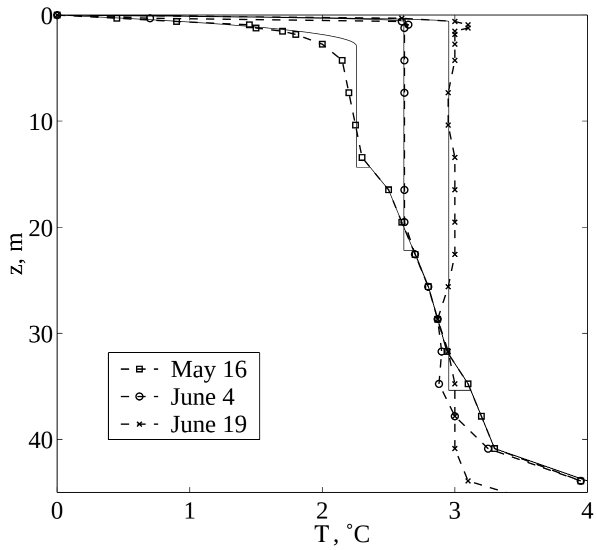

Figure 5.8: Successive profiles in Lake Peters, Alaska, 16 May – 19 June 1959 (Barnes and Hobbie 1960). Solid curves: mixed-layer model. Symbols: measured profiles. A one-band radiation decay law is used with $\gamma = 0.3$ m^{-1}. The surface radiation flux, I_0, increases linearly from $4 \cdot 10^{-7}$ K·m·s^{-1} to $8 \cdot 10^{-6}$ K·m·s^{-1} over the period of simulation.

lakes is not as detailed and accurate as from Lake Vendyurskoe, and some caution is required when interpreting the results. For Lake Peters and Lake Char, the temperature profiles are taken from temperature-depth plots; for Lake Rindozero, thermistor chains measurements are used. For Lake Babine, two temperature records obtained with an electronic bathythermograph are shown together with thermistor chain measurements [each chain has eleven thermistors with 2 m spacing on the upper instrument, 5 m spacing on the lower chain (Farmer, 1975)]. Highly resolved radiation measurements are unavailable for Lake Peters, Lake Char and Lake Babine, and we have used the one-band decay law approximation. The surface radiation flux, I_0, is

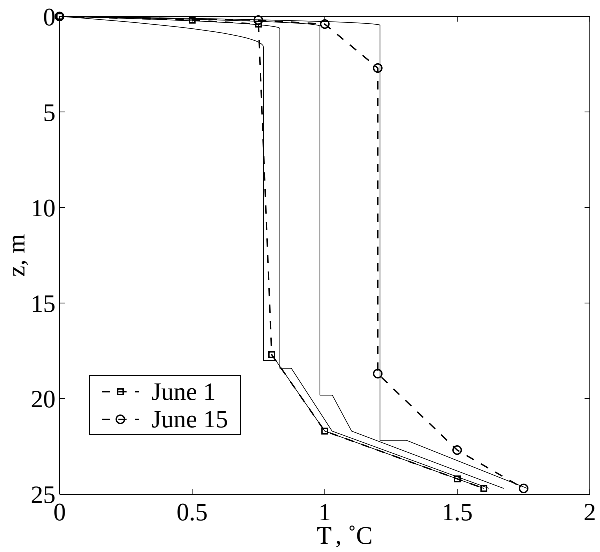

Figure 5.9: Successive temperature profiles in Lake Char, Canada, 1 – 15 June 1971 (Schindler et al. 1974). Solid curves: mixed-layer model. Symbols: measured profiles. A one-band radiation decay law is used with $\gamma = 0.1$ m^{-1}. The surface radiation flux increases linearly from $I_0 = 8 \cdot 10^{-7}$ K·m·s^{-1} to $I_0 = 1 \cdot 10^{-5}$ K·m·s^{-1} over the simulation.

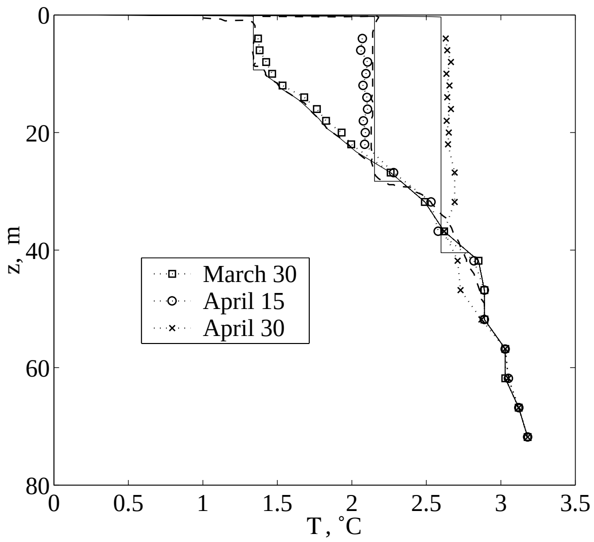

Figure 5.10: Successive temperature profiles in Lake Babine, Canada, 30 March – 30 April 1973 (Farmer, 1975). Solid curves: mixed-layer model. Dashed curves: electronic bathythermograph profiles, 30 March and 15 April. Dotted curves with symbols: thermistor chain profiles, 30 March, 15 and 30 April. A one-band decay law approximation is used with $\gamma = 0.56$ m^{-1} and a time-independent value of $I_0 = 1.2 \cdot 10^{-5}$ K·m·s^{-1}.

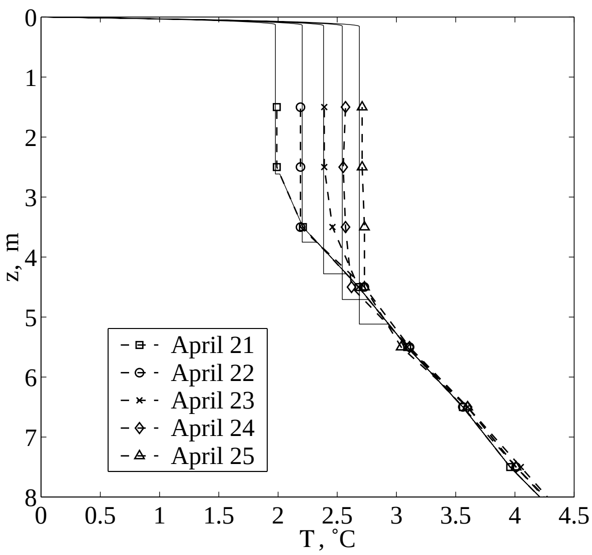

Figure 5.11: Successive temperature profiles in Lake Rindozero, Karelia, Russia, 21 – 25 April 1995 [*Malm* et. al 1996, 1997a, 1997b]. Solid curves: mixed-layer model. Curves with symbols: measured profiles. A two-band radiation decay approximation is used with $a_1 = 0.5$, $a_2 = 0.5$, $\gamma_1 = 7.1$ m^{-1} and $\gamma_2 = 1.5$ m^{-1}, and a constant value of $I_0 = 7 \cdot 10^{-6}$ K·m·s^{-1}.

either approximated by a linearly increasing function of time, or kept constant over the period of simulation, although time dependent radiation flux time series can be resolved by integration of the mixed layer heat content as a function of time (Farmer, 1975).

Despite uncertainties in the input parameters and temperature records, the model shows satisfactory consistency with the observations. Particularly good agreement is found between the model prediction and observed temperature profile 15 April 1973 in Lake Babine. The CBL depth and water transparency differ greatly between the five lakes considered here. In the three polar lakes, Lakes Peters, Char and Babine, the convective layer is a few tens of meters deep, but is less than 10 m deep in Lakes Vendyurskoe and Rindozero. Attenuation coefficients for solar radiation also differ by more than an order of magnitude. Given the independent estimation of model constants, consistent predictions over the wide range of limnological conditions reinforces our confidence in our simplified model.

5.4 The Effect of Salinity

As discussed above, in many lakes the effect of salinity stratification cannot be neglected, although the absolute values of salinity are small. When the temperature in the bottom layer exceeds the temperature of maximum density, convective mixing would have occurred were it not for the increase of salinity that maintains static stability. Convective episodes in Lake Vendyurskoe are compared with corresponding model predictions.

The salt concentrations referred to here are derived from measurements of conductivity, temperature and pressure, and converted into “salinity” using the standard oceanographic conversion algorithms. Lacking full chemical analysis of the dissolved salts, we recognize that small unknown discrepancies will exist between the density contribution of dissolved solids in any particular lake and that due to salinity derived from the oceanographic algorithms; however, we anticipate these discrepancies are minor. For consistency with the inversion algorithm, values of salinity are given using the standard oceanographic convention of “practical salinity units”.

Figure 5.12 shows the temperature (a) and salinity profiles (b) during a convective episode in Lake Vendyurskoe, Karelia, Russia, 20 April to 2 May 1994 (Bengtsson *et al.* , 1995; Bengtsson, 1996).

The profiles were acquired at station CS4-6 in the central part of the lake (see Figure 6 of Bengtsson 1996). The temperature near the lake bottom in Figure 5.12(a) exceeds the fresh water temperature of maximum density. However, the salinity profile ensures that static stability is maintained. Absolute values of S are much less than 1 ppt, as indicated in Figure 5.12(b). Nonetheless, a weak salinity stratification appears to be sufficient to prevent convective overturning of the near-bottom layer, the temperature of which is close to that of maximum density. At this temperature the thermal expansion coefficient tends to zero and thermally induced density changes are small. However, the rate of mixed-layer deepening is virtually unaffected by salinity stratification. Results from a test computation (not shown), performed with a lower boundary artificially set at $z = 9$ m where the temperature is less than T_r, and with the salinity set to zero throughout, differed little from the results shown in Figure 5.12 (the mixed-layer depth was only 0.1 m deeper with no salinity at the end of the simulation and the difference in mixed-layer temperature was negligibly small). This is because the bottom of the mixed layer has not reached the layer of significant gradient of salinity, and the mixed-layer temperature is still well below the temperature of maximum density at the end of the period considered. Although the salinity gradient enters the entrainment equation through the buoyancy frequency in the quiescent layer, its effect on the entrainment rate is small. Changes in $\overline{N}$ due to the salinity gradient produce a

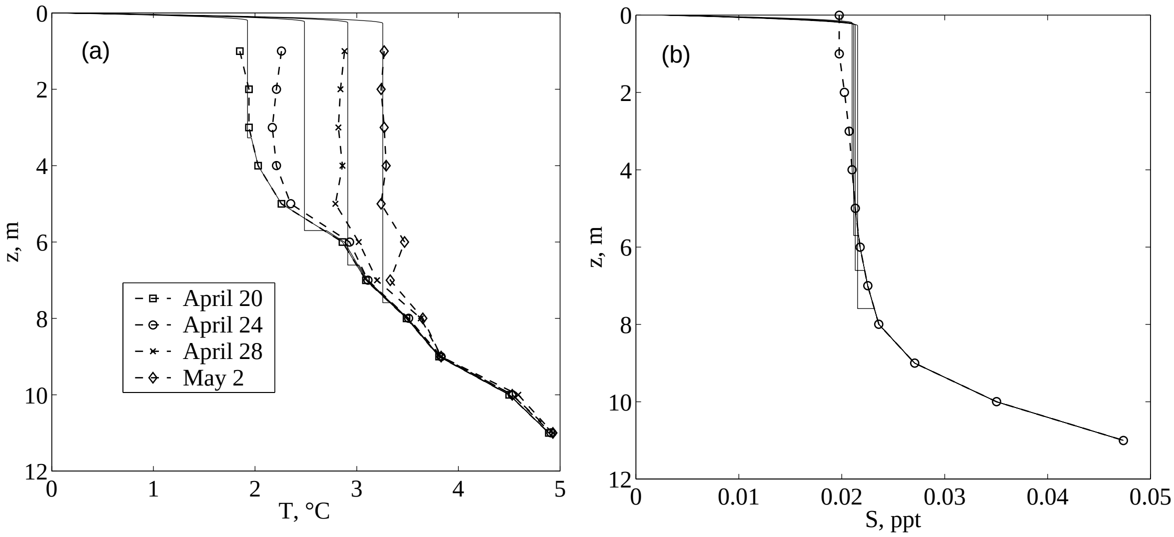

Figure 5.12: Successive vertical profiles of (a) temperature and (b) salinity in Lake Vendyurskoe, Karelia, Russia, 20 April – 2 May, 1994 (Bengtsson et. al 1995, 1996). Solid curves: model. Curves with symbols: measured temperature profiles on 20, 24, 28 April and 2 May 1994. Salinity profile was recorded 20 April 1994. A two-band radiation decay law is used with $a_1 = 0.5$, $a_2 = 0.5$, $\gamma_1 = 2.7$ m^{-1} and $\gamma_2 = 0.7$ m^{-1}, and a constant value of $I_0 = 8 \cdot 10^{-6}$ K·m·s^{-1}.

correction to the wave term, the last term on the left-hand side of Eq. (5.16), but the effect is minor relative to the entrainment terms (see section 5.3). The salinity also affects the buoyancy jump across the entrainment layer. Its contribution is small relative to that of the temperature jump.

Measurements at two stations CS4-9 (depth ∼12 m.) and CS4-9 (depth 7.5 m.) were used in model simulations of convective episode in Lake Vendyurskoe over the period 16 – 24 April 1999 (Terzhevik *et al.* , 2000; Kirillin *et al.* , 2001). The situation is different from the previous one. The simulated temperature profiles shown in Figures 5.13a and 5.14a display a curious feature. A negative temperature jump across the interfacial layer develops by the end of the simulation period. This is possible due to the stabilizing effect of salinity stratification. By late spring 1999 the CBL has reached a depth where there is a substantial salinity gradient that tends to slow the penetration. Further heating of the mixed layer results in a negative temperature jump below the mixed layer, clearly remarkable in Fig. 5.14. However, the salinity stratification (figures 5.13b and 5.14b) is sufficient to stabilize the profile even in the presence of the temperature structure, so that the buoyancy jump across the interfacial layer remains negative, see Figures 5.13c and 5.14c.

At the station CS4-9 (5.13), the temperature near the lake bottom exceeds T_r. The water column remains statically stable, however, due to the stabilising effect of salt concentration. Notice that the absolute values of S are very small, two orders of magnitude less than a typical oceanic value. Nonetheless, a weak salinity stratification appears to be sufficient to prevent convective overturning of the near-bottom layer whose temperature is close to T_r. As seen in Fig. 5.13, the simulated profiles of temperature, salinity and buoyancy are in fair agreement with observations. Figure 5.15 shows salinity profiles just beneath the ice. Computed values of salinity just beneath the ice agree well with values observed at both stations. The profiles of salinity in the conduction layer at the station CS4-6 (right plot in Fig. 5.15) are also reproduced fairly good by the model. Salinity profiles at the station CS4-9 vary considerably (left plot in

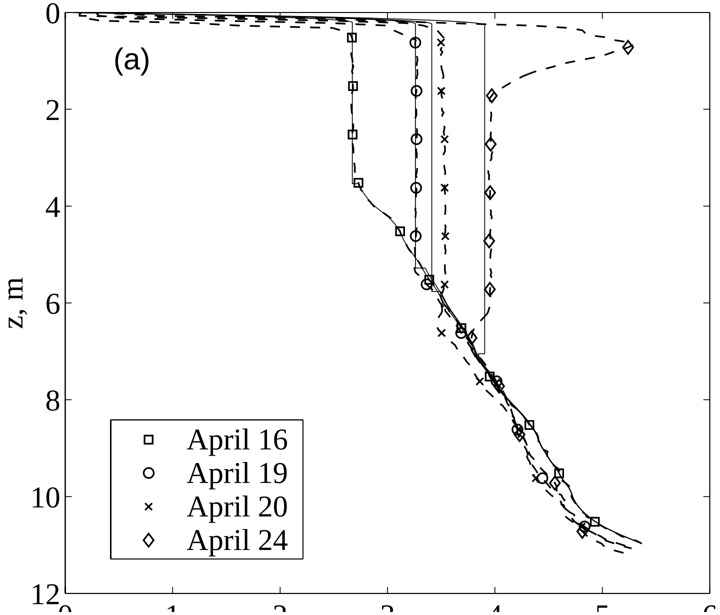

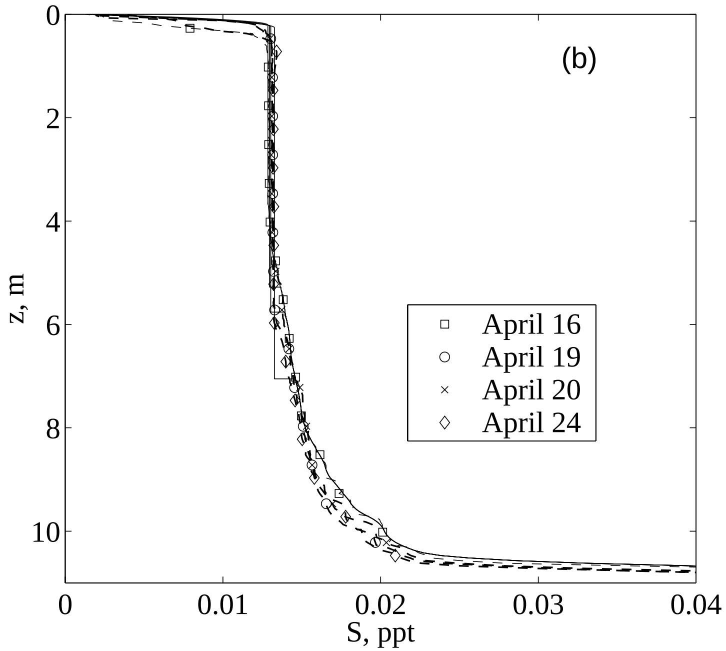

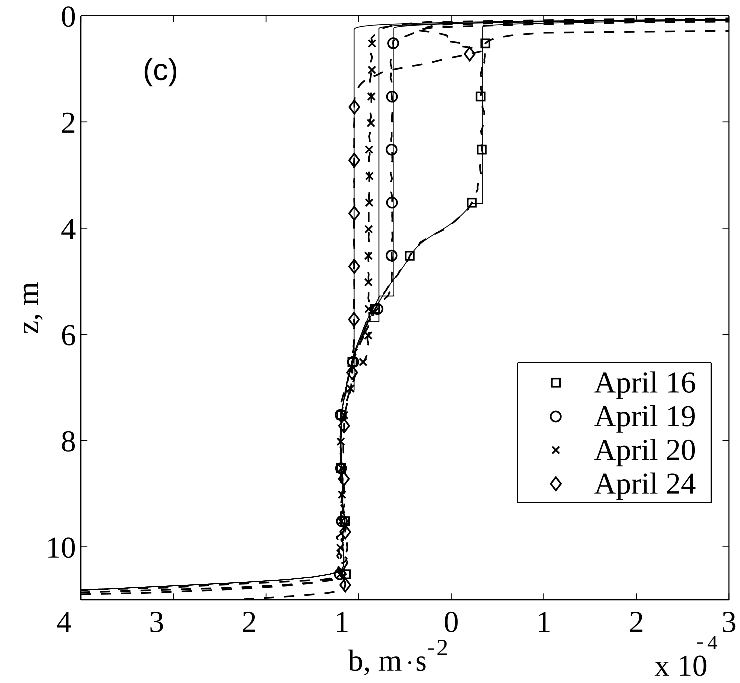

Figure 5.13: Successive vertical profiles of (a) temperature, (b) salinity, (c) buoyancy, in Lake Vendyurskoe, Karelia, Russia, 16 – 24 April 1999 (Terzhevik et. al 2000). Solid curves: mixed-layer model. Curves with symbols show profiles measured at the station **CS4-9** where depth to the bottom is 11.5 m. A two-band radiation decay law is used with $a_1 = 0.5$, $a_2 = 0.5$, $\gamma_1 = 2.7$ m^{-1} and $\gamma_2 = 0.7$ m^{-1}, and a constant value of $I_0 = 1.3 \cdot 10^{-6}$ K·m·s^{-1}.

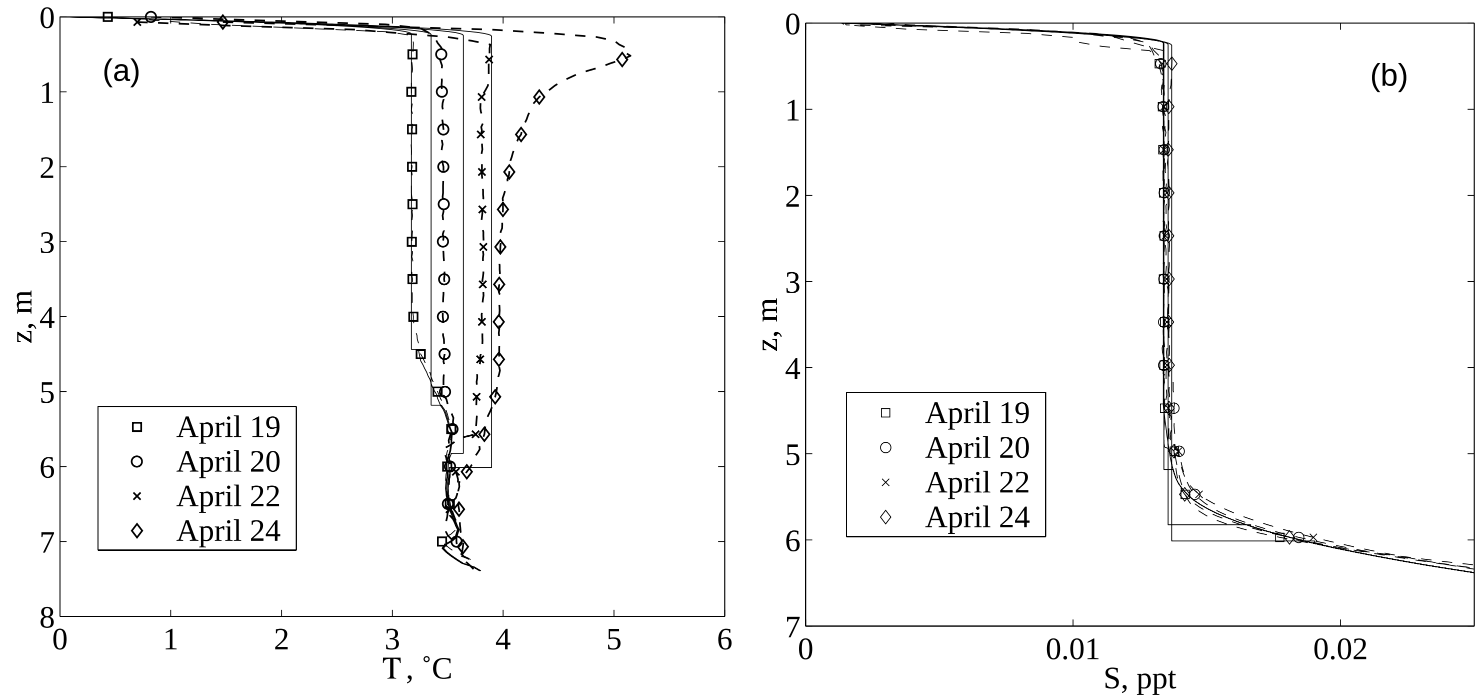

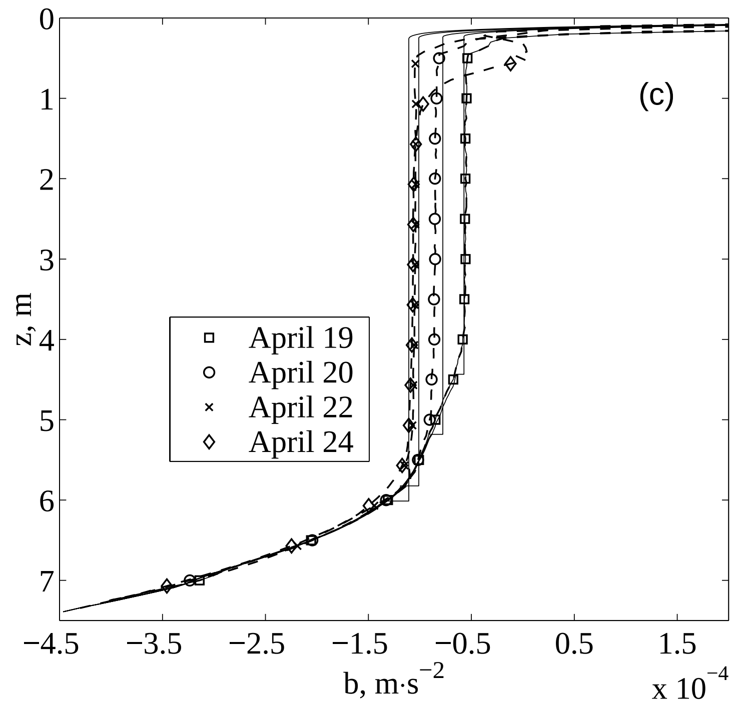

Figure 5.14: Successive vertical profiles of (a) temperature, (b) salinity, (c) buoyancy, in Lake Vendyurskoe, Karelia, Russia, 16 – 24 April 1999 (Terzhevik et. al 2000). Solid curves: mixed-layer model. Curves with symbols show profiles measured at the station **CS4-6** where depth to the bottom is 8.9 m. A two-band radiation decay law is used with $a_1 = 0.5$, $a_2 = 0.5$, $\gamma_1 = 2.7$ m^{-1} and $\gamma_2 = 0.7$ m^{-1}, and a constant value of $I_0 = 1.3 \cdot 10^{-6}$ K·m·s^{-1}.

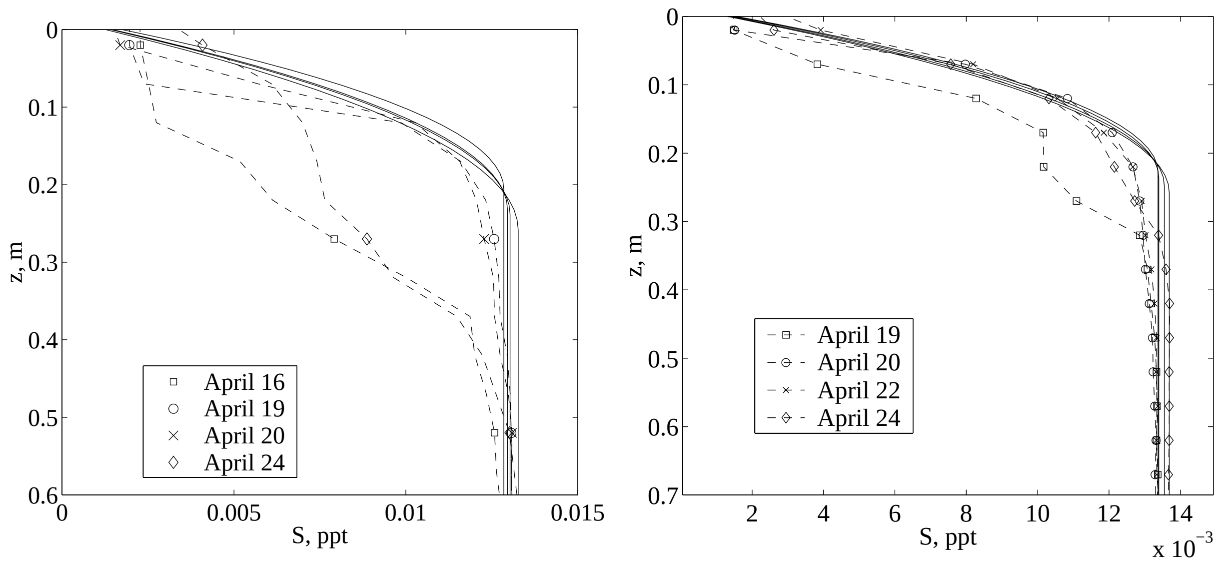

Figure 5.15: Salinity profiles on expanded scale 16 – 24 April 1999 (Terzhevik et. al 2000) just beneath the ice. Left panel: station **CS4-9**, (Fig. 5.13); right panel: station **CS4-6**, (Fig. 5.14).

Fig. 5.15). These variations are produced probably by horizontal motions and are not predicted by the model. The CBL temperature structure prediction in Figs. 5.13a and 5.14a degrades somewhat towards the end of the simulation period. The last profile is qualitatively different, displaying a blob of warm water above the mixed layer. This feature cannot be explained by our four-layer parameterization, but is hardly surprising. Convection energetics near the temperature of maximum density are more complicated and the bulk scaling, Eq. (5.11), underlying our mixed-layer model is not applicable. Clearly, as T_m tends to T_r, the velocity scale, w_R, given by Eq. (5.11) tends to zero. The third-order temperature-velocity correlation should be included in the expression for vertical buoyancy flux in order to arrive at a non-zero convective velocity scale (see Mironov *et al.* 2001 for further discussion). Our mixed-layer model is inapplicable where the bulk of the water column exceeds the temperature of maximum density (cf. the observations of Woodcock 1965 discussed in section 5.1). In this situation solar heating establishes a stable density stratification; static instability only occurs where the temperature increases with depth from T_r to its maximum value. In Figure 5.13(a), it is the upper part of the layer with temperature in excess of T_r that is unstably stratified. We therefore halt our computations when the mixed-layer temperature reaches the temperature of maximum density.

Chapter 6

Conclusions

6.1 General results

- Self-similarity analysis of the temperature profile in the thermocline.

  The concept of self-similarity of the thermocline is discussed. The physical background of the self-similarity hypothesis is analyzed. It is shown that the self-similarity of the temperature profile can be explained as being equivalent of the traveling wave type solution of the heat transfer equation in one-dimensional form.

  The solution is achieved accounting the stratification below the thermocline that extends the applicability of the self-similarity thermocline's representation on wide range of geophysical flows including shallow lakes, atmospheric CBL and the seasonal thermocline in the ocean. Accounting of the underlying stratification in non-turbulent fluid by means of the dimensionless temperature gradient at the thermocline's base, Γ allows the temperature profile within the thermocline to vary in shape collapsing asymptotically into a temperature jump at the UML base as the underlying gradient infinitely grows.

  The solution generalizes previously proposed empirical descriptions of the temperature profile in the thermocline. The turbulent heat flux profile resulting from the solution indicates the direct ratio between mixing intensity and the potential energy, that is in accordance with the theory of mixing in stratified fluids driven by internal waves breaking (Kantha, 1977; Zilitinkevich *et al.* , 1988).

  The solution is tested against observations in the Ocean, the Earth and Mars atmospheres, laboratory modeling and measurements in lakes. The vertical extensions of the natural processes vary from several meters to tenth of kilometers but, when scaled using proposed dimensionless variables, all temperature profiles tend to group at the curve given by proposed solution.

  The self-similar description of the temperature profile make it possible to extend bulk modeling approach analogous to mixed-layer modeling on the stratified part of water column. The fact that the temperature flux at the thermocline's base is taken into account, allows incorporating the description in models of shallow lakes, where the heat flux at the water-sediments boundary can be significant, and in models of convection capped by strong inversion in the atmospheric CBL.

- Model of lake temperature evolution.

The model of seasonal temperature evolution in lakes is developed using the source code and general concepts of the `TeMix` model (Mironov *et al.* , 1991). The model makes use of two-layered representation of temperature profile based on achieved self-similarity solution.

In contrast to the previous `TeMix` algorithm, differential heating of water layer by penetrating solar radiation is taken into account that sufficiently improves the model predictions especially in the shallow lake conditions.

The model performance is investigated on data from the Lake Müggelsee. The comparison of the modeling results with observations shows that the model adequately predicts vertical temperature structure in shallow lakes. The model calculations for summer periods of 1980-1996 have allowed distinguishing the overestimation of the solar radiation data in measurements performed over the lake in 1980-1989. It demonstrates the sensitivity of the model to the input data quality and testifies to the reliability of the model predictions.

Comparison of the modeling results with two-equation turbulence models is performed. Predictions of the mixed layer depth as they given by the current model are in the good agreement with the vertical turbulence structure predicted by the k-ϵ model. At the same time, the bulk algorithm underlying the `TeMix` model provides better results in modeling the surface temperature in shallow lakes than that of k-ϵ and Mellor-Yamada models. The latter two models show essential numerical instability when applied to shallow water bodies under conditions of strongly varying surface heat flux. This fact and the high computational requirements make difficult any utilization of the two-equation turbulence models in ecological and meteorological applications, where prediction of the thermal structure in shallow lakes is necessary. The `TeMix` model in its turn is free from these limitations combining adequate predictions with low computer costs.

The model predicts fairly good the seasonal and interannual variability of the thermal regime in a polymictic lake including stratification formation and destroying. The output characteristics of the model: the mean temperature, the depth and the temperature of the upper mixed layer, provide with information sufficient for various applications related to the lake physics.

The role of water transparency temporal variability in heat budget of a shallow lake is investigated using modeling results and observational data from the Lake Müggelsee. It is found, that for summer periods with low values of the average wind speeds, the surface temperature variations are correlated with the light extinction in lake water. It supposes a backward effect of the plankton growth on the lake temperature.

- Convection in ice-covered lakes.

  The entrainment regimes typical of convection under the ice are analyzed. It is shown that the entrainment equation suitable for the surface-flux-driven convection in the atmosphere and the ocean also applies to convection beneath lake ice, provided that the Deardorff convective velocity scale based on the surface buoyancy flux, is replaced with the appropriate scale that accounts for the vertically distributed character of radiation heating.

  A bulk mixed-layer model is applied to simulate the deepening of convectively mixed layer. The model utilizes a self-similar zero-order-jump representation of the evolving temperature profile. A stationary solution to the heat transfer equation is used to describe the structure of the stably stratified layer just beneath the ice. The mixed-layer scaling and the TKE budget equation integrated over the mixed layer are used to derive the entrainment equation. The model predictions compare well with data from observations in a number of temperate and polar lakes.

An extension of the mixed-layer model for the case of salt water is proposed and tested against observations. Although the salinity is very low in most temperate and polar lakes, its dynamical effect can be significant close to the temperature of maximum density. In particular, when the temperature increases with depth and exceeds the temperature of maximum density in the bottom layer, the water column would have undergone convective overturning were it not for the salinity increase with depth that maintains static stability.

A regime of convection similar to that in ice-covered fresh-water lakes may be encountered in puddles over melting sea ice. Since the puddle water is nearly fresh and has a temperature below that of maximum density, solar heating would drive convective motions just as it does in ice-covered lakes. The difference between the two regimes lies in the boundary conditions. The temperature of the puddle surface changes with time, while in a lake the temperature at the ice-water interface is fixed at the freezing point. Conversely, the lake bottom temperature changes with time, while in the puddle it is fixed at the freezing point. Knowledge of convection in puddles is of practical importance, since convective motions intensify the vertical heat transport towards the ice, thus influencing the rate of ice melting.

Finally, radiatively-driven convection in ice-covered lakes represents a nearly ideal test case for turbulence models. As pointed out by (Farmer, 1975), it is a rare example of geophysical convective flows where there is no mean shear, providing an important simplification of particular value in the study of gravitational instability and its consequences. Data sets generated through temperature and turbulence measurements in the CBL beneath lake ice and through LES can be used to test and further develop turbulence models of convective flows.

6.2 Practical applications

Integration of the model developed here into the model of shallow lake ecosystems (Schellenberger *et al.* , 1983) will be a logical extension of the present study. One can expect essential improvement of the ecological components prediction when the vertical temperature stratification is taken into account (Ford & Thornton, 1979; Denman & Gargett, 1983). The mixed layer depth is the length scale determining the vertical distribution of lake plankton as well as overall biomass production. The stratification regime determines also the internal and external nutrients loading and, consequently, the trophic state of a lake (Golosov & Kirillin, 2000).

Integration of the current algorithm with improved parameterizations of ice-water and water-sediments exchange, which have being currently developed on the base of the `TeMix` code (Zverev, 2000) is envisaged in the near future and will result in a comprehensive model of the “ice – water column – sediments” system. Its development is targeted in the project “Representation of lakes in numerical models for environmental applications” undertaken currently by joined scientific team of meteorological and limnological institutions.

The parameterized description of the vertical temperature distribution developed here can be also used in two- and three-dimensional models of water dynamics, where simplified but physically sound parameterization of the vertical transport is desirable. This approach was used e. g. by Kirillin *et al.* (1998) for modeling of coastal currents in large lakes.

The interaction of the atmosphere with the underlying surface is strongly dependent on the surface temperature and its time-rate-of-change. It is common for NWP systems to assume that the water surface temperature can be kept constant over the forecast period. The assumption is to some extent justified for seas and deep lakes. It is doubtful for small-to-medium size relatively shallow lakes, where the diurnal variations of the surface temperature reach several degrees. A large number of such lakes will become resolved-scale features as the horizontal resolution is increased. The use of a horizontal grid-size of about three kilometers will soon become a common practice in short-range weather forecast. In climate modeling systems with coarser resolution, many small-to-medium size lakes remain sub-grid scale features. However, the presence of these lakes cannot be ignored due to their aggregate effect on the grid-scale surface fluxes. This effect is still poorly understood and parameterized. A renewed interest to the problem of lakes has led to the development of several parameterizations for use in NWP and CM systems (e. g. Ljungemyr *et al.* 1996, Goyette *et al.* 2000, Tsuang *et al.* 2001). Some assume a complete mixing down to the lake bottom and characterize the entire water column by a single value of temperature. Although this assumption results in a bulk model that is very cheap computationally, it is an oversimplification from the physical point of view since most lakes are stratified over a considerable part of the year. Turbulence closure models, e.g. models based on the transport equation for the turbulence kinetic energy (Tsuang *et al.* , 2001), would do the work of describing the lake thermocline better. However, closure models are expensive computationally. Thus, a lake model for environmental applications is required that is physically sound, but at the same time computationally efficient. A very good compromise between physical realism and computational economy can be achieved with the current parameterized model, where the structure of the stratified layer between the upper mixed layer and the basin bottom is described using the concept of self-similarity of the temperature profile in the thermocline.

Acknowledgements

I thank the administration of the Institute for Water Ecology and Inland Fisheries (IGB) for making this research possible and for comprehensive support during my work. It is a pleasure to record my best acknowledgments to the team of the Department of Shallow Lakes and Lowland Rivers of IGB and personally to Horst Behrendt and Dieter Opitz for their unaffected interest and helpful discussions.

I am glad to express my thanks to Leonard Oganesyan for inspiring this work. Numerous encouraging discussions with Dmitrii Mironov (German Weather Service) helped to elaborate the general direction of the research. I am indebted to Sergey Ryanzhin for his invaluable help at the organizing stage of the study.

Illuminating discussions with Sergey Golosov (Insitute of Limnology RAS, Russia), Christian Hochfeld (Institute for Applied Ecology), Oliver Schmoll (Federal Environmental Agency, Germany), Arkady Terzhevik (Northern Water Problems Institute, Russia) contributed this work a lot. I wish to thank Christof Engelhardt and Alexander Sukhodolov (IGB) for the valuable help during the experimental phase of this work and co-operation in many ways.

Measurements data from following sources were used in the study: data from the Mars atmosphere provided by the NASA Planetary Data System; cloudiness data and atmosphere soundings from First ISCLP Field Experiment provided by the International Satellite Cloud Project; North-American lakes temperature data collected by the North Temperate Lakes LTER team.

The source code of the turbulence model GOTM was applied here, developed and made available for free usage by the GOTM development team (`www.gotm.net`).

I am grateful to professors Wilfried Endlicher, Gerhard Jirka and Gunnar Nützmann for their attention to my work.

Bibliography

Arsenyev, S. A., & Felsenbaum, A. I. 1977. Integral Model of the Ocean Active Layer. *Izv. Akad. Nauk SSSR, Fizika Atmosfery i Okeana*, **13**, 1034–1043. English edition: pp. 707-712.

Baker, A. N. 1967. Algae from Lake Miers, a Solar-Heated Antarctic Lake. *N. Z. J. Bot.*, **5**, 453–468.

Ball, F. K. 1960. Control of Inversion Height by Surface Heating. *Q. J. R. Meteorol. Soc.*, **86**, 483–494.

Barenblatt, G. 1996. *Scaling, Self-Similarity and Intermediate Asymptotics*. Cambridge Texts in Applied Mathematics. London: Cambridge University Press. 386 pp.

Barenblatt, G. I. 1978. On Self-Similarity of Temperature and Salinity Distribution in Upper Thermocline. *Izv. Akad. Nauk SSSR. Fizika Atmosfery i Okeana*, **14**, 1160–1166. english edition: pp. 820-823.

Barnes, D. F., & Hobbie, J. E. 1960. Rate of Melting at the Bottom of Floating Ice. *US Geol. Serv. Profess. Papers*, **400**, B392–B394.

Batchelor, G. K. 1959. Small-Scale Variation of Convected Quantities Like Temperature in Turbulent Fluid. *J. Fluid Mech.*, **5**, 113–133.

Batchvarova, E., & Gryning, S.-E. 1991. Applied Model for the Growth of the Daytime Mixed Layer. *Bound.-Layer Meteor.*, **56**, 261–274.

Behrendt, H., Driescher, E., & Schellenberger, G. 1990. Lake Müggelsee – The Use of Lake Water and its Consequences. *GeoJournal*, **22**(2), 175–183.

Behrendt, H., Nixdorf, B., & Pagenkopf, W.-G. 1993. Phenomenological Description of Polymixis and Influence on Oxygen Budget and Phosphorus Release in Lake Müggelsee. *Int. Revue ges. Hydrobiol.*, **78**(3), 411–421.

Bengtsson, L. 1996. Mixing in Ice-Covered Lakes. *Hydrobiologia*, **322**, 91–97.

Bengtsson, L., Malm, J., Terzhevik, A., Petrov, M., Boyarinov, P., Glinsky, A., & Palshin, N. 1995. *A Field Study of Thermo- and Hydrodynamics in a Small Karelian Lake During Late Winter 1994*. Tech. rept. 3185. Department of Water Resources Engineering, Institute of Technology, University of Lund, Lund, Sweden. 72 pp.

Betts, A. K. 1973. Non-Precipitating Cumulus Convection and its Parameterization. *Q. J. R. Meteorol. Soc.*, **99**(419), 178–196.

Betts, A. K. 1974. Reply to the Comment on the Paper “Non-Precipitating Cumulus Convection and its Parameterization”. *Q. J. R. Meteorol. Soc.*, **100**, 469–471.

Birge, E. A. 1910. The Apparent Sinking of Ice in Lakes. *Science*, **32**, 81–82.

Brunt, D. 1946. Patterns in Ice and Cloud. *Weather*, **1**, 184–185.

Burchard, H., & Bolding, K. 2001. Comparative Analysis of Four Second-Moment Turbulence Closure Models for the Oceanic Mixed Layer. *J. Phys. Oceanogr.*, **31**, 1943–1968.

Burchard, H., Bolding, K., & Villarreal, M. R. *GOTM, a General Ocean Turbulence Model*. User manual. Available at `http://www.gotm.net`.

Canuto, V. M., Howard, A., Cheng, Y., & Dubovikov, M. S. 2001. Ocean Turbulence. Part I: One-Point Closure Model. Momentum and Heat Vertical Diffusivities. *J. Phys. Oceanogr.*, **31**, 1413–1426.

Carson, D. J. 1973. The Development of Dry Inversion-Capped Convectively Unstable Boundary Layer. *Q. J. R. Meteorol. Soc.*, **99**(421), 450–467.

Chorley, L. G., Caughey, S. J., & Readings, C. J. 1975. The Development of of the Atmospheric Boundary Layer: Three Case Studies. *Meteor. Mag.*, **104**, 349–360.

Dake, J. M. K., & Harleman, D. R. F. 1969. Thermal stratification in lakes: analytical and laboratory studies. *Water Resour. Res.*, **5**(2), 484–495.

Deardorff, J. W. 1970a. Convective Velocity and Temperature Scales for the Unstable Planetary Boundary Layer and for Rayleigh Convection. *J. Atmos. Sci.*, **27**, 1211–1213.

Deardorff, J. W. 1970b. Preliminary Results from Numerical Integrations of the Unstable Planetary Boundary Layer. *J. Atmos. Sci.*, **27**, 1209–1211.

Deardorff, J. W. 1979. Prediction of Convective Mixed-Layer Layer Entrainment for Realistic Capping Inversion Structure. *J. Atmos. Sci.*, **36**, 424–436.

Deardorff, J. W. 1980. Stratocumulus-Capped Mixed Layers Derived from a Three-Dimensional Model. *Boundary-Layer Meteorol.*, **18**, 495–527.

Deardorff, W. J., & Willis, G. E. 1982. Dependence of Mixed-Layer Entrainment on Shear Stress and Velocity Jump. *J. Fluid Mech.*, **115**, 123–149.

Deardorff, W. J., Willis, G. E., & Stockton, B. H. 1980. Laboratory Studies of the Entrainment Zone of a Convectivly Mixed Layer. *J. Fluid Mech.*, **100**, 41–46.

Denman, K. L. 1973. A Time Dependent Model of the Upper Ocean. *J. Phys. Oceanogr.*, **3**, 173–184.

Denman, K. L., & Gargett, A. E. 1983. Time and space scales of vertical mixing and advection of phytoplankton in the upper ocean. *Limnol. Oceanol.*, **28**(5), 801–815.

Driescher, E., Behrendt, H., Schellenberger, G., & Stellmacher, R. 1993. Lake Müggelsee and Its Environment – Natural Conditions and Anthropogenic Impact. *Int. Revue ges. Hydrobiol.*, **78**(3), 327–343. Special issue: Lake Müggelsee – Limnology of a Eutrophic Shallow Polymictic Lake.

Efimov, S. S., & Tsarenko, V. M. 1980. On a Self-Similarity of the Temperature Distribution in the Upper Thermocline. *Izv. Akad. Nauk SSSR. Fizika Atmosfery i Okeana*, **16**(6), 620–627.

Emery, William J., & Thomson, Richard E. 2001. *Data Analysis Methods in Physical Oceanography*. second edn. Amsterdam: Elsevier.

Ertel, Hans. 1954. Theorie der Thermischen Sprungschiht in Seen. *Acta Hydrophys.*, **2**, 151–171.

Farmer, D. M. 1975. Penetrative Convection in the Absence of Mean Shear. *Q. J. R. Meteorol. Soc.*, **101**, 869–891.

Farmer, D. M., & Carmack, E. 1981. Wind mixing and restratification in a lake near the temperature of maximum density. *J. Phys. Oceanogr.*, **11**(11), 1516–1533.

Fedorovich, E. E., & Mironov, D. V. 1995. A Model for a Shear-Free Convective Boundary Layer with Parameterized Capping Inversion Structure. *J. Atmos. Sci.*, **52**(1), 83–95.

Fofonoff, P., & Millard, Jr., R. C. 1983. *Algorithms for Computation of Fundamental Properties of Seawater*. Tech. rept. 44. UNESCO Tech. Pap. in Mar. Sci. 53 pp.

Ford, D. E., & Thornton, K. W. 1979. Time and length scales for the one-dimensional assumption and its relation to ecological models. *Water Resour. Res.*, **15**, 113–120.

Forel, F.-A. 1892. *Le Léman. Monographie Limnologique.* Vol. 1. Lausanne: F. Rouge, Éditeur, Librarie de l'Université.

Forel, F.-A. 1901. *Handbuch der Seekunde*. Stuttgart: Verlag von J. Engelhorn.

Fung, I., Harrison, D. E., & Lacis, A. A. 1984. The Variability of Net Longwave Radiation at the Ocean Surface. *Rev. Geophys. Space Physics*, **22**, 177–193.

GGO manual. 1982. *Recommendations for Calculation of Radiative Budget Components on the Oceanic Surface*. GGO (State Geophysical Observatory), Leningrad. 92 p., in russian.

Gill, A. E., & Turner, J. S. 1976. A Comparison of Seasonal Thermocline Models with Observation. *Deep-Sea Res.*, **23**, 391–401.

Golosov, S. D., & Kirillin, G. B. 2000. Modelling the Lake Response to an External Phosphorus Load. *Pages 388–392 of:* Peltonen, A., Grönlund, E., & Viljanen, M. (eds), *Proceedings of the 3rd International Lake Ladoga Symposium*. University of Joensuu, Publications of Karelian Institute.

Golosov, S. D., & Kreiman, K. D. 1992. Heat Exchange and Thermal Structure in the Water-Sediments System. *Vodnye Resursy*, **19**(6), 12–18.

Götzinger, G. 1909. Studien über Das Eis Des Lunzer Unter- und Obersees. *Internat. Rev. ges. Hydrobiol. Hydrograph.*, **2**, 386–396.

Goyette, S., McFarlane, N. A., & Flato, G. M. 2000. Application of the Canadian Regional Climate Model to the Laurentian Great Lakes Region: Implementation of a Lake Model. *Atmosphere-Ocean*, **38**, 481–503.

Granin, N., Jewson, D., Gnatovskiy, R., Levin, L., Zhdanov, A., Averin, A., Gorbunova, L., Tsekhanovskii, V., Doroschenko, L., Min'ko, N., & Grachev, M. 1999a. Turbulent Mixing in the Water Layer Just Below the Ice and its Role in Development of Diatomic Algae in Lake Baikal. *Dokl. Akad. Nauk SSSR*, **366**, 835–839.

Granin, N. G., Gnatovskiy, R. Yu., Zhdanov, A. A., Tsekhanovskii, V. V., & Gorbunova, L. A. 1999b. Convection and Mixing under the Ice of Lake Baikal. *Sibirskij Ecologicheskij Zhurnal*, **6**, 597–600.

Gryning, S.-E., & Batchvarova, E. 1994. Parameterization of the Depth of of the Entrainment Zone Above the Daytime Mixed Layer. *Quart. J. Roy. Meteor. Soc.*, **120**, 47–58.

Hahn, C. J., & Warren, S. G. 1999. *Extended Edited Synoptic Cloud Reports from Ships and Land Stations Over the Globe, 1952-1996.* Tech. rept. ORNL/CDIAC-123, NDP026C. Carbon Dioxide Information Analysis Center, Oak Ridge National Laboratory, U.S. Dept. of Energy, Oak Ridge, Tennessee. (Also available from Data Support Section, National Center for Atmospheric Research, Boulder, CO.).

Hawes, I. 1983. Turbulence and its Consequences for Phytoplankton Development in Two Ice-Covered Antarctic Lakes. *British Antarctic Survey Bulletin*, **60**, 69–81.

Hinson, D. P., Simpson, R. A., Twicken, J. D., Tyler, G. L., & Flasar, F. M. 1999. Initial Results from Radio Occultation Measurements with Mars Global Surveyor. *J. Geophys. Res.*, **104**(E11), 26297–27012.

Hinze, J. O. 1959. *Turbulence*. McGraw Hill Book Co. 517 pp.

Hocking, G. C., & Straškraba, M. 1999. The Effect of Light Extinction on Thermal Stratification in Reservoirs and Lakes. *Internat. Rev. Hydrobiol.*, **84**(6), 535–556.

Imberger, J. 1994. Transport Processes in Lakes. *Pages 99–193 of:* Margalef, R. (ed), *Limnology Now: A Paradigm of Planetary Problems*. Elsevier Science B.V.

Imberger, J. 2001. Characterizing the Dynamical Regimes of a Lake. *Pages 77–92 of:* Casamitjana, X. (ed), *Proc. 6th International Workshop on Physical Processes in Natural Waters*. Spain: University of Girona.

Imberger, J., & Hamblin, P.F. 1982. Dynamics of lakes, reservoirs and cooling ponds. *Annu. Rev. Fluid Mech.*, **14**(1), 153–187.

Imberger, J., & Patterson, J. C. 1981. A dynamic reservoir simulation model - DYRESM 5. *Pages 310–361 of:* Fischer, H. B. (ed), *Transport Models for Inland and Coastal Waters*. New-York: Academic Press.

Imberger, J., & Patterson, J. C. 1990. Physical Limnology. *Pages 303–475 of:* Wu, T. (ed), *Advances in Applied Machanics*. Boston: Academic Press.

Ivey, G. N., & Nokes, R. I. 1989. Vertical Mixing Due to the Breaking of Internal Waves on Sloping Boundaries. *J. Fluid Mech.*, **204**, 479–500.

Jerlov, N. G. 1976. *Marine Optics*. 2nd edition edn. Elsevier Oceanography Series. Amsterdam: Elsevier Scientific Publishing Company.

Jirka, G. H., & Watanabe, M. 1980. Thermal Structure of Cooling Ponds. *Journal of the Hydraulics Division*, **106**(5), 701–715.

Jirka, G. H., Watanabe, M., Octavio, K. H., Cerco, C. F., & Harleman, D. R. F. 1978. *Mathematical Predictive Models for Cooling Lakes and Ponds. Part A: Model Development and Design Consierations*. Tech. rept. 238. Massachusetts Institute of Technology, Cambridge, Mass.

Kamenkovich, V. M., Koshlyakov, M. N., & Monin, A. S. 1987. *Synoptic Eddies in the Ocean*. 2 edn. Leningrad: Gidrometeoizdat.

Kantha, L. H. 1977. Notes on the Role of Internal Waves in Thermocline Erosion. *Pages 173–177 of:* Kraus, E. B. (ed), *Modelling and Prediction of the Upper Layers of the Ocean*. Oxford: Pergamon press.

Katsaros, K. B. 1981. Convection Patterns in a Pond. *Bull. Am. Meteorol. Soc.*, **62**, 1446–1453.

Katsaros, K. B. 1983. Response. *Bull. Am. Meteorol. Soc.*, **64**, 277–279.

Kelley, D. E. 1997. Convection in Ice-Covered Lakes: Effects on Algal Suspension. *J. Plankton Res*, **19**, 1859–1880.

Kirillin, G. 2001a. On Self-Similarity of the Pycnocline. *In:* Boyer, D., & Rankin, R. (eds), *Proceedings of the 3rd International Symposium on Environmental Hydraulics*. 6pp. (Proceedings CD-ROM is available at <www.eas.asu.edu/iseh2001/book/>).

Kirillin, G. 2001b. On Self-Similarity of Thermocline in Shallow Lakes. *Pages 221–225 of:* Casamitjana, X. (ed), *Proc. 6th International Workshop on Physical Processes in Natural Waters*. Spain: University of Girona.

Kirillin, G., Oganesyan, L., & Terzhevik, A. 1998. *Analytical Modelling of Coastal Hydrodynamics of Large Reserviors*. Lund, Sweden: Report No 3221, Department of Water Resources Engineering, Lund Institute of Technology, Lund University.

Kirillin, G., Mironov, D., & Terzhevik, A. 2001. Radiatively-Driven Spring Convection in Ice-Covered Lakes: The Effect of Salt Concentration. *Pages 199–203 of:* Casamitjana, X. (ed), *Proc. 6th International Workshop on Physical Processes in Natural Waters*. Spain: University of Girona.

Kitaigorodski, S. A. 1960. On the Computaion of the Thickness of the Wind-Mixing Layer in the Ocean. *Bull. Acad. Sci. USSR, Geophys. Ser.*, **3**, 284–287.

Kitaigorodski, S. A., & Miropolski, Yu. Z. 1970. On the Theory of the Open Ocean Active Layer. *Izv. Akad. Nauk SSSR. Fizika Atmosfery i Okeana*, **6**, 178–188.

Kitaigorodskii, S. A., & Joffre, S. M. 1988. In Search of Simple Scaling for the Heights of the Stratified Atmospheric Boundary Layer. *Tellus*, **40A**, 419–433.

Kohl, E. 1969. Das Klima der Stadt Berlin. *Wiss. Abh. d. Geogr. Ges. DDR*, **10**, 67–84.

Kraus, E. B. 1972. *Atmosphere-Ocean Interaction*. London: Oxford University Press.

Kraus, E. B., & Rooth, C. 1961. Temperature and Steady State Vertical Heat Flux in the Ocean Surface Layers. *Tellus*, **13**(2), 231–238.

Kraus, E. B., & Turner, J. S. 1967. A One-Dimentional Model of the Seasonal Thermocline: The General Theory and its Consequences. *Tellus*, **19**, 98–106.

Kreiman, K. D., & Kirillin, G. B. 1998. Laboratory Modeling of Turbulent Entrainment in a Stratified Fluid. *Izv. Akad. Nauk SSSR. Fizika Atmosfery i Okeana*, **34**(4), 600–605.

Li, G. H., & Gregory, S. 1974. Diffusion of Ions in the Sea Water and in Deep Sea Sediments. *Geochim. Cosmochim. Acta*, **38**, 703–714.

Lilly, D. K. 1968. Models of Cloud-Topped Mixed Layers under a Strong Inversion. *Q. J. R. Meteorol. Soc.*, **94**, 292–309.

Linden, P. F. 1975. The Deepening of the Mixed Layer in a Stratified Fluid. *J. Fluid Mech.*, **71**, 385–405.

Ljungemyr, P., Gustafsson, N., & Omsted, A. 1996. Parameterization of Lake Thermodynamics in a High-Resolution Weather Forecasting Model. *Tellus*, **48A**(5), 608–621.

Mahrt, L., & Lenschow, D. H. 1976. Growth Dynamics of the Convectively Mixed Layer. *J. Atmos. Sci.*, **33**, 41–51.

Mälkki, P., & Tamsalu, R. 1985. Physical Features of the Baltic Sea. *Finn. Mar. Res.* 110 pp.

Malm, J., Terzhevik, A., Bengtsson, L., Boyarinov, P., Glinsky, A., Palshin, N., & Petrov, M. 1996. *A field study of thermo- and hydrodynamics in three small Karelian lakes during winter 1994/1995*. Tech. rept. 3197. Dept. Water Resour. Eng., Univ. of Lund. 220 pp.

Malm, J., Terzhevik, A., Bengtsson, L., Boyarinov, P., Glinsky, A., Palshin, N., & Petrov, M. 1997a. Temperature and Salt Content Regimes in Three Shallow Ice-Covered Lakes. 1. Temperature, Salt Content, and Density Structure. *Nordic Hydrology*, **28**, 99–128.

Malm, J., Terzhevik, A., Bengtsson, L., Boyarinov, P., Glinsky, A., Palshin, N., & Petrov, M. 1997b. Temperature and Salt Content Regimes in Three Shallow Ice-Covered Lakes, 2. Heat and Mass Fluxes. *Nordic Hydrology*, **28**, 129–152.

Matthews, P. C. 1988. *Convection and Mixing in Ice-Covered Lakes*. Ph.D. thesis, Cambridge University.

Matthews, P. C., & Heaney, S. A. 1987. Solar Heating and its Influence on Mixing in Ice-Covered Lakes. *Freshwater Biol.*, **18**, 135–149.

Mellor, G. L., & Yamada, T. 1974. A hierarchy of turbulence closure models for planetary boundary layers. *J. Atmos. Sci.*, **13**, 1791–1806.

Mellor, G. L., & Yamada, T. 1982. Development of a turbulent closure model for geophysical fluid problems. *Rev. Geophys.*, **20**(4), 851–875.

Mironov, D. 1991. Calculation of Parameters of Hydro- and Thermodynamical Interaction at the Air-Water Interface over Lakes. *Pages xx–xx of:* Zilitinkevich, S. S. (ed), *Modelling Air-Lake Interaction. Physical Background*. Advances in Physics. Berlin: Springer-Verlag.

Mironov, D., Terzhevik, A., Kirillin, G., Jonas, T., Malm, J., & Farmer, D. 2002. Radiatively-Driven Convection in Ice-Covered Lakes: Observations, Scaling and Mixed-Layer Model. *J. Geophys. Res.*, **107**(C4), 1–16.

Mironov, D. V., & Terzhevik, A. Yu. 2000. Spring Convection in Ice-Covered Fresh-Water Lakes. *Izv. Akad. Nauk SSSR. Fizika Atmosfery i Okeana*, **36**, 627–634.

Mironov, D. V., Golosov, S. D., Zilitinkevich, S. S., Kreiman, K. D., & Terzhevik, A. Yu. 1991. Seasonal Changes of Temperature and Mixing Conditions in a Lake. *Pages 74–90 of:* Zilitinkevich, S. S. (ed), *Modelling Air-Lake Interaction. Physical Background*. Berlin: Springer-Verlag.

Mironov, D. V., Danilov, S. D., & Olbers, D. J. 2001. Large-Eddy Simulation of Radiatively-Driven Convection in Ice-Covered Lakes. *Pages 71–75 of:* Casamitjana, X. (ed), *Proc. Of the 6th Workshop on Physical Processes in Natural Waters*. Girona, Spain: University of Girona.

Mironov, D.V., & Karlin, L.N. 1989. Penetrative convection due to surface cooling with vertically distributed heating. *Dokl. Akad. Nauk SSSR*, **309**(6), 1336–1340.

Miropolsky, Yu. Z., Filyushkin, B. N., & Chernyshkov, P. V. 1970. On the Parametric Description of Temperature Profiles in the Ocean Active Layer. *Okeanologiya*, **10**, 1101–1107. English edition: pp. 892-897.

Munk, W. H., & Anderson, E. R. 1948. Notes on a Theory of the Thermocline. *J. Marine Res.*, **7**, 276–295.

Neumann, H. G. 1958. Zellmuster Auf der Oberfläche Eines Teiches. *Beitr. Phys. Atmosph.*, **30**, 246–253.

Nieuwstadt, F. T. M., & Duynkerke, P. G. 1996. Turbulence in the Atmospheric Boundary Layer. *Atmos. Res.*, **40**, 111–142.

Nieuwstadt, F. T. M., & Tennekes, H. 1981. A Rate Equation for the Nocturnal Boundary-Layer Height. *J. Atmos. Sci.*, **38**, 1418–1428.

Niiler, P. P., & Kraus, E. B. 1977. One-Dimensional Models of the Upper Ocean. *Pages 143–172 of:* Kraus, E. B. (ed), *Modelling and Prediction of the Upper Layers of the Ocean*. Oxford: Pergamon press.

Octavio, K. A. H., Jirka, G. H., & Harleman, D. R. F. 1977. *Vertical Heat Transport Mechanisms in Lakes and Reservoirs*. Tech. rept. 227. Massachusets Institute of Technology, Boston, Massachusetts.

Orlov, V. S. 1996. The Role of Solar Radiation and Boundary Conditions in Simulation of the Mixed Oceanic Layer. *Izv. Akad. Nauk SSSR. Fizika Atmosfery i Okeana*, **31**(5), 690–695. English edition.

Ostrovsky, I., Yakobi, Y. Z., Walline, P., & Kalikhman, I. 1996. Seiche-Induced Mixing: Its Impact on Lake Productivity. *Limnol. Oceanogr.*, **41**(2), 323–332.

Payne. 1972. Albedo of the Sea Surface. *J. Atmos. Sci.*, **29**(5), 959–970.

Petrov, M. P., & Sutyrin, G. G. 1984. Diurnal Cycle of Convection in an Ice-Covered Lake. *Meteorologija i Gidrologija*, **1**, 91–98.

Prézelin, B. B., Tilzer, M. M., Schofield, O., & Haese, C. 1991. The Control of the Production Process of Phytoplankton by the Physical Structure of the Aquatic Environment with Special Reference to its Optical Properties. *Aquatic Sci.*, **?**, 136–186.

Price, J. F., Weller, R. A., & Pinkel, R. 1986. Diurnal Cycling: Observations and Models of the Upper Ocean Response to Diurnal Heating. *J. Geophys. Res.*, **C91**, 8411–8427.

Pushistov, P. Yu., & Ievlev, K. V. 2000. Numerical Eddy-Resolving Model of Non-Stationary Penetrative Convection in Spring Solar Heating of Ice-Covered Lakes. *Bull. Inst. Comp. Math. and Math. Geoph. Series "Numerical Modelling in Atmosphere, Ocean Environment Studies"*, **5**, 55–63.

Randall, D. A., & Wielicki, B. A. 1997. Measurements, Models, and Hypotheses in the Atmospheric Sciences. *Bull. Am. Meteorol. Soc.*, **78**, 399–406.

Reshetova, O., & Chalikov, D. 1977. Universal Structure of the Active Layer in the Ocean. *Okeanologiya*, **17**, 774–777. English edition: pp. 509-511.

Rodhe, W. 1949. The Ionic Composition of Lake Waters. *Verh. Internat. Ver. Limnol.*, **10**, 377–386.

Rodi, W. 1987. Examples of Calculation Methods for Flow and Mixing in Stratified Flows. *J. Geophys. Res.*, **92**, 5305–5328.

Rossby, C. G., & Montgomery, R. B. 1935. The Layer of Frictional Influence in Wind and Ocean Currents. *Pap. Phys. Oceanogr. Meteorol.*, **3**(3), 1–101. M.I.T. and Woods Hole Oceanog. Inst.

Royer, T., & Young, W. (eds). 1997. *The Future of Physical Oceanography (Proceedings of the APROPOS Workshop)*.

Rumiantsev, V. A., Razumov, E. V., & Zilitinkevich, S. S. 1986. *Parameterized Model of Seasonal Changes of Temperature and Mixing Conditions in a Lake (with Application to Sevan Problem)*. Leningrad. 74 pp. (in russian).

Schellenberger, G., Behrendt, H., Kozerski, H.-P., & Mohaupt, V. 1983. Ein Mathematisches Ökosystemmodell Für Eutrophe Flachgewässer. *Acta hydrophys.*, **28**(1-2), 109–172.

Schindler, D. W., Welch, H. E., Kalff, J., Brunskill, G. J., & Krisch, N. 1974. Physical and Chemical Limnology of Char Lake, Cornwallis Island (75°N Lat.). *J. Fish. Res. Board Can.*, **31**, 585–607.

Schmidt, W. 1915. Über Den Energiegehalt der Seen. *Internat. Rev. ges. Hydrobiol. Hydrogr.*, **suppl.**

Shapiro, G. I. 1980. Effect of Fluctuations in a Turbulent Entrainment Layer on Heat and Mass Transfer in the Upper Thermocline. *Izv. Akad. Nauk SSSR. Fizika Atmosfery i Okeana*, **16**, 433–436.

Simpson, J. J., & Dickey, T. D. 1981. Alternative Parameterizations of Downward Irradiance and Their Dynamical Significance. *J Phys Oceanogr*, **11**, 876–882.

Soloviev, A.V. 1979. Fine thermal structure of the ocean surface layer in the POLYMODE-77 region. *Izv. Akad. Nauk SSSR. Fizika Atmosfery i Okeana*, **15**(7), 750–757.

Soloviev, A.V., & Vershinskii, N.V. 1982. The vertical structure of the thin surface layer of the ocean under conditions of low wind speed. *Deep Sea Res.*, **29**, 1437–1449.

Spigel, R. H., Imberger, J., & Rayner, K. N. 1986. Modeling the Diurnal Mixed Layer. *Limnol. Oceanogr.*, **31**(3), 533–556.

Strebel, D. E., Landis, D. R., Huemmrich, K. F., & Meeson, B. W. 1994. *Collected Data of the First ISLSCP Field Experiment, Volume 1:Surface Observations and Non-Image Data Sets*. Published on CD-ROM by NASA.

Svensson, U. 1978. *A mathematical model for the seasonal thermocline*. Ph.D. thesis, Dept. Water Resour. Eng., Univ. of Lund, Sweden. Rep. 1002,187 p.

Tamsalu, R., & Myrberg, K. 1998. A Theoretical and Experimental Study of the Self-Similarity Concept. *MERI. Report series of the Finnish Institute of Marine Research*, **37**, 3–13 (1238–1328).

Tamsalu, R., Mälkki, P., & Myrberg, K. 1997. Self-Similarity Concept in Marine System Modelling. *Geophysica*, **2**, 51–68.

Tennekes, H. 1973. A Model for the Dynamics of the Inversion Above a Convective Boundary Layer. *J. Atmos. Sci.*, **30**(4), 558–567.

Terzhevik, A., Boyarinov, P., Filatov, N., Mitrokhov, A., Palshin, N., Petrov, M., Jonas, T., Schurter, M., & Ali Maher, O. 2000. Field Study of Winter Hydrodynamics in Lake Vendyurskoe (Russia). *Pages 110–113 of:* Semovski, S. V. (ed), *Proc. 5th Workshop on Physical Processes in Natural Waters*. Irkutsk, Russia: Limnological Institute, Siberian Branch of RAS.

Thompson, R.O.R.Y., & Imberger, J. 1980. Response of a Numerical Model of a Stratified Lake to Wind Stress. *Pages 562–570 of:* Carstens, T., & McClimans, T. (eds), *Second International Symposium on Stratified Flows*. Trondheim, Norway: IAHR.

Thorpe, S. A. 1973. Turbulence in a Stably Stratified Fluids: A Review of Laboratory Experiments. *Boundary-Layer Meteorol.*, **5**, 95–119.

Townsend, A. A. 1964. Natural Convection in Water over an Ice Surface. *Q. J. R. Meteorol. Soc.*, **90**, 248–259.

Tsuang, B.-J., Tu, C.-Y., & Arpe, K. 2001. *Lake Parameterization for Climate Models*. Tech. rept. 316. Max Planck Institute for Meteorology, Hamburg. 72 pp.

Tucker, W. A., & Green, A. W. 1977. A time-dependent model of the lake-averaged, vertical temperature distribution of lakes. *Limnol. Oceanogr.*, **22**(4), 687–699.

Turner, J. S. 1978. The Temperature Profile Below the Surface Mixed Layer. *Ocean Model.*, **11**, 6–8.

Turner, J. S. 1986. Turbulent Entrainment: The Development of the Entrainment Assumption, and its Application to Geophysical Flows. *J. Fluid Mech.*, **173**, 431–471.

Webb, D. J., & Suginohara, N. 2001. Oceanography. Vertical Mixing in the Ocean. *Nature*, **409**(6816), 37.

Woodcock, A. H. 1965. Melt Patterns in Ice over Shallow Waters. *Limnol. Oceanogr.*, **10**, R290–R297.

Woodcock, A. H., & Lukas, R. B. 1983. Comments Concerning "Convection Patterns in a Pond". *Bull. Am. Meteorol. Soc.*, **64**, 274–277.

Woodcock, A. H., & Riley, G. A. 1947. Patterns in Pond Ice. *J. Meteorol.*, **4**, 100–101.

Woods, J. D. 1980. Diurnal and Seasonal Variation of Convection in the Wind-Mixed Layer of the Ocean. *Q. J. R. Meteorol. Soc.*, **106**(449), 379–394.

Wyatt, L. R. 1978. Mixed Layer Development in an Annular Tank. *Ocean Model.*, **17**, 6–8.

Zilitinkevich, S., & Mironov, D. 1996. A Multi-Limit Formulation for the Equilibrium Depth of a Stably Stratified Boundary Layer. *Boundary-Layer Meteorology*, **81**, 325–351.

Zilitinkevich, S., Fedorovich, E., & Mironov, D. 1992. Turbulent Heat Transfer in Stratified Geophysical Flows. *Pages 1123–1139 of:* Sundén, B., & Žukauskas, A. (eds), *Recent Advances in Heat Transfer*. Elsevier Science Publ.

Zilitinkevich, S. S. 1987. A Theoretical Model of Turbulent Penetrative Convection. *Izv. Akad. Nauk SSSR. Fizika Atmosfery i Okeana*, **23**, 593–610.

Zilitinkevich, S. S. 1991. *Turbulent Penetrative Convection*. Adlershot: Avebury Technical. 179 pp.

Zilitinkevich, S. S., & Deardorff, J. W. 1974. Similarity Theory for the Planetary Boundary Layer of Time-Dependent Height. *J. Atmos. Sci.*, **31**, 1449–1452.

Zilitinkevich, S. S., & Rumyantsev, V. A. 1990. A Parameterized Model of Seasonal Temperature Changes in Lakes. *Environmental Software*, **5**(1), 12–25.

Zilitinkevich, S. S., Kreiman, K. D., & Felzenbaum, A. I. 1988. Turbulence, Heat Exchange and Self-Similarity of the Temperature Profile in a Thermocline. *Dokl. Akad. Nauk SSSR*, **300**(5), 1226–1230.

Zilitinkevich, S.S., & Mironov, D.V. 1992. Theoretical Model of the Thermocline in a Freshwater Basin. *J. Phys. Oceanogr.*, **22**(9), 988–996.

Zimmerman, M. J., Waldron, M. C., Schreiner, S. P., Freedman, M. L., Giammatteo, P. A., Hains, J. J., Nestler, J. M., Speziale, B. J., & Schindler, J. E. 1981. High Frequency Energy Exchange and Mixing Dynamics of Lakes. *Verh. Internat. Verein. Limnol.*, **21**, 88–93.

Zubov, N. N. 1943. *L'dy Arktiki (Arctic Ice)*. Moskva (Glavsevmorput Publ. House, Moscow): Izdatel'stvo Glavsevmorput. 360 pp.

Zverev, I. S. 2000. *Modeling the Annual Cycle of the Thermal Regime of a Shallow Lake*. Ph.D. thesis, Institute of Limnology, Russian Academy of Sciences, S-Petersburg. (in russian).

Zwart, B. 1976. Natuur Experimenteerde Met KNMI – Vijver. *Zenit*, **4**, 86–88.

Acronyms

CBL	Convective Boundary Layer
CM	Climate Modeling
CTD	Conductivity-Temperature-Depth
DNS	Direct Numerical Simulation
HTE	Heat Transfer Equation
IGB	Institut für Gewässerökologie und Binnenfischerei (Institute for Water Ecology and Inland Fisheries)
IL	Interfacial Layer
LES	Large Eddy Simulation
MGS	Mars Global Surveyor experiment
MO	Monin-Obukhov (scaling)
NWP	Numerical Weather Prediction
TKE	Turbulent Kinetic Energy
UML	Upper Mixed Layer

List of symbols

Some intermediate notations are not included in the list and explained as they appear in text.

Sub- and Superscripts

$\dot{\square}$	Derivative with regard to t,
$\square'$	Derivative with regard to ζ,
$\bar{\square}$	Vertical co-ordinate averaging,
$\langle\square\rangle$	Reynolds averaging,
$\widetilde{\square}$	Turbulent pulsation,
$\square_D$	Bottom value,
$\square_S$	Surface value,
$\square_h$	Value at the UML base,
$\Delta\square$	Difference across the thermocline ($\square_D - \square_h$),

Greek

α_T	Thermal expansion coefficient,
α_S	Saline contraction coefficient,
β	Buoyancy parameter,
γ	Light extinction coefficient,
Γ	Dimensionless temperature (density) gradient,
δ	Upper "conduction" layer thickness (Chapter 5),
ϵ	Turbulent dissipation rate,
ζ	Dimensionless vertical co-ordinate,
ϑ	Dimensionless temperature,
$\varkappa$	Molecular temperature diffusion coefficient,
μ	Molecular diffusivity of salt in water,
ξ	Dimensionless vertical co-ordinate in conduction layer,

ϱ	Water density,
ς	Dimensionless vertical co-ordinate in ML,
χ	Dimensionless temperature conductivity coefficient,
Φ	Dimensionless vertical heat flux,
φ	Latitude,

Latin

A	Lake surface albedo,
b	Buoyancy,
B	Vertical buoyancy flux,
$C_\square$	Dimensionless constants,
D	Lake depth, m
g	Gravity acceleration,
h	UML depth, m
I	solar radiation,
K	Turbulent heat (temperature) conductivity,
$K_{\mathbf{XY}}$	Coefficient of cross-correlation between quantities *X* and *Y*,
l	Turbulent mixing length scale,
L_*	Monin-Obukhov length scale,
N	Brunt-Väisälä frequency,
Q	Vertical heat (temperature) flux,
S	Salinity,
T	Temperature, K(°C)
t	Time co-ordinate,
u_*	Surface friction velocity,
w_*	Deardorff convective velocity scale,
w_R	Radiatively-driven convective velocity scale,
w_{*R}	$w_* + w_R$,
z	Vertical co-ordinate,